Title

Multiomic Analysis of the Gut Microbiome in Psoriasis Reveals Distinct Host–Microbe Associations

Journal

JID Innovations, 2(3)

ISSN

2667-0267

Authors

Chang, Hsin-Wen
Yan, Di
Singh, Rasnik
et al.

Publication Date

2022-05-01

DOI

10.1016/j.xjidi.2022.100115

Peer reviewed

Multiomic Analysis of the Gut Microbiome in Psoriasis Reveals Distinct Host–Microbe Associations

Hsin-Wen Chang[1], Di Yan[2], Rasnik Singh[3], Audrey Bui[4], Kristina Lee[1], Alexa Truong[5], Jeffrey M. Milush[6], Ma Somsouk[7] and Wilson Liao[1]

Psoriasis is a chronic, inflammatory skin disease that affects 2–3% of the global population. Besides skin manifestations, patients with psoriasis have increased susceptibility to a number of comorbidities, including psoriatic arthritis, cardiovascular disease, and inflammatory bowel disease. To understand the systemic component of psoriasis pathogenesis, we performed a pilot study to examine the fecal metagenome, host colonic transcriptome, and host peripheral blood immune profiles of patients with psoriasis and healthy controls. Our study showed increased functional diversity in the gut microbiome of patients with psoriasis. In addition, we identified microbial species that preferentially associate with patients with psoriasis and which have been previously found to associate with other autoimmune diseases. Intriguingly, our data revealed three psoriasis subgroups that have distinct microbial and host features. Integrating these features revealed host–microbe associations that are specific to psoriasis or particular psoriasis subgroups. Our findings provide insight into the factors that may affect the development of comorbidities in patients with psoriasis and may hold diagnostic potential for early identification of patients with psoriasis at risk for these comorbidities.

JID Innovations (2022);**2:**100115 doi:10.1016/j.xjidi.2022.100115

INTRODUCTION

Psoriasis is a prevalent immune-mediated disease characterized by inflamed skin lesions and epidermal hyperproliferation. A total of 2–3% of the global population is affected by psoriasis, and the disease is known to be heterogeneous and multifactorial. It has been well established that psoriasis has different subtypes on the basis of distinct disease characteristics. Plaque psoriasis (psoriasis vulgaris) is the most prevalent psoriasis subtype, with others being guttate, inverse, erythrodermic, and pustular. Psoriasis pathogenesis is multifactorial with a strong genetic component (Elder et al., 2010). Recent studies have suggested that the microbiome, diet, and other environmental factors may also have a role in psoriasis pathogenesis (Afifi et al., 2017; Benhadou et al., 2018; Chang et al., 2018; Codoñer et al., 2018; Fahlén et al., 2012; Fyhrquist et al., 2019; Gao et al., 2008; Loesche et al., 2018; Takemoto et al., 2015; Tett et al., 2017; Yan et al., 2017). At the molecular level, aberrant activation of IL-17 signaling pathway is one of the major contributors to the disease (Brembilla et al., 2018). Therapeutically blocking components in IL-17 signaling pathway usually controls skin inflammation. However, the effectiveness of psoriasis treatments varies across patients, further highlighting the heterogeneous nature of psoriasis.

In addition to the skin manifestations, patients with psoriasis are at higher risk of developing a number of other comorbidities. Psoriatic arthritis is one of the most prevalent comorbidities among patients with psoriasis because up to one third of patients with psoriasis transition into psoriatic arthritis (Ritchlin et al., 2017). Patients with psoriasis also have a 2.5-fold higher risk of developing Crohn's disease and a 1.7-fold higher risk of developing ulcerative colitis, linking psoriasis to inflammatory bowel disease (IBD) (Fu et al., 2018). Other common psoriasis comorbidities include cardiovascular disease (Prodanovich et al., 2009) and type 2 diabetes (Wan et al., 2018). Although the association between psoriasis and its comorbidities is firmly established, the underlying cause and triggers are yet to be elucidated. Developing these comorbidities in patients with psoriasis not only increases the disease burden for the patients but also complicates strategies in treatment and diagnosis. The ability to risk stratify patients with psoriasis for the development of certain comorbidities would greatly enhance strategies toward prevention, early detection, and treatment.

Although the skin microbiome has been the focus for cutaneous autoimmune disease, dysbiosis in the gut microbiome has been observed in psoriasis (Codoñer et al., 2018; Eppinga et al., 2016; Hidalgo-Cantabrana et al., 2019; Scher

[1]*Department of Dermatology, University of California San Francisco, San Francisco, California, USA;* [2]*Ronald O. Perelman Department of Dermatology, New York University Langone Health, New York, New York, USA;* [3]*Department of Dermatology, Henry Ford Health System, Detroit, Michigan, USA;* [4]*Department of Biology, St. Bonaventure University, St. Bonaventure, New York, USA;* [5]*Department of Nutritional Sciences & Toxicology, University of California Berkeley, Berkeley, California, USA;* [6]*Department of Medicine, University of California San Francisco, San Francisco, California, USA; and* [7]*Division of Gastroenterology, Department of Medicine, University of California San Francisco, San Francisco, California, USA*

Correspondence: Wilson Liao, Department of Dermatology, University of California San Francisco, 2340 Sutter Street, San Francisco, California 94143-0808, USA. E-mail: wilson.liao@ucsf.edu

Abbreviations: IBD, inflammatory bowel disease; RNA-seq, RNA sequencing

Received 6 April 2021; revised 8 December 2021; accepted 11 December 2021; accepted manuscript published online 10 March 2022; corrected proof published online 12 May 2022

Cite this article as: JID Innovations 2022;2:100115

et al., 2015; Tan et al., 2018). Moreover, gut microbiome dysbiosis has been implicated in many psoriasis comorbidities such as psoriatic arthritis (Scher et al., 2015), IBD (Gevers et al., 2014; Knights et al., 2014; Lloyd-Price et al., 2019; Morgan et al., 2012), and type 2 diabetes (Zhou et al., 2019). Together, these findings suggest that the gut microbiome might be an important contributing factor for psoriasis pathogenesis and the emergence of psoriasis comorbidities. To better understand the systemic component of pathogenesis associated with psoriasis, we performed a detailed multiomics analysis with a cohort of patients with psoriasis and healthy individuals. We utilized shotgun metagenomic sequencing to profile both the taxonomic composition and functional capacity of the gut microbiome. In addition, we carried out RNA sequencing (RNA-seq) to profile the host intestinal transcriptome. Host peripheral blood was also collected to measure both systemic immune populations and their cytokine-producing capacity. Our study revealed several microbial features associated with psoriasis. Next, using clustering analysis, we identified three psoriasis subgroups, each with distinct microbial features that may predispose to certain psoriasis comorbidities. Finally, we performed multiomics analysis by integrating all our omics data and revealed disease and subgroup-specific host–microbe associations. Our work highlights the heterogeneity of psoriasis and the potential role of microbial and host–microbe associations in psoriasis pathogenesis and comorbidities. Moreover, this pilot study provides an analytical framework that can be applied to study host–microbe association in other diseases.

RESULTS

Study design and cohort summary

We recruited a cohort of 33 subjects with psoriasis not on systemic therapy and 15 age- and sex-matched healthy individuals (Table 1) to study the gut microbial features associated with psoriasis and their potential contribution to psoriasis pathogenesis. All patients with psoriasis were clinically diagnosed with psoriasis at the University of California San Francisco Psoriasis and Skin Treatment Center (San Francisco, CA) and had a mean PASI of 14.2, representing moderate-to-severe disease. To characterize microbial composition, we collected stool samples and subjected each sample to shotgun metagenomic sequencing that provides both taxonomic composition and functional capacity. For the subsequent analyses, we focused on bacterial species, microbial UniRef90 gene families, and microbial MetaCyc pathways. To link the changes of microbial features in psoriasis gut to the host response, we collected biopsies from the sigmoid colon and subjected these samples to RNA-seq. We also isolated PBMCs from blood samples to measure immune cell profiles and cytokine production capacity. Together, our study design (Figure 1) provided a comprehensive survey on both host biology and microbiome capacity in a cohort of patients with psoriasis in comparison with those in the healthy controls.

Microbial diversity and community structure between psoriasis and healthy gut microbiome

Gut microbiome dysbiosis has been previously associated with decreased microbial diversity. Low microbial diversity has been observed in several human diseases, including IBD, obesity, and autism (Gevers et al., 2014; Hsiao et al., 2013; Turnbaugh et al., 2009). It has been hypothesized that losing microbial diversity rise from a missing group of beneficial microbes in the gut microbiome, which can lead to many detrimental consequences such as loss of control in the growth of opportunistic pathogens and lack of production of beneficial microbial-derived compounds. Alpha diversities

Table 1. Demographic Information of Metagenomics Cohort

Characteristic	Healthy	Psoriasis	*P*-Value
Sample size	15	33	NA
Sex (% female)	47%	52%	1
Age (mean age), y	45.8 ± 13.9	43.2 ± 14.6	0.5654
Mean PASI score	NA	14.2 ± 13.3	NA
Median PASI score	NA	10.1	NA

Abbreviation: NA, not applicable.

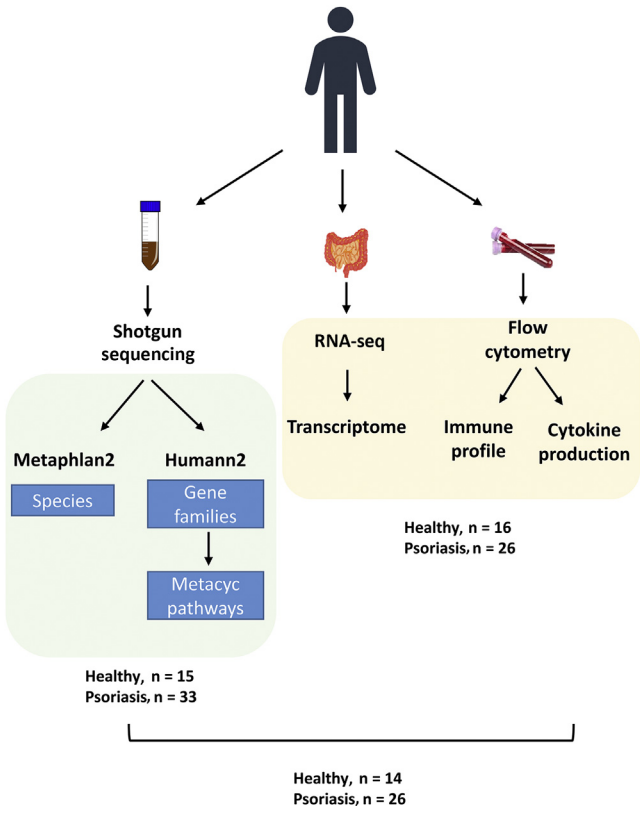

Figure 1. Multiomic study design. In this study, we collected six different datasets for multiomic analysis: shotgun metagenomic sequencing from stool samples generated profiles of (i) microbial species, (ii) microbial gene families, and (iii) microbial gene pathways. RNA-seq from sigmoid colon biopsies generated (iv) host colonic transcriptome data. Flow cytometry analyses from PBMCs generated (v) immune population profiles and (vi) cytokine production profiles. The datasets measuring microbial features are in the green box, and the datasets measuring host features are in the yellow box. Stool samples were collected from 15 healthy subjects and 33 patients with psoriasis. Sigmoid colon biopsies and PBMCs were collected from 16 healthy subjects and 26 patients with psoriasis. A total of 14 healthy subjects and 26 patients with psoriasis had six fully complete datasets. RNA-seq, RNA sequencing.

assess the microbial diversity within a community by calculating richness (numbers of species) and evenness (even distribution of each species within a community) (Lozupone and Knight, 2005). To compare the microbial diversity in patients with psoriasis with that in healthy subjects, we calculated different alpha diversity indices to estimate the overall diversity (Shannon), evenness (Simpson), and richness (chao1) of each community. We observed higher evenness of microbial functional diversities associated with patients with psoriasis, whereas similar taxonomical diversity was observed between patients with psoriasis and healthy controls (Figure 2a and Supplementary Figure S1a and b). The overall microbial community structures were similar between psoriasis samples and healthy samples because no distinct clusters were observed in principal coordinate analysis plots for taxonomic and functional profiles (Supplementary Figure S1c and d). All patients with psoriasis in our cohort had a normal-appearing lower gastrointestinal endoscopic examination, so drastic differences in diversity and community structure in the psoriasis microbiome as observed with other gastrointestinal diseases might not be expected.

Identification of the microbial features associated with the psoriasis gut microbiome

We hypothesized that even though the gut microbiome from patients with psoriasis has seemingly normal overall microbial community structure and diversity, the differences between psoriasis and healthy microbiome may be in specific microbial features. To identify the microbial features that are differentially abundant between gut microbiome from patients with psoriasis and healthy individuals, we performed differentially abundance analysis using DEseq2 (Love et al., 2014), which is designed for RNA-seq analysis but is widely adapted for microbiome data (McMurdie and Holmes, 2014). We estimated differential abundant features using a negative binomial model after controlling for known confounding factors for gut microbiome such as sex, age, and experimental batch. Our analysis revealed bacterial species and microbial gene families and pathways that are differentially abundant between microbiome in patients with psoriasis and healthy individuals (Figure 2b and Supplementary Tables S1−3). Among bacterial species that are differentially abundant between psoriasis and healthy gut microbiome, we found an increase of *Bacteroides vulgatus* and *Parasutterella excrementihominis* and a decrease of *Phascolarctobacterium succinatutens* (Figure 2c).

Microbial gene family analysis reveals three psoriasis subgroups with distinct microbial and host features

We then performed a hierarchical clustering analysis on the microbial gene families differentially abundant between patients with psoriasis and healthy controls and identified three distinct groups in our cohort (Figure 3a). To confirm that these subgroups were not observed by chance, we performed bootstrapped gap statistics on both the Euclidean distance and Bray–Curtis distance, which confirmed the presence of the three distinct groups in the cohort (Supplementary Figure S2a and b). Among the three groups identified by clustering, group 1 consists of a mixture of healthy and psoriasis samples (14 healthy samples and 15 psoriasis samples), group 2 consists of all patients with psoriasis (nine psoriasis samples), and group 3 consists of almost all patients with psoriasis (one healthy sample and nine psoriasis samples) (Figure 3b). For the subsequent investigations of these psoriasis subgroups, we termed the subjects with psoriasis from these subgroups PSO1, PSO2, and PSO3. The clustering was not confounded by body mass index, age, and sex or diet (Supplementary Figure S3a–c and g and Supplementary Table S4). All psoriasis subgroups had similar disease severity, disease duration, and age of disease onset (Supplementary Figure S3d–f). However, we found that each psoriasis subgroup had a number of distinct microbial and host features (Figure 3c). Some of the interesting features associated with each psoriasis subgroup are highlighted below.

Both PSO2 and PSO3 are dominated by subjects with psoriasis, suggesting that these are two distinct psoriasis-specific subgroups. We identified several common microbial features shared by these psoriasis subgroups as well as some microbial features that are distinct to each subgroup (Figure 3c and Supplementary Tables S5–7). Although psoriasis samples have a lower abundance in *P. succinatutens* than healthy controls (Figure 2c), the reduced abundance of *P. succinatutens* is specific to PSO2 and PSO3 but not to PSO1 (Figure 3c). In addition, samples in PSO2 and PSO3 are less abundant with *Turicibacter sanguinis* and unclassified *Turicibacter* species (Figure 3c). Samples in PSO2 are more abundant with *Bacteroides xylanisolvens* and less abundant with *Prevotella copri, Streptococcus thermophilus,* and *Coprococcus sp ART55 1* (Figure 3c). On the contrary, samples in PSO3 have a lower abundance in *Ruminococcaceae bacterium D16* and *Lachnospiraceae bacterium 1 1 57FAA* (Figure 3c). In addition to distinct taxonomic features, PSO2 has a distinct profile in microbial functions, especially in microbial pathways. Both abundant and depleted pathways were found in PSO2 relative to those in other psoriasis subgroups, suggesting a shift of microbial functions in PSO2 (Figure 3c). Microbial communities in PSO2 have lower abundance in the arginine and polyamine biosynthesis superfamily, suggesting a lower capacity for polyamine production (Figure 3c). In contrast to PSO2, we did not identify microbial pathways that are uniquely associated with PSO1 and PSO3.

From the perspective of host response, PSO2 and PSO3 patients have distinct intestinal transcriptomic signatures (Figure 3c and Supplementary Table S8). Gut biopsies from PSO2 patients have increased expression in *ATP13A5* and *PDE9A* and reduced expression in sulfotransferases, *SULT1C2* and *SULT1C3*. In contrast, most of the transcriptomic signatures associated with PSO3 have increased expression compared with those associated with other psoriasis samples (Figure 3c). To gain more insight into the host intestinal immune response, we deconvoluted the immune cell composition in sigmoid colon bulk RNA-seq using the digital cytometry framework CIBERSORTx (Newman et al., 2019). As part of the CIBERSORTx framework, we first defined gene signatures of various immune cell populations in the sigmoid colon using single-cell RNA-seq generated from healthy sigmoid colon (James et al., 2020). We then used CIBERSORTx to apply the gene signature matrix to the bulk RNA-seq to infer the composition of cell populations.

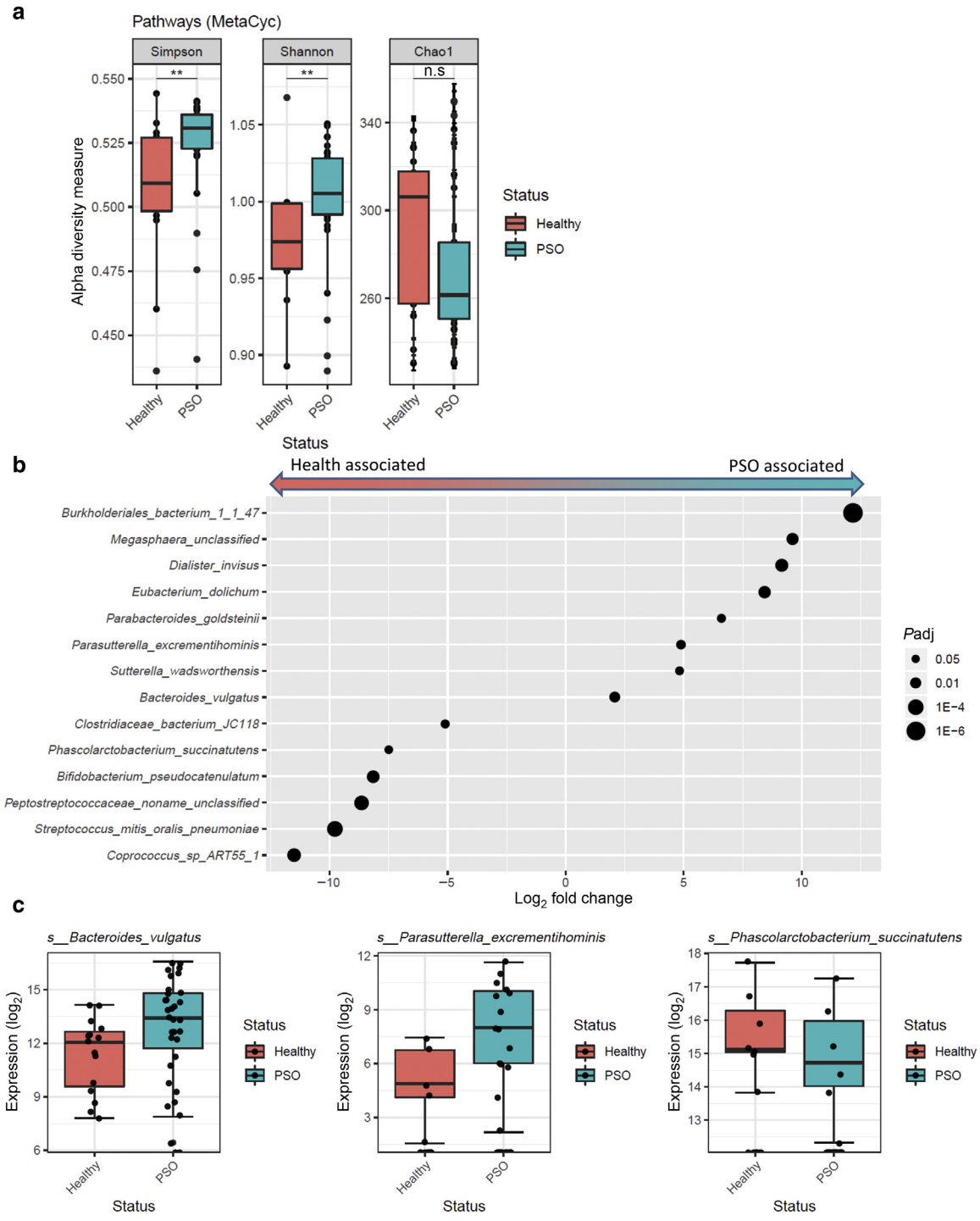

Figure 2. Microbial features associated with PSO and healthy subjects. Boxplots compare alpha diversities of gut microbiome in patients with PSO and those in the healthy subjects. Alpha diversity was measured by Shannon index, Simpson diversity index, and chao1 estimation for (**a**) microbial Uniref90 gene families. Statistical significance was determined by Wilcoxon test. (**b**) Dot plot summary of DA microbial species identified by DEseq2. Each dot represents a DA microbial species with dot size–present adjusted *P*-value, and x-axis represents $\log_2$ fold change. (**c**) Boxplots of select DA microbial species. Blue boxes represent PSO sample, and red boxes represent healthy samples. $^{**}P < 0.01$. adj, adjusted; DA, differential abundant; n.s., not significant; PSO, psoriasis.

Sigmoid colon from patients in PSO3 has more abundant CD8+ T cells and less abundant NK cells and activated CD4+ T cells than that from other psoriasis subgroups (Figure 4a and Supplementary Table S9).

In addition to colonic transcriptomic signatures, flow cytometry analysis revealed distinct immune features in circulatory blood between the two psoriasis-dominant groups. Patients in PSO3 have higher activated memory CD4+ effector T cells than those in PSO2, whereas the frequency of memory CD4+ effector T cells and total CD4+ effector T cells are comparable between these two psoriasis subgroups (Figure 4b). Similarly, memory CD8+ T cells have

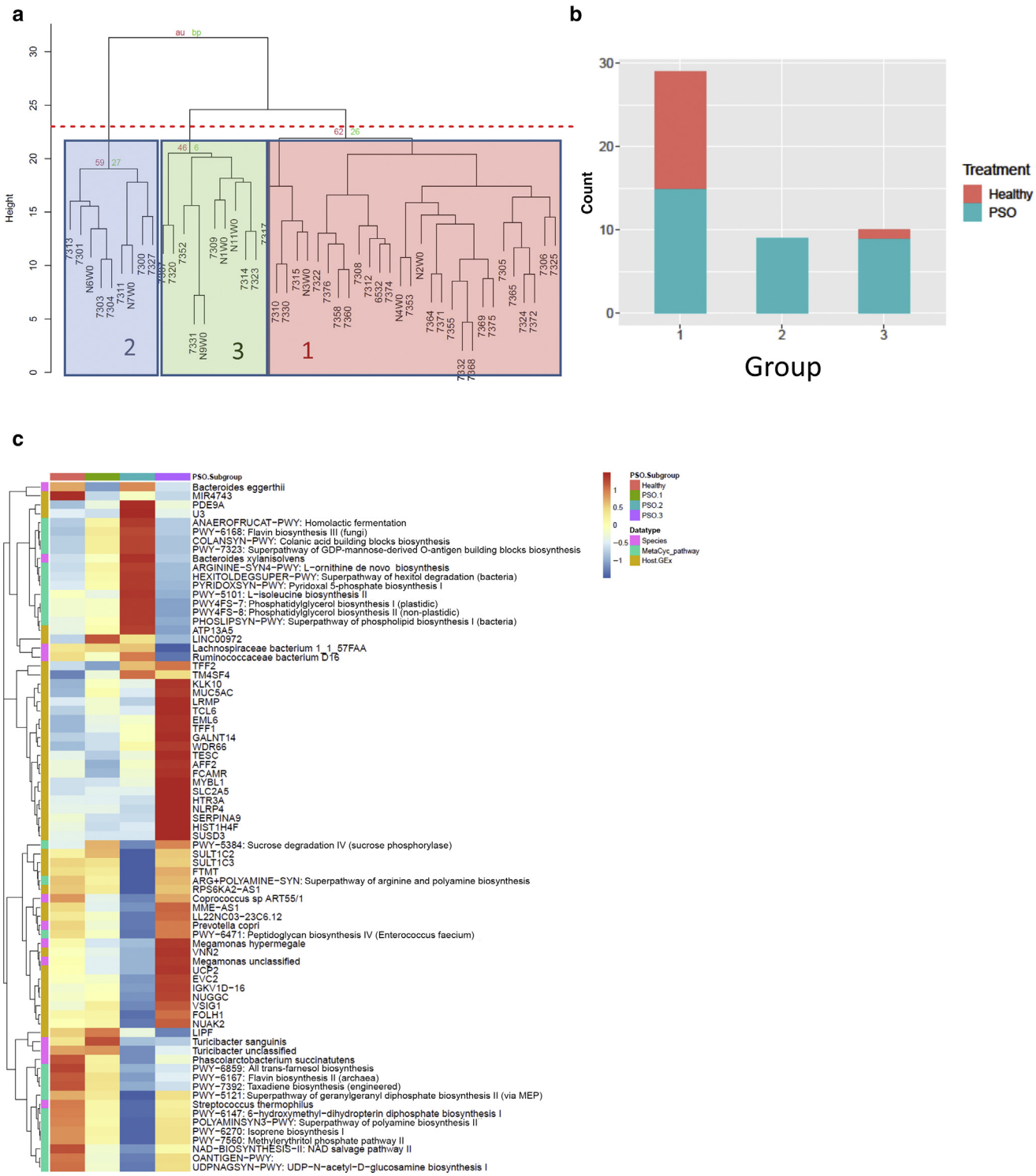

Figure 3. PSO subgroups identified by a differential abundance of microbial gene families. (**a**) The hierarchical cluster dendrogram shows the membership of all samples in this cohort. The colored boxes represent the grouping of each sample into three distinct groups. The red box depicts group 1, the blue box depicts group 2, and the green box depicts group 3. The red dotted line represents where the tree is cut to derive the three subgroups. The AU bootstrap confidence scores and BP values are represented in red and green, respectively, at the major branches. (**b**) The stacked bar plot represents the distribution of disease status of the three groups identified by cluster analysis. The height of each bar represents the size of each group, and the color represents the disease status, with red for healthy subjects and blue for PSO samples. (**c**) Heatmap of microbial and host features associated with each PSO subgroup. Columns represent PSO subgroups, and rows represents microbial features identified from shotgun metagenomics or host features from colonic RNA-seq. Differential abundance microbial features with nonzero counts for at least 10 samples were plotted on the heatmap to exclude features with high dropout rates. The color of each cell represents the average abundance and is scaled by means of the features. The data type of each feature is indicated in the side bar: pink represents microbial species, blue represents microbial pathway, and yellow represents host GEx. AU, arbitrary unit; BP, bootstrap probability; GEx, gene expression; PSO, psoriasis; RNA-seq, RNA sequencing.

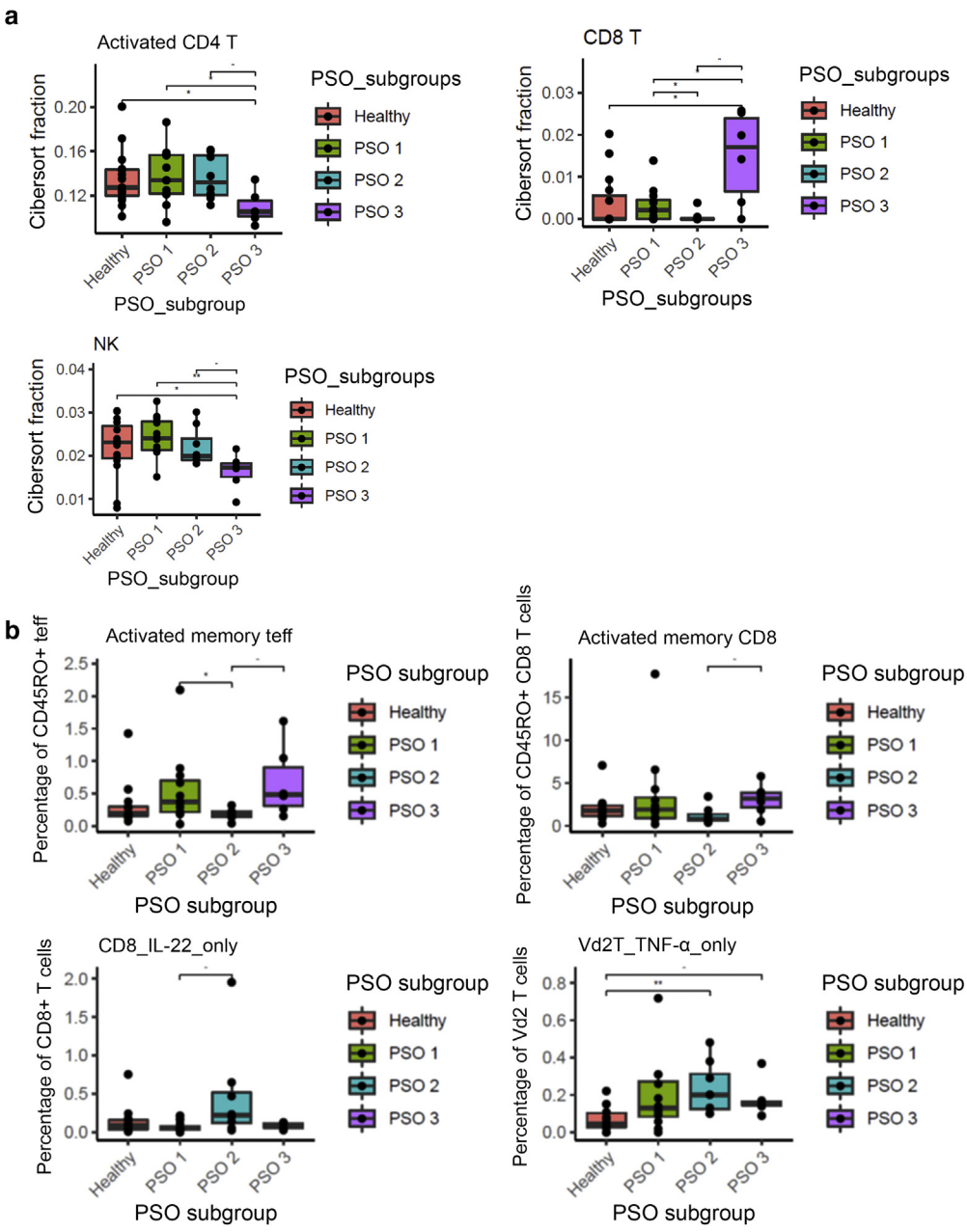

Figure 4. PSO subgroup–specific microbial and host features.
(**a**) Boxplots show differences in sigmoid colon immune cell compositions deconvoluted by CIBERSORTx between different PSO subgroups. (**b**) Boxplots showing circulating host immune responses measured by flow cytometry. The statistical significance in boxplots was determined by Wilcox test on pairwise comparison of each group of interest. *P*-values were depicted by symbols: ****$P < 0.0001$, ***$P < 0.001$, **$P < 0.01$, and *$P < 0.05$. Comparisons with $P > 0.05$ are not shown. PSO, psoriasis; Teff, effector T cell.

a more activated population in PSO3 patients (Figure 4b). Despite lower T-cell activation, patients in PSO2 have a higher capacity to produce IL-22 by circulating CD8+ T cells and TNF-α by circulating γδ T cells (Figure 4b) than healthy controls or those in PSO1. Together, our data reveal differential underlying circulatory immune responses associated with PSO2 and PSO3. PSO2 patients have a higher capacity for proinflammatory cytokine production, whereas PSO3 patients have higher baseline T-cell activation.

Distinct correlations between psoriasis severity with microbial features in each psoriasis subgroups

To further understand the relationship between the psoriasis subgroups and psoriasis heterogeneity, we tested whether microbial features in these psoriasis subgroups are significantly correlated with psoriasis parameters. In PSO1 patients, disease severity is positively correlated with the microbial pathways involved in purine degradation (Figure 5). Disease severity in PSO2 patients is positively correlated with several microbial pathways, including pentose phosphate biosynthesis and L-arginine biosynthesis (Figure 5). The microbial L-rhamnose degradation pathway is positively correlated with disease duration in PSO2 (Figure 5). The microbial L-isoleucine biosynthesis pathway is correlated with disease duration positively in PSO1 patients and negatively in PSO2 patients (Figure 5). No significant correlations between microbial features and disease information were observed in PSO3.

Multiomic analysis in patients with psoriasis and subgroups reveals distinct host–microbe associations

To gain a comprehensive view of the crosstalk between the gut microbiome and host biology, we constructed multiomic

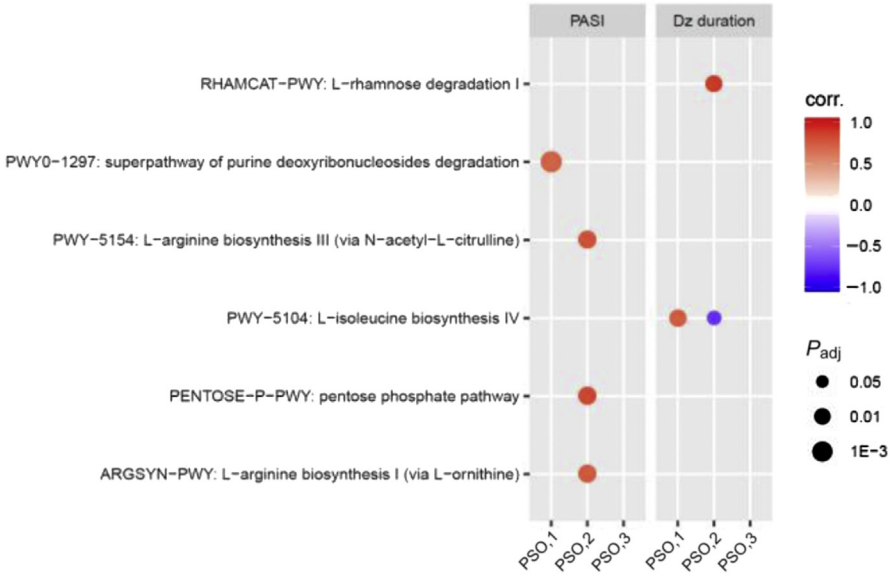

Figure 5. Correlations between microbial features and psoriasis-related clinical features. Dot plot summarizes the correlation between microbial features and disease parameters of PASI scores and disease duration. Each dot represents a significant correlation between a disease parameter and a microbial feature. The direction and strength of the correlation are presented by dot color (red represents positive correlation, and blue represents negative correlation). The dot size represents false discovery rate–adjusted *P*-values. adj, adjusted; corr., correlation value; Dz, disease.

correlation networks by integrating microbial and host features across different measurements (Supplementary Table S10). A subset of 40 subjects from our cohort with complete measurements from shotgun metagenomic sequencing, gut RNA-seq, and circulating immune profiling were included in the multiomic analysis. This multiomic cohort consists of 26 subjects with psoriasis and 14 age- and sex-matched healthy subjects (Table 2). Multiomic networks were constructed within each disease status and within each psoriasis subgroup to reveal disease-specific and subgroup-specific host–microbe relationships. The resulting multiomic networks consist of nodes that represent host or microbial features and edges that represent significant correlations between nodes. The network in patients with psoriasis is denser and consists of more edges than the multiomic network in healthy subjects (Figure 6a). The final multiomic network consists of 73 significant correlations within healthy subjects and 97 significant correlations within patients with psoriasis (Table 3). Intriguingly, the multiomic network in each psoriasis subgroup displayed a distinct network structure. Multiomic networks in PSO1 and PSO2 were more interconnected than the network in PSO3 (Figure 6a). It is interesting that PSO3 had fewer edges and nodes than other psoriasis subgroups and all psoriasis samples combined (Table 3). Overall, our data revealed distinct multiomic network structures in patients with psoriasis and healthy controls as well as among different psoriasis subgroups.

Table 2. Demographic Information of Subjects with Full Set of Multiomics Data

Characteristic	Healthy	Psoriasis	*P*-Value
Sample size	14	26	NA
Sex (% female)	43%	58%	0.5096
Age (mean age), y	44.8 ±13.8	44.7 ±15.5	0.9789
Mean PASI score	NA	11 ±8.9	NA
Median PASI score	NA	7.7	NA

Abbreviation: NA, not applicable.

The different multiomic networks might reflect the different host–microbe associations in subjects with psoriasis and healthy subjects. One of the modules in psoriasis-associated multiomic network positively links microbial pathways involved in microbial ppGpp biosynthesis and pyrimidine ribonucleosides salvage pathways with circulating IL-17 production in both CD4+ effector T cells and regulatory T cells (Figure 6b). The associations between these microbial pathways and IL-17 production were only observed in psoriasis samples despite that these microbial pathways are also being abundant in healthy samples (Supplementary Figure S4a).

Besides psoriasis-specific host–microbe associations, our analysis also identified host–microbe associations that are specific in psoriasis subgroups. A multiomic network identified in PSO1 consists of a module that links microbial gene families with activated nonmemory CD4+ T cells and IL-17 production capacity in CD4+ effector T cells (Figure 6c), suggesting potential microbial controls in T-cell activation and effector function in this psoriasis subgroup. Indeed, 95 of 124 host–microbe associations in PSO1 link the features of host circulating immunity to microbial features, which is higher than the networks in PSO2 and PSO3 patients (Table 3). In addition, we also identified some subgroup-specific associations in psoriasis-dominant PSO2 and PSO3. In PSO2, the expression of proinflammatory chemokine *CXCL8* is positively correlated with microbial putrescine biosynthesis pathway in PSO2 patients (Figure 6d). We identified a module in PSO3 network that negatively correlates microbial tetrapyrrole biosynthesis pathway with several genes in B-cell biology, including *CD79B*, *PAX5*, *TCL1A*, and *MYBL1* (Figure 6e). Tetrapyrroles are metal-binding compounds that serve as different cofactors, such as heme, cobalamin (vitamin B12), and coenzyme F430, and have crucial roles in regulating diverse cell functions.

DISCUSSION

The pathogenesis of psoriasis is highly heterogeneous, which poses challenges in diagnosis and disease control.

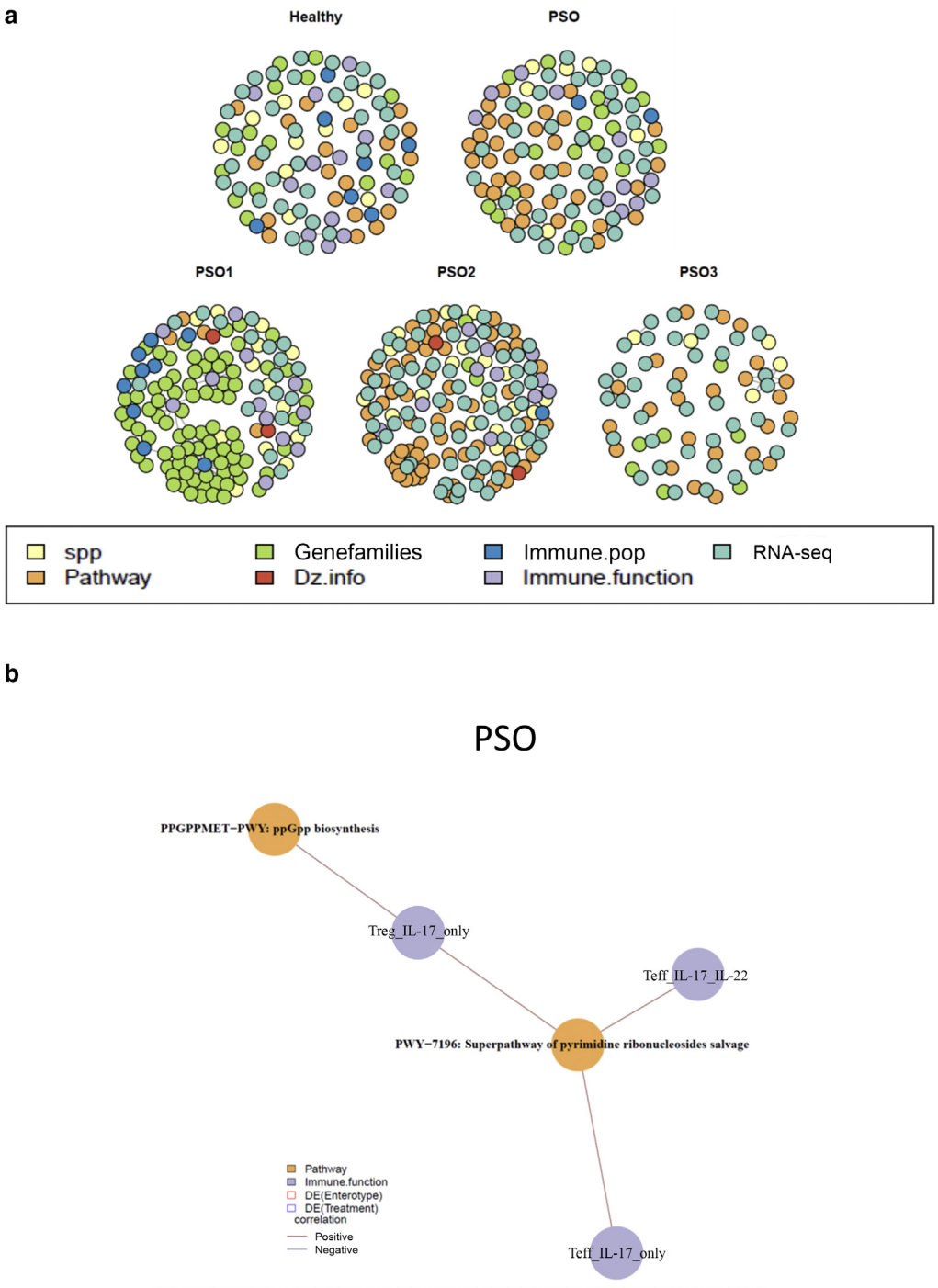

Figure 6. Multiomic networks associated with PSO and PSO-specific subgroups. (**a**) Overview of multiomic networks within healthy subjects, patients with PSO, and each PSO subgroup. Each node represents a microbial or host feature, and each edge represents a significant association between the two nodes. The color of nodes represents the measurement type of the node. Host–microbe modules are identified using greedy optimization of modularity. (**b**) PSO-specific modules associate microbial features with circulating IL-17 production. (**c–e**) PSO subgroup–specific modules are also identified in each PSO-specific subgroup. For each module, the color of nodes represents the measurement type of the node, and the color of edges indicates the direction of the correlation (red edges represent positive associations, and blue edges represent negative associations). DE, differentially expressed; PSO, psoriasis; RNA-seq, RNA sequencing.

Accumulating evidence from recent studies suggests that the heterogeneity of psoriasis pathogenesis may be the result of the interplay between microbiome and host immune response. Our study focused on studying the heterogeneity of psoriasis pathogenesis through the lens of multiomic datasets assessing both host and microbial features. In this study, we show that psoriasis gut microbiome has increased *B. vulgatus* and *P. excrementihominis* and reduced *P. succinatutens* compared with the ones in healthy controls. These microbial features have also been associated with intestinal inflammation. Increased intestinal colonization of *B. vulgatus* and elevated *B. vulgatus* reactive serum antibodies have been reported in patients with ulcerative colitis (Matsuda et al., 2000). It is intriguing that the gut microbiome of patients with psoriasis in our cohort shares some microbial features associated with IBD or irritable bowel syndrome despite no intestinal symptoms reported in our patients.

Enterotypes defined by different microbiome compositions have been previously described in healthy subjects (Arumugam et al., 2011). Our study revealed three psoriasis subgroups in our cohort as defined by the differential abundance of microbial gene families. Each psoriasis subgroup has distinct microbial and host features (Table 4). The reduced *Turicibacter* species in PSO2 and PSO3 are

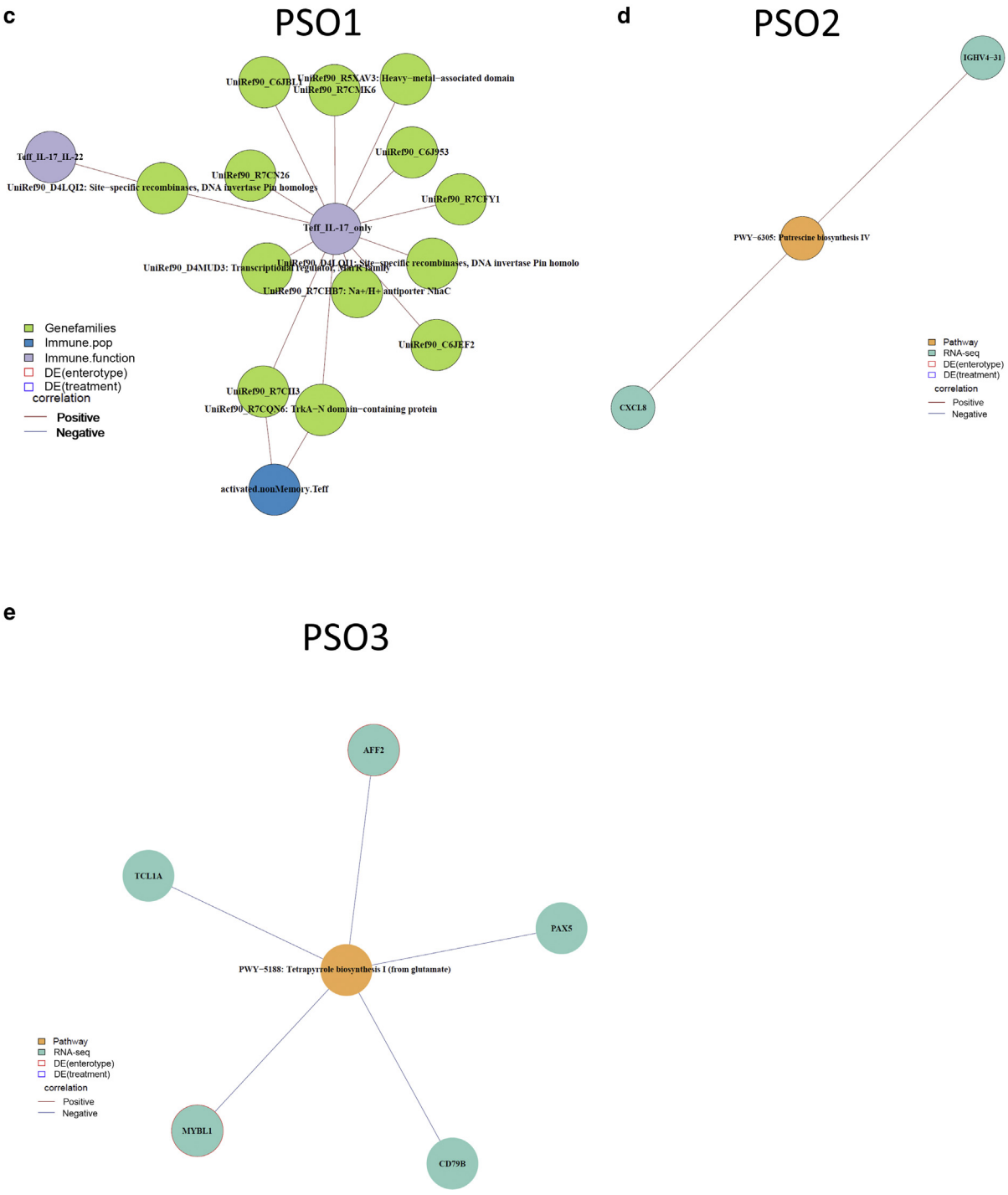

Figure 6. *Continued.*

reminiscent of the gut microbiome associated with pediatric Crohn's disease (El Mouzan et al., 2018; Wang et al., 2016). PSO2 has the most distinct microbial functional profile (Figure 3c) from that of other psoriasis subgroups. The gut microbiome in PSO2 shows a higher biosynthetic capacity of several important immune regulators, including pyridoxal 5-phosphate (vitamin B6), L-ornithine, and flavin. We also found lower capacity in arginine and polyamine biosynthesis in PSO2. Some of these molecules have been linked to immune-mediated intestinal inflammation. For example, vitamin B6 plays a crucial role in lymphocyte trafficking into the intestines (Yoshii et al., 2019). Vitamin B6 deficiency has been linked to several immune-mediated diseases, including rheumatoid arthritis and IBD (Selhub et al., 2013; Yoshii et al., 2019). Having increased capacity of vitamin B6 biosynthesis may have a protective role for subjects in PSO2 from autoimmune diseases. On the contrary, polyamines play a crucial role in intestinal mucosa maintenance and resident immune cell development (Yoshii et al., 2019). Interestingly, it has been shown that spermine, a class of polyamine,

Table 3. Summary of Multiomic Networks

Characteristic	Healthy	Psoriasis	PSO1	PSO2	PSO3
Number of subjects	14	26	12	8	6
Number of edges	73	97	124	126	53
Number of features	99	110	143	160	74
Total number of modules	30	35	28	55	26
Number of modules with at least three features	16	15	15	21	10
Number of edges with host immune features	22	13	95	12	0
Number of edges with host transcriptome	51	84	27	109	53

reduces the secretion of proinflammatory IL-18 cytokine by inhibiting NLRP6 inflammasome activation (Levy et al., 2015). Our data suggest that gut microbial communities in PSO2 have increased vitamin B6 biosynthesis and reduced polyamine production, but the clinical implication requires further study.

Although both PSO2 and PSO3 are psoriasis-enriched subgroups, we have observed some differences in host circulatory and intestinal immune profiles between the two subgroups. PSO2 has increased memory CD8+ T-cell population in peripheral blood and higher IL-22 production capacity from CD8+ T cells (Figure 4 and Supplementary Table S9). Although PSO3 has no obvious immune signatures in peripheral blood, PSO3 has higher CD8+ T cells and lower active CD4+ T cells in sigmoidal gut as identified by in silico immunoprofiling. Conventionally, CD8+ T cells are known for their cytotoxic activities and are important for clearing infected cells or cancerous cells. Recent studies have been focusing on cytokine-producing CD8+ T cells because they were found in psoriatic skin to be an important source of proinflammatory IL-17 and IL-22 (Hijnen et al., 2013; Liu et al., 2021). Interestingly, expanded proinflammatory cytokine-producing CD8+ T cells have been found in PBMCs of patients with psoriatic arthritis (Diani et al., 2019). Our findings confirm the presence of cytokine-producing CD8+ T cells in patients with psoriasis and implicate differential roles of CD8+ T cells in different psoriasis subgroups.

Many of the host transcriptomic signatures found in PSO3 are similar to the ones reported in patients with IBD or IBD animal models, including elevated expression of folate hydrolase (*FOLH1*) (Noble et al., 2010; Rais et al., 2016), one of the serotonin receptors (*HTR3A*) (Shajib et al., 2019), and mitochondrial *UCP2* (Jin et al., 2017; Yu et al., 2009). Elevated *FOLH1* expression has been reported in intestinal biopsies of patients with IBD, and inhibiting *FOLH1* activity ameliorates IBD-associated abnormalities in mouse models (Noble et al., 2010; Rais et al., 2016). *UCP2* encodes for mitochondrial UCP2 and has been implicated in several autoimmune diseases (Yu et al., 2009). Expression of *UCP2* is elevated in a dextran sodium sulfate–induced mouse model of IBD, and the severity of IBD can be ameliorated by knocking down *UCP2* expression through an expression by small interfering RNA (Jin et al., 2017). In addition to the IBD-related signatures, patients in PSO3 also have a reduced abundance of *Ruminococcaceae* and *Lachnospiraceae*, which is also observed in the gut microbiome of psoriatic arthritis (Scher et al., 2015). It is worth noting that all patients in PSO3 reported having joint pain or swelling, whereas only a fraction of patients in PSO1 or PSO2 did (Supplementary Figure S3h). Both IBD and psoriatic arthritis are common psoriatic comorbidities, and our study suggests an intriguing possibility that these psoriasis subgroups might represent psoriasis populations with differential risk for developing comorbidities such as IBD and psoriatic arthritis.

Our multiomic analysis revealed interesting associations between microbial pathways with circulating IL-17A production and expression of proinflammatory chemokines, CXCL1 and CXCL3, in the colon (Figure 6b). These host–microbe associations are only observed in patients with psoriasis but not in healthy subjects (Supplementary Figure S4a and b), suggesting that psoriasis-specific host–microbe associations might be crucial drivers of the proinflammatory changes in patients with psoriasis. In addition to

Table 4. Summary of Host and Microbial Features of Psoriasis Subgroups

Characteristic	PSO2 and PSO3 Common Features	PSO2-Specific Features	PSO3-Specific Features
Metagenomics (stool)	*Turicibacter spp.* ↓ *Phascolarctobacterium succinatutens* ↓	*Bacteroides xylanisolvans* ↑ *Prevetella copri* ↓ *Streptococcus thermophilus* ↓ *Coprococcus* sp ART55 1 arginine and polyamine biosynthesis ↓ pyridoxal 5-phosphate biosynthesis ↑	*Megamonas spp.* ↑ *Ruminococcaceae bacterium D16* ↓ *Lachnospiraceae bacterium 1 1 57FAA* ↓
Transcriptomics (sigmoid colon)	NA	SULT1C2 and SULT1C3 ↓ FOHL1 ↓ PDE9A ↑	FOHL1 ↑ UCP2 ↑ HTR3A ↑
Gut immune cell population (sigmoid colon digital cytometry)	NA	NA	CD8 T cells ↑ Activated CD4 T cells ↓ NK cells ↓
Immune population (PBMC flow cytometry)	NA	Reduced activated memory CD4 and CD8	NA
Cytokine production (PBMC flow cytometry)	NA	Higher IL-22 production in CD8 and higher TNF-α production in γδ T cells	NA

Abbreviation: NA, not applicable.

psoriasis-specific host–microbe associations, our analysis also revealed specific host–microbe associations in each psoriasis subgroup in our cohort. Together, our data suggest that the host–microbe interaction can be context dependent, whereby the same microbial species or function may have a different effect on the basis of the disease state or disease subgroup.

We are aware of several limitations of our study that could be improved by future work. Although multidimensional, our analysis is limited by a modest cohort size, so it would be important to validate our findings in a larger independent psoriasis cohort. In addition to validation, a larger cohort will allow for the application of machine learning approaches to better characterize psoriasis subgroups. Owing to the scope of the study, we focused our efforts on cross-sectional observations of our cohort. Host–microbe interaction can be relatively dynamic over time, and some of the features or associations identified may be relatively transient. Collecting longitudinal data may assist in the identification of stable associations compared with transient associations. In addition, a longitudinal dataset would allow for better tracking of host–microbe associations associated with the development of comorbidities. In this study, we have identified several microbial species that are differentially abundant in psoriasis gut compared with those in healthy controls. However, their roles in psoriasis and inflammation are not previously well understood. Testing the microbial species identified in this study for their roles in eliciting local and system inflammation can shed some insights into their roles in modulating psoriasis. Even with these limitations, the findings of this study provide valuable insights into the complexity of psoriasis biology that can help us to better identify patients with psoriasis with a higher risk of comorbidities and unique biological pathways. To date, most of the disease-related microbiome studies are still focusing on signatures identification aimed to identify specific microbes or microbial functions that contribute to the pathogenesis of the disease. Our results suggest that pathogenesis of psoriasis and its comorbidities is highly individualized and that both host and microbiome should be considered when assessing disease risks and strategizing disease management in both clinical and scientific settings. The findings of this study are relevant because they may have diagnostic potential for psoriasis comorbidities and may provide insights in developing personalized disease management strategies for patients with psoriasis.

MATERIALS AND METHODS

Cohort recruitment and sample collection

Adult patients with psoriasis and healthy volunteers recruited from the San Francisco Bay area were enrolled in the study after providing written informed consent. All procedures performed on human subjects were reviewed and approved by Institutional Review Board at the University of California San Francisco (Institutional Review Board protocols 10-02830 and 10-01218). Individuals with abnormal coagulation parameters, positive HIV screening test, and history of bleeding disorders, abdominal surgery, gastrointestinal cancer, IBD, AIDS, immunodeficiency or immunosuppressive medications, or concurrent inflammatory skin condition were excluded. All patients with psoriasis had a diagnosis of psoriasis from a physician for at least 6 months before study enrollment, which was verified by study staff. To assess the psoriatic microbiome in an untreated state, subjects were excluded if they had received systemic biologic therapy in the last 6 months, nonbiologic systemic medications (methotrexate, cyclosporine, corticosteroids, cyclophosphamide, retinoids, and photochemotherapy) or antibiotics in the last month, or phototherapy or topical therapy in the last 2 weeks before the clinical visit. Healthy volunteers had no personal or family history of psoriasis. Gut biopsies, stool samples, and blood samples were collected on the same day. Gut biopsies were taken from the sigmoid colon of each subject. All patients with psoriasis in our cohort had a normal-appearing lower gastrointestinal endoscopic examination. Two biopsies were preserved in RNAlater solution (Ambion, Austin, TX) and kept at 4 °C overnight before storage at –80 °C. Stool samples were collected before gut biopsies and stored at –80 °C. Blood samples were taken on the same day as and preceded the gut biopsies. PBMCs were isolated from whole blood and stored in liquid nitrogen. We collected a total of 48 stool samples (15 from healthy subjects and 33 from patients with psoriasis) for shotgun metagenomics, and a total of 42 gut biopsies and blood samples (16 from healthy subjects and 26 from patients with psoriasis) were collected for host transcriptomics and immune profiling.

Diet habit analysis

We assessed dietary habits of healthy controls and patients with psoriasis by an in-person distribution of the 2009–2010 National Health and Nutrition Examination Survey dietary screener questionnaire. The questionnaire consists of 25 questions about nutrient intake frequencies of different food groups. The differences in intake frequencies of each food group were compared between disease status and psoriasis subgroups with Fisher's exact test, and results with $P < 0.05$ were considered significant. To further assess the quality of dietary habits, we summarized diet survey by calculating a Mediterranean diet score that would quantify the overall quality of diet. The traditional Mediterranean diet has been shown to reduce the risk of developing heart disease, metabolic syndrome, diabetes, and depression. The foundation for the Mediterranean diet consists of an abundance of fresh fruits, vegetables, whole grains, legumes, and omega-3 fatty acids and limited food such as milk, cheese, red meats, and sweets with added sugars. We adopted Mediterranean score calculation from a previous study (Panagiotakos et al., 2006). Briefly, we used six components of the Mediterranean diet (nonrefined cereals, fruit, vegetables, potatoes, whole grains, and legumes). For the consumption of food groups that aligned with the Mediterranean diet, we assigned scores 0, 1, 2, 3, 4, and 5 when a participant reported no consumption, rare (one time per month), frequent (2–3 times per /month), very frequent (one time per week), weekly (2–6 times per week), and daily (1–2 times per day), respectively. For non-Mediterranean diet food components, we assigned scores on a reverse scale with scores 0, 1, 2, 3, 4, and 5 when a participant reported daily (1–2 times per day), weekly (2–6 times per week), very frequent (one time per week), rare (one time per month), and no consumption, respectively. All scores were then combined to produce a total score that ranged from 0 to 50, where the higher the score, the better the diet. To test for statistical significance between both participant groups, we utilized the Wilcox test to compare the means and *P*-values of our data.

Shotgun metagenomics

DNA was extracted from fecal samples with the modified cetyl trimethylammonium bromide method. The quality of the extracted

DNA was assessed by gel electrophoresis and Quant-iT PicoGreen dsDNA Assay (Life Technologies, Carlsbad, CA). The extracted DNA was submitted to Vincent J. Coates Genomic Sequencing Laboratory at the California Institute of Technology for Quantitative Biosciences (San Francisco, CA) (www.qb3.berkeley.edu/gsl) for metagenomic library construction and sequencing. The metagenomic libraries were constructed using PrepX DNA library kit (Takara Bio, Kusatsu, Japan) and sequenced on HiSeq4000 (Illumina, San Diego, CA) for pair-end 150 base pair sequencing. An average of 22 million pair-end total reads were generated per sample. Reads were first mapped to human genome (GRCh38, GENCODE release 25) by bowtie2 (version 2.2.8) to identify human DNA. The nonhuman reads were extracted and sorted by using samtool (version 0.1.19). This data processing workflow results in an average of 16 million nonhuman reads per sample. The resulting nonhuman reads were used for the subsequent taxonomic and functional profiling.

Taxonomic profiles were generated using MetaPhlAn2 (version 2.6.0), which uses a library of ~1 million unique clade-specific marker genes for taxonomic profiling (Franzosa et al., 2018). The abundance table of bacterial species was extracted for the subsequent analysis. Functional profiles were generated by HUMAnN2 (version 0.11.1), which is an assemble-free method to infer the functional capacities for each microbiome (Franzosa et al., 2018). For each sample, HUMAnN2 maps read the pangenomes of species identified in the sample and performed additional translated searches on unclassified reads. The resulting dataset is the abundance table of microbial gene families (UniRef90), which is summarized into the higher-level MetaCyc gene pathways. Our analysis identified a total of 339 bacterial species, 409 MetaCyc pathways, and 650,048 UniRef90 gene families in our dataset.

Subsequent metagenomic analyses were performed using the R package phyloseq (McMurdie and Holmes, 2013). The abundance of microbial species, UniRef90 gene families, and MetaCyc pathway was normalized to relative abundance to account for different library sizes and input as phyloseq objects and used for calculating microbial community diversities. Owing to the high dimensionality and high dropout rate of the microbial gene families table, we focus our analysis on the microbial gene families with at least three counts for at least 80% of the total samples, which results in 3,356 UniRef90 gene families. Alpha diversity was calculated as four indices: observed (number of observed microbial features), chao1, Shannon, and Simpson index, which summarize both richness and evenness of the community. The alpha diversities were compared by disease status and psoriasis subgroups with two-sided Wilcox test. Dissimilarities between each microbiome isolated are represented by Bray–Curtis dissimilarity matrix and visualized on a principal coordinate analysis plot.

Unfiltered counts per million tables were used for differential abundance analysis. Differential abundant microbial features between psoriasis samples and healthy samples were identified using DESeq2 (version 1.18.1) (Love et al., 2014) with the design ~sex+age.bin+batch+Status. Microbial features with adjusted $P < 0.05$ and absolute $\log_2$ fold change > 0.6 are considered statistically significant. Differential abundant microbial features associated with each subgroup identified in this cohort were identified by pairwise comparison of each subgroup using DESeq2 (version 1.18.1) (Love et al., 2014). Microbial features with adjusted $P < 0.1$ and absolute $\log_2$ fold change > 0.6 are considered statistically significant. Differential abundance microbial features with none zero counts for at least 10 samples were plotted on the heatmap to exclude features with high dropout rates.

Clustering analysis to identify subgroups in the cohort

The subgroups in this cohort were identified by complete linkage hierarchical clustering on the differentially abundant microbial UniRef90 gene families identified as described earlier. The clustering was done using the R package pheatmap (version 1.0.12), which implements hclust for hierarchical clustering, or the gapstat_ord function in phyloseq (version 1.22.3). Gap statistics on differentially abundant UniRef90 gene families estimated three clusters present in our dataset. Gap statistics were done using the clusGap function from the cluster package (version 2.0.7-1) with bootstrapping 1,000 times (B = 1,000). The optimal number of clusters was determined as the smallest k that is within one standard error from the local maximal as suggested in Tibshirani et. al. (2001). The hierarchical dendrogram was cut by cutree function for three clusters (k = 3) in stats package (version 3.4.2) to assign membership of clusters for each sample.

Host RNA-seq

RNA was extracted from sigmoidal colon biopsies by RNeasy Plus Universal Kits (Qiagen, Hilden, Germany). Total RNA integrity was assessed using Agilent 2100 Nano and Pico RNA kit, and all samples have RNA integrity number score >7. cDNA libraries construction and sequencing were done by Beijing Genomics Institute (Shenzhen, China). In brief, ribosomal RNA was removed from the total RNA by Ribo-Zero Gold Kit (Illumina), and library was constructed by TruSeq Stranded Total RNA Library Prep kit (Illumina). cDNA libraries were sequenced on HiSeq4000 (Illumina) for paired-end 100 base pair sequencing. The average sequencing depth is 66 million per sample. Sequencing reads were mapped to the human genome (GRCh38, GENCODE release 25) using STAR (version 2.4.2a). The number of counts mapped to each transcript is summarized by HTSeq-count (version 0.6.0) and used as input for differential analysis in DESeq2 (version 1.18.1) (Love et al., 2014). Raw read counts were normalized by median of ratios method using DESeq2. Differentially expressed genes between psoriasis samples and healthy samples were determined by DESeq2 with the model design ~sex+age+batch+status. Genes with adjusted $P < 0.05$ and absolute $\log_2$ fold change > 0.6 are considered significantly different between psoriasis samples and healthy samples. A similar analysis was performed to identify differentially expressed genes between different subgroups (genecluster.group) in this cohort with the DESeq2 model design ~sex+age+batch+genecluster.group. Results of pairwise comparisons were extracted, and significant differentially expressed genes were determined with the same significant criteria. The expression of the top 5,000 most variable genes was transformed by variance stabilizing transformation for principal component analysis.

In silico cytometry methods

The colon immune cell composition was imputed from the sigmoid colon bulk RNA-seq data by CIBERSORTx (https://cibersortx.stanford.edu/) (Newman et al., 2019). In brief, single-cell RNA-seq dataset associated with sigmoid colon was extracted from colon immune atlas of Gut Cell Atlas project by Seurat (James et al., 2020). The first part of the CIBERSORTx workflow computed the signature matrix of immune cell populations in the sigmoid colon using the sigmoid colon single-cell RNA-seq dataset. The second part of the CIBERSORTx workflow imputed cell fractions in the sigmoid colon

by comparing bulk sigmoid colon RNA-seq with sigmoid colon immune cell signature matrix with the following parameters: relative run mode, 100 permutations, disabled quantile normalization, and S-mode batch correction, which was implemented to account for cross-platform deconvolution. The cell compositions were compared by disease status and psoriasis subgroups with two-sided Wilcoxon test or Kruskal–Wallis test, and results with $P < 0.05$ were considered significant. Statistical analyses were performed with R.

Multiomic analysis

We integrated six different datasets collected from three different measurement types: shotgun metagenomic sequencing, flow cytometry, and host RNA-seq from 14 healthy subjects and 26 patients with psoriasis. We included the following datasets for data integration: (i) bacterial species from shotgun metagenomics with nonzero count in at least 10 samples, (ii) microbial MetaCyc pathway from shotgun metagenomics with nonzero count in at least 10 samples, (iii) microbial UniRef90 gene families from shotgun metagenomics with at least three counts for 80% of the total samples with metagenomic data, (iv) cell population from flow cytometry, (v) cytokine production capacity from flow cytometry, and (vi) top 500 most variable genes plus all differentially expressed genes identified by DEseq2 from host RNA-seq. More information about datasets included in the multiomic analysis is summarized in Supplementary Table S10. Pairwise datasets from different measurement types were integrated by Spearman's rank-order correlation. We constructed interaction networks with only strong and robust correlations that fit the following criteria: correlations need to have a false discovery rate–adjusted $P < 0.1$ and absolute correlation coefficient > 0.6. We required microbial or host features with a nonzero count for >70% of samples within the group of interest. Multiomic analyses were done within all subjects (both healthy subjects and subjects with psoriasis), within healthy subjects alone, within subjects with psoriasis alone, and within each psoriasis subgroups. The significant host–microbe associations identified in our analyses are listed in Supplementary Table S11. The multiomic networks were visualized using the R package, igraph (version 1.2.4.1) The community modules within each network were identified using fast greedy modularity optimization algorithm (Clauset et al., 2004[1]).

Host flow cytometry

Flow cytometry for cell population. Frozen PBMCs were thawed and counted, and one million cells were plated in a 96-well V-bottom plate. The cells were centrifuged for 5 minutes at 400*g* and surfaced stained with a predetermined antibody staining cocktail for 15 minutes at room temperature. The cells were washed with sort buffer, centrifuged, resuspended in BD Perm/Wash Buffer (BD Biosciences, Franklin Lakes, NJ), and centrifuged for 5 minutes at 700*g*. The supernatant was aspirated, and the cells were stained for FoxP3 by adding diluted fluorophore-labeled anti-human FoxP3 antibody in BD Perm/Wash Buffer for 30 minutes at room temperature. Cells were centrifuged for 5 minutes at 700*g*, the supernatant was aspirated, and the wash was repeated with BD Perm/Wash buffer. The cells were resuspended a final time in 50 ul of PBS and held at 4 °C until analyzed on a BD LSR-II instrument (BD Biosciences). Brilliant Violet Buffer was added to each staining step. Fluorescent-minus-one controls were used for setting gates. A minimum of 300,000 events were analyzed for each sample. The gating strategy is provided in Supplementary Figure S5, and the antibodies used are listed in Table 5.

Flow cytometry for cytokine production. Frozen PBMCs were thawed and counted and one million cells were plated in a 96-well U-bottom plate. PBMCs were left unstimulated in complete culture media (RPMI + 10% heat-inactivated fetal bovine serum supplemented with penicillin/streptomycin/L-glutamine) or stimulated with 5 ng/ml of phorbol myristate acetate and 0.5 ug/ml of ionomycin for 4 hours in the presence of brefeldin A (10 ug/ml). After 4 hours of stimulation, the cells were centrifuged and stained with an antibody staining cocktail listed for 15 minutes at room temperature. The cells were washed with sort buffer, centrifuged, and resuspended in BD Perm/Wash Buffer and centrifuged for 5 minutes at 700*g*. The supernatant was aspirated, and the cells were stained for intracellular antigens by adding diluted fluorophore-labeled antibodies in BD Perm/Wash Buffer for 30 minutes at room temperature. Cells were centrifuged for 5 minutes at 700*g*, the supernatant was aspirated, and the wash was repeated with BD Perm/Wash buffer. The cells were resuspended a final time in 50 ul of PBS and held at 4 °C until analyzed on a BD LSR-II instrument. Brilliant Violet Buffer was added to each staining step. Fluorescent-minus-one controls were used for setting gates. A minimum of 300,000 events were analyzed

Table 5. List of the Antibodies Used for the Flow Cytometry

Marker	Antibody	Cell Type
Phenotype panel		
AARD	AARD	Viability
CD45	CD45-APCH7	Lymphocytes
CD3	CD3-PerCpCy55	T cells
CD4	CD4-APC	CD4+ T cells
CD8	CD8-BV650	CD8+ T cells
FoxP3	FoxP3-A488	Treg
CD25	CD25-PECF594	Treg
TCRgd	TCRgd-BV711	γδ T cells
HLADR	HLADR-BV421	Activation
CD38	CD38-PE	Activation
CD117	CD117-BV786	ILCs
NKp44	NKp44-BV605	ILC3
CD45RO	CD45RO-PECy7	Memory
Functional panel		
AARD	AARD	Viability
CD45	CD45-APC-Cy7	Lymphocytes
CD3	CD3-PerCpCy55	T cells
CD4	CD4-APC	CD4+ T cells
CD8	CD8-BV650	CD8+ T cells
FoxP3	FoxP3-A488	Treg
CD127	CD127-PE-Dazzle594	Low in Tregs
TCRVS2	TCRVS2-BV711	Vd2 T cells
NKp44	NKp44-BV605	ILC3
CD117	CD117-BV786	ILC3
TNF-α	TNFa-A700	Cytokine
IFNγ	IFNg-PE-Cy7	Cytokine
IL-17	IL17-BV421	Cytokine
IL-22	IL22-PE	Cytokine

Abbreviations: APC, allophycocyanin; PE, phycoerythrin; Treg, regulatory T cell.

[1] Clauset A, Newman MEJ, Moore C. Finding community structure in very large networks. arXiv 2004.

for each sample. Reported data represent the stimulated cytokine expression minus the unstimulated cytokine expression referred to as background corrected cytokine expression. fcs files were analyzed by FlowJo (version 10; Tree Star, Ashland, OR), and the immune profiles were exported as txt files, which are imported into R for statistical analysis. Wilcox test was used to assess the significance of the differences between disease status or disease subgroups. The gating strategy is provided in Supplementary Figure S6, and the antibodies used are listed in Table 5.

Data availability statement

Expression data have been deposited in the National Center for Biotechnology Information Gene Expression Omnibus and is accessible through Gene Expression Omnibus Series accession number GSE150851. Metagenomics sequence data are accessible through Sequence Read Archive BioProject PRJNA634145. All clinical and experimental data available are shown in Supplementary Table S12.

ORCIDs

Hsin-Wen Chang: http://orcid.org/0000-0003-2881-245X
Di Yan: http://orcid.org/0000-0003-1338-9847
Rasnik Singh: http://orcid.org/0000-0002-7372-6692
Audrey Bui: http://orcid.org/0000-0003-3055-463X
Kristina Lee: http://orcid.org/0000-0002-5879-817X
Alexa Truong: http://orcid.org/0000-0002-4748-5581
Jeffrey M. Milush: http://orcid.org/0000-0002-0773-6411
Ma Somsouk: http://orcid.org/0000-0001-6116-3645
Wilson Liao: http://orcid.org/0000-0001-7883-6439

AUTHOR CONTRIBUTIONS

Conceptualization: WL, HWC; Methodology (Colonic Biopsies Collection): MS; Formal Analysis (Diet): AT; Flow Cytometry Data Analysis: JMM, HWC; Methodology (Flow Cytometry): JMM; Methodology (In Silico Cytometry): AB; Methodology: WL, HWC, JMM, MS; Methodology (Patient Recruitment): DY, RS, KL; Supervision: WL; Formal Analysis (Bioinformatics): HWC; Writing - Original Draft Preparation: WL, HWC

ACKNOWLEDGMENTS

Metagenomic sequencing was performed by the Vincent J. Coates Genomics Sequencing Laboratory at the University of California Berkeley (Berkeley, CA), supported by the National Institutes of Health S10 OD018174 Instrumentation Grant. Flow cytometry was performed by the San Francisco General Hospital Flow Core Facility, supported by a grant from the National Institutes of Health, University of California San Francisco-Gladstone Institute of Virology and Immunology Center for AIDS Research (P30 AI027763). This work was performed at the University of California San Francisco (San Francisco, CA). This study was supported in part by a National Psoriasis Foundation Translational Research Award and National Institutes of Health grants to WL (R01AR065174 and U01AI119125) and a National Psoriasis Foundation Medical Research Fellowship to DY.

CONFLICT OF INTEREST

WL has received research grant funding from AbbVie, Amgen, Janssen, Leo, Novartis, Pfizer, Regeneron, and TRex Bio. The remaining authors state no conflict of interest.

SUPPLEMENTARY MATERIAL

Supplementary material is linked to the online version of the paper at www.jidonline.org, and at https://doi.org/10.1016/j.xjidi.2022.100115.

REFERENCES

Afifi L, Danesh MJ, Lee KM, Beroukhim K, Farahnik B, Ahn RS, et al. Dietary behaviors in psoriasis: patient-reported outcomes from a U.S. National survey. Dermatol Ther (Heidelb) 2017;7:227–42.

Arumugam M, Raes J, Pelletier E, Le Paslier D, Yamada T, Mende DR, et al. Enterotypes of the human gut microbiome [published corrections appear in Nature 2014;506:516 and Nature 2011;474:666]. Nature 2011;473:174–80.

Benhadou F, Mintoff D, Schnebert B, Thio HB. Psoriasis and microbiota: a systematic review. Diseases 2018;6:47.

Brembilla NC, Senra L, Boehncke W-H. The IL-17 Family of cytokines in psoriasis: IL-17A and beyond. Front Immunol 2018;9:1682.

Chang HW, Yan D, Singh R, Liu J, Lu X, Ucmak D, et al. Alteration of the cutaneous microbiome in psoriasis and potential role in Th17 polarization. Microbiome 2018;6:154.

Codoñer FM, Ramírez-Bosca A, Climent E, Carrión-Gutierrez M, Guerrero M, Pérez-Orquín JM, et al. Gut microbial composition in patients with psoriasis. Sci Rep 2018;8:3812.

Diani M, Casciano F, Marongiu L, Longhi M, Altomare A, Pigatto PD, et al. Increased frequency of activated CD8+ T cell effectors in patients with psoriatic arthritis. Sci Rep 2019;9:10870.

El Mouzan MI, Winter HS, Assiri AA, Korolev KS, Al Sarkhy AA, Dowd SE, et al. Microbiota profile in new-onset pediatric Crohn's disease: data from a non-Western population. Gut Pathog 2018;10:49.

Elder JT, Bruce AT, Gudjonsson JE, Johnston A, Stuart PE, Tejasvi T, et al. Molecular dissection of psoriasis: integrating genetics and biology. J Invest Dermatol 2010;130:1213–26.

Eppinga H, Sperna Weiland CJ, Thio HB, van der Woude CJ, Nijsten TEC, Peppelenbosch MP, et al. Similar depletion of protective *Faecalibacterium prausnitzii* in psoriasis and inflammatory bowel disease, but not in hidradenitis suppurativa. J Crohns Colitis 2016;10:1067–75.

Fahlén A, Engstrand L, Baker BS, Powles A, Fry L. Comparison of bacterial microbiota in skin biopsies from normal and psoriatic skin. Arch Dermatol Res 2012;304:15–22.

Franzosa EA, McIver LJ, Rahnavard G, Thompson LR, Schirmer M, Weingart G, et al. Species-level functional profiling of metagenomes and metatranscriptomes. Nat Methods 2018;15:962–8.

Fu Y, Lee CH, Chi CC. Association of psoriasis with inflammatory bowel disease: a systematic review and meta-analysis. JAMA Dermatol 2018;154:1417–23.

Fyhrquist N, Muirhead G, Prast-Nielsen S, Jeanmougin M, Olah P, Skoog T, et al. Microbe-host interplay in atopic dermatitis and psoriasis. Nat Commun 2019;10:4703.

Gao Z, Tseng CH, Strober BE, Pei Z, Blaser MJ. Substantial alterations of the cutaneous bacterial biota in psoriatic lesions. PLoS One 2008;3:e2719.

Gevers D, Kugathasan S, Denson LA, Vázquez-Baeza Y, Van Treuren W, Ren B, et al. The treatment-naive microbiome in new-onset Crohn's disease. Cell Host Microbe 2014;15:382–92.

Hidalgo-Cantabrana C, Gómez J, Delgado S, Requena-López S, Queiro-Silva R, Margolles A, et al. Gut microbiota dysbiosis in a cohort of patients with psoriasis. Br J Dermatol 2019;181:1287–95.

Hijnen D, Knol EF, Gent YY, Giovannone B, Beijn SJP, Kupper TS, et al. CD8(+) T cells in the lesional skin of atopic dermatitis and psoriasis patients are an important source of IFN-γ, IL-13, IL-17, and IL-22. J Invest Dermatol 2013;133:973–9.

Hsiao EY, McBride SW, Hsien S, Sharon G, Hyde ER, McCue T, et al. Microbiota modulate behavioral and physiological abnormalities associated with neurodevelopmental disorders. Cell 2013;155:1451–63.

James KR, Gomes T, Elmentaite R, Kumar N, Gulliver EL, King HW, et al. Distinct microbial and immune niches of the human colon. Nat Immunol 2020;21:343–53.

Jin X, Chen D, Zheng RH, Zhang H, Chen YP, Xiang Z. miRNA-133a-UCP2 pathway regulates inflammatory bowel disease progress by influencing inflammation, oxidative stress and energy metabolism. World J Gastroenterol 2017;23:76–86.

Knights D, Silverberg MS, Weersma RK, Gevers D, Dijkstra G, Huang H, et al. Complex host genetics influence the microbiome in inflammatory bowel disease. Genome Med 2014;6:107.

Levy M, Thaiss CA, Zeevi D, Dohnalová L, Zilberman-Schapira G, Mahdi JA, et al. Microbiota-modulated metabolites shape the intestinal microenvironment by regulating NLRP6 inflammasome signaling. Cell 2015;163:1428–43.

Liu J, Chang HW, Huang ZM, Nakamura M, Sekhon S, Ahn R, et al. Single-cell RNA sequencing of psoriatic skin identifies pathogenic Tc17 cell subsets and reveals distinctions between $CD8^+$ T cells in autoimmunity and cancer. J Allergy Clin Immunol 2021;147:2370–80.

Lloyd-Price J, Arze C, Ananthakrishnan AN, Schirmer M, Avila-Pacheco J, Poon TW, et al. Multi-omics of the gut microbial ecosystem in inflammatory bowel diseases. Nature 2019;569:655–62.

Loesche MA, Farahi K, Capone K, Fakharzadeh S, Blauvelt A, Duffin KC, et al. Longitudinal study of the psoriasis-associated skin microbiome during therapy with ustekinumab in a randomized phase 3b clinical trial. J Invest Dermatol 2018;138:1973–81.

Love MI, Huber W, Anders S. Moderated estimation of fold change and dispersion for RNA-seq data with DESeq2. Genome Biol 2014;15:550.

Lozupone C, Knight R. UniFrac: a new phylogenetic method for comparing microbial communities. Appl Environ Microbiol 2005;71:8228–35.

Matsuda H, Fujiyama Y, Andoh A, Ushijima T, Kajinami T, Bamba T. Characterization of antibody responses against rectal mucosa-associated bacterial flora in patients with ulcerative colitis. J Gastroenterol Hepatol 2000;15:61–8.

McMurdie PJ, Holmes S. phyloseq: an R package for reproducible interactive analysis and graphics of microbiome census data. PLoS One 2013;8:e61217.

McMurdie PJ, Holmes S. Waste not, want not: why rarefying microbiome data is inadmissible. PLoS Comput Biol 2014;10:e1003531.

Morgan XC, Tickle TL, Sokol H, Gevers D, Devaney KL, Ward DV, et al. Dysfunction of the intestinal microbiome in inflammatory bowel disease and treatment. Genome Biol 2012;13:R79.

Newman AM, Steen CB, Liu CL, Gentles AJ, Chaudhuri AA, Scherer F, et al. Determining cell type abundance and expression from bulk tissues with digital cytometry. Nat Biotechnol 2019;37:773–82.

Noble CL, Abbas AR, Lees CW, Cornelius J, Toy K, Modrusan Z, et al. Characterization of intestinal gene expression profiles in Crohn's disease by genome-wide microarray analysis. Inflamm Bowel Dis 2010;16:1717–28.

Panagiotakos DB, Pitsavos C, Stefanadis C. Dietary patterns: A Mediterranean diet score and its relation to clinical and biological markers of cardiovascular disease risk. Nutr Metab Cardiovasc Dis 2006;16:559–68.

Prodanovich S, Kirsner RS, Kravetz JD, Ma F, Martinez L, Federman DG. Association of psoriasis with coronary artery, cerebrovascular, and peripheral vascular diseases and mortality. Arch Dermatol 2009;145:700–3.

Rais R, Jiang W, Zhai H, Wozniak KM, Stathis M, Hollinger KR, et al. *FOLH1*/GCPII is elevated in IBD patients, and its inhibition ameliorates murine IBD abnormalities. JCI Insight 2016;1:e88634.

Ritchlin CT, Colbert RA, Gladman DD. Psoriatic arthritis [published correction appears in N Engl J Med 2017;376:2097]. N Engl J Med 2017;376:957–70.

Scher JU, Ubeda C, Artacho A, Attur M, Isaac S, Reddy SM, et al. Decreased bacterial diversity characterizes the altered gut microbiota in patients with psoriatic arthritis, resembling dysbiosis in inflammatory bowel disease. Arthritis Rheumatol 2015;67:128–39.

Selhub J, Byun A, Liu Z, Mason JB, Bronson RT, Crott JW. Dietary vitamin B6 intake modulates colonic inflammation in the IL10−/− model of inflammatory bowel disease. J Nutr Biochem 2013;24:2138–43.

Shajib MS, Chauhan U, Adeeb S, Chetty Y, Armstrong D, Halder SLS, et al. Characterization of serotonin signaling components in patients with inflammatory bowel disease. J Can Assoc Gastroenterol 2019;2:132–40.

Takemoto A, Cho O, Morohoshi Y, Sugita T, Muto M. Molecular characterization of the skin fungal microbiome in patients with psoriasis. J Dermatol 2015;42:166–70.

Tan L, Zhao S, Zhu W, Wu L, Li J, Shen M, et al. The Akkermansia muciniphila is a gut microbiota signature in psoriasis. Exp Dermatol 2018;27:144–9.

Tett A, Pasolli E, Farina S, Truong DT, Asnicar F, Zolfo M, et al. Unexplored diversity and strain-level structure of the skin microbiome associated with psoriasis. NPJ Biofilms Microbiomes 2017;3:14.

Tibshirani R, Hastie T. Hastie. Estimating the number of clusters in a data set via the gap statistic. Royal Stat Soc 2002;457. https://doi.org/10.1111/1467-9868.00293.

Turnbaugh PJ, Hamady M, Yatsunenko T, Cantarel BL, Duncan A, Ley RE, et al. A core gut microbiome in obese and lean twins. Nature 2009;457:480–4.

Wan MT, Shin DB, Hubbard RA, Noe MH, Mehta NN, Gelfand JM. Psoriasis and the risk of diabetes: a prospective population-based cohort study. J Am Acad Dermatol 2018;78:315–22.e1.

Wang F, Kaplan JL, Gold BD, Bhasin MK, Ward NL, Kellermayer R, et al. Detecting microbial dysbiosis associated with pediatric Crohn disease despite the high variability of the gut microbiota. Cell Rep 2016;14:945–55.

Yan D, Issa N, Afifi L, Jeon C, Chang HW, Liao W. The role of the skin and gut microbiome in psoriatic disease. Curr Dermatol Rep 2017;6:94–103.

Yoshii K, Hosomi K, Sawane K, Kunisawa J. Metabolism of dietary and microbial vitamin B family in the regulation of host immunity. Front Nutr 2019;6:48.

Yu X, Wieczorek S, Franke A, Yin H, Pierer M, Sina C, et al. Association of UCP2 -866 G/A polymorphism with chronic inflammatory diseases. Genes Immun 2009;10:601–5.

Zhou W, Sailani MR, Contrepois K, Zhou Y, Ahadi S, Leopold SR, et al. Longitudinal multi-omics of host–microbe dynamics in prediabetes. Nature 2019;569:663–71.

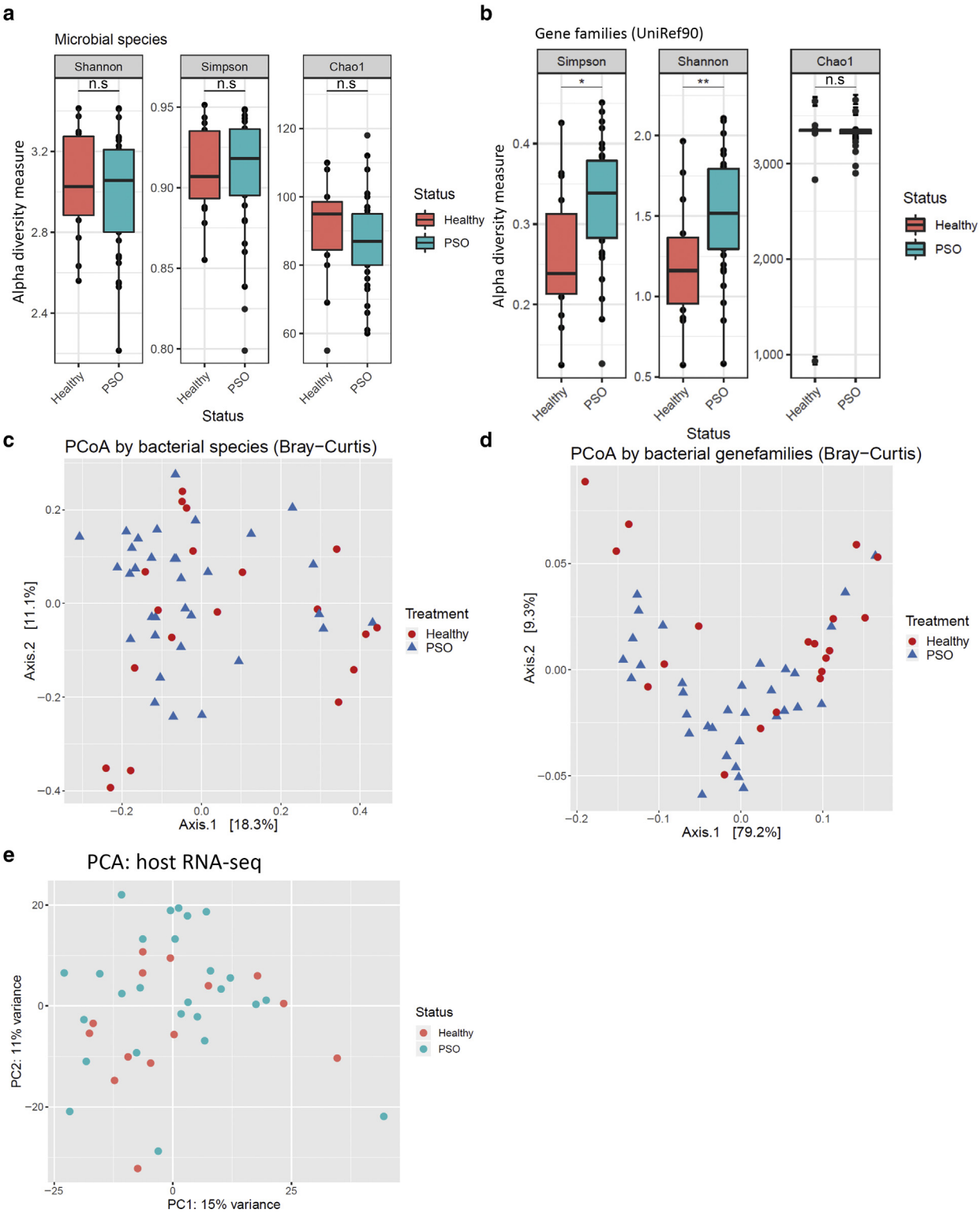

Supplementary Figure S1. Microbial diversity metrics. (**a**) Boxplot comparing the alpha diversity of gut microbiome in patients with PSO and healthy subjects. Alpha diversity was measured by Shannon index, Simpson diversity index, and chao1 estimation for microbial species. PCoA of the microbial community structures based on Bray–Curtis distance matrix for (**b**) microbial species and (**c**) microbial gene families. (**d**) PCA of host transcriptome by top 5,000 most variable genes. In all plots, red denotes healthy samples, and blue denotes PSO samples. n.s., not significant; PC, principal component; PCA, principal component analysis; PCoA, principal coordinate analysis; PSO, psoriasis; RNA-seq, RNA sequencing.

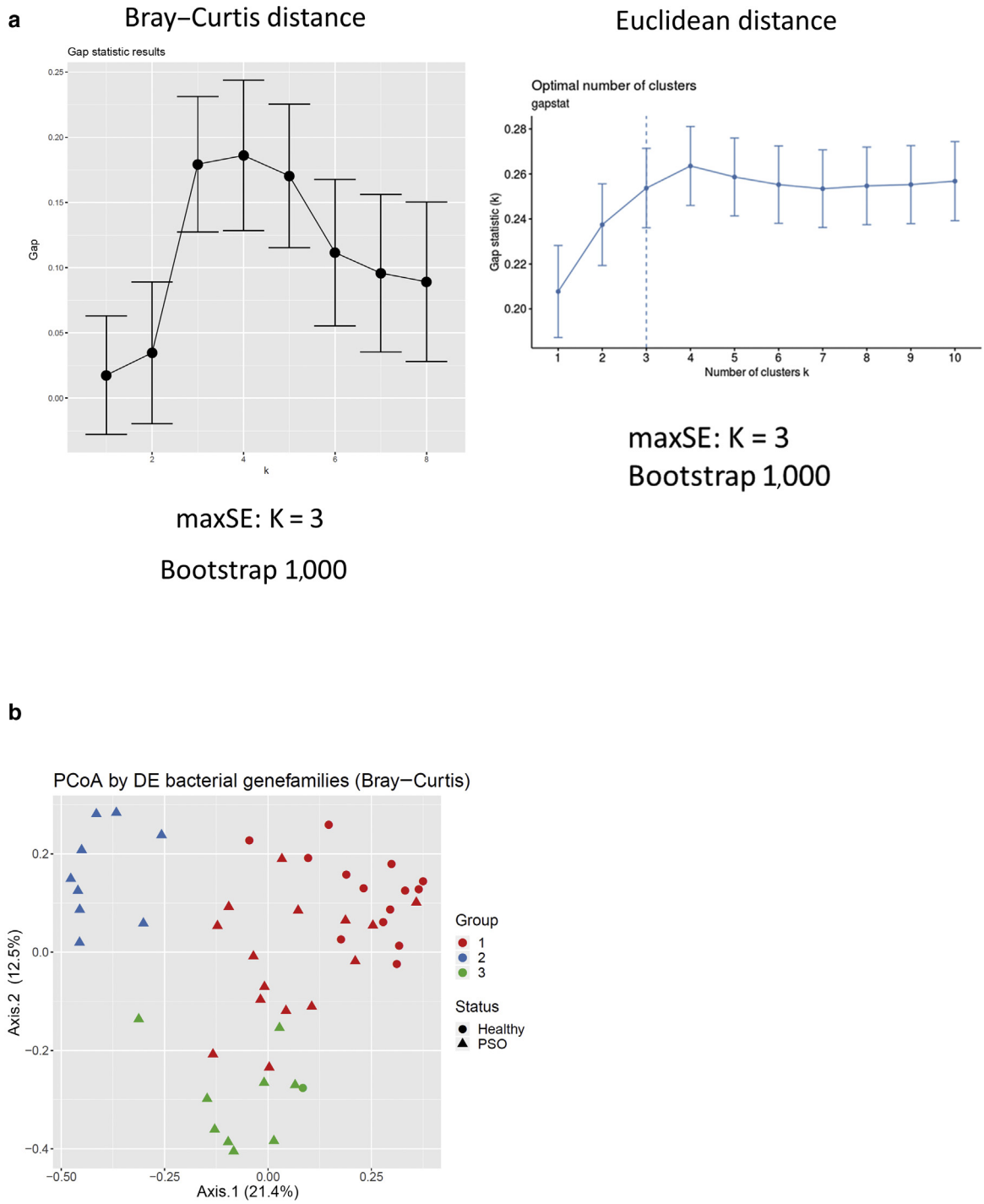

Supplementary Figure S2. Bray-Curtis analysis. (**a**) Gap statistics calculated using Bray–Curtis and Euclidean dissimilar matrix of the DA UniRef90 gene families with bootstrapping for 1,000 times. (**b**) PCoA plot shows the Bray–Curtis dissimilarity matrix of the DA UniRef90 gene families grouped the cohort into three groups that are similar to the grouping defined by hierarchical clustering (as represented by the color of each point). The shapes represent the disease status (round circles depict healthy samples, and triangles depict PSO samples). DA, differentially abundant; DE, differentially expressed; maxSE, maximum numeric vector of function values; PCoA, principal coordinate analysis; PSO, psoriasis.

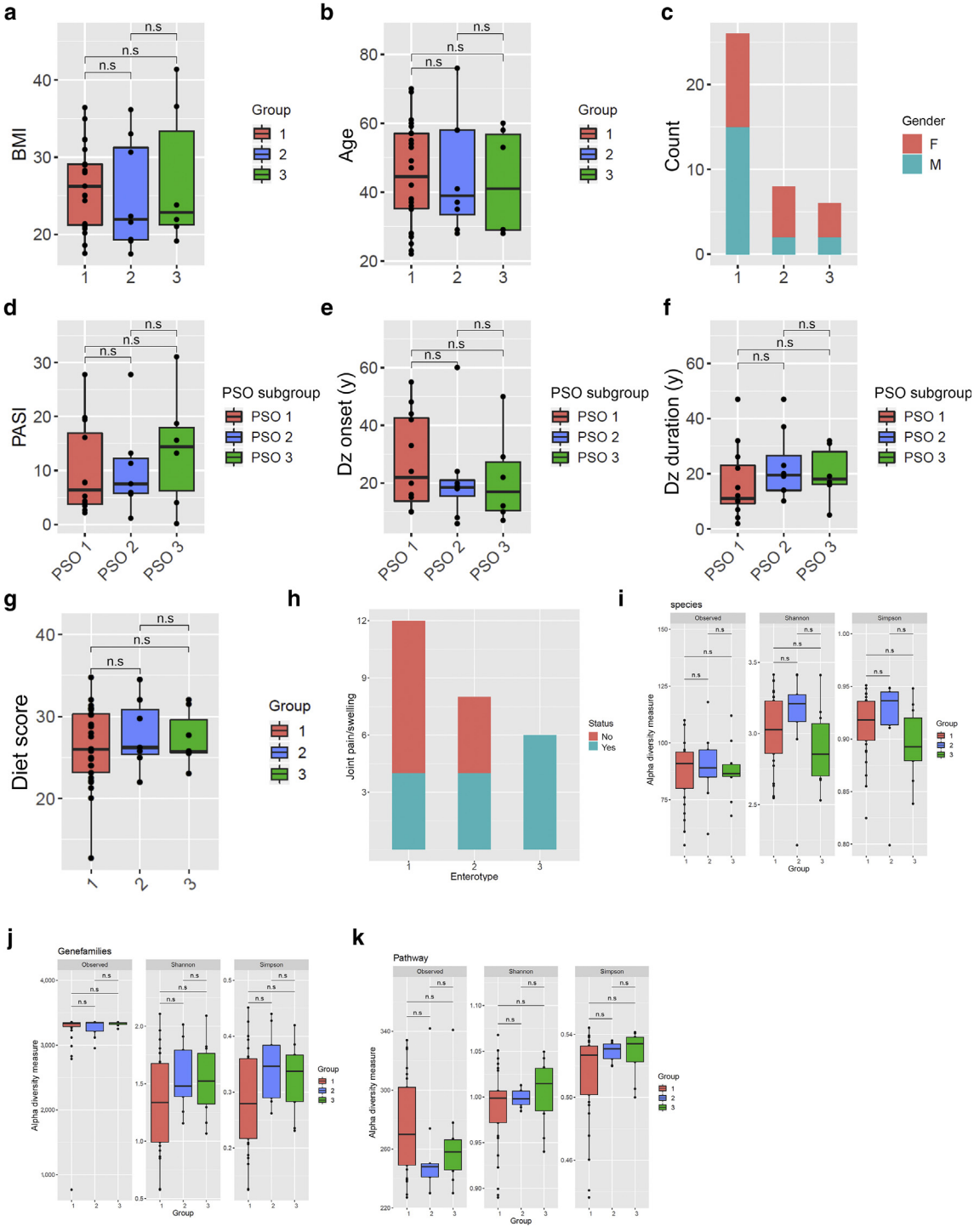

Supplementary Figure S3. Comparisons of metadata and microbial diversity in the three subgroups identified in the cohort. Only subjects with a complete dataset from the three measurement types are included. (**a–c**) Comparisons of BMI, age, and gender in the three groups. (**d–f**) Comparisons of PASI, disease onset, and disease duration in each PSO subgroup. (**g, h**) Comparison of diet scores and self-reported joint pain or swelling in the three groups. Comparisons of observed microbial, Shannon index, and Simpson diversity index in the three groups for (**i**) microbial species, (**j**) UniRef90 gene families, and (**k**) MetaCyc pathway. BMI, body mass index; Dz, disease; F, female; M, male; n.s., not significant; PSO, psoriasis; y, year.

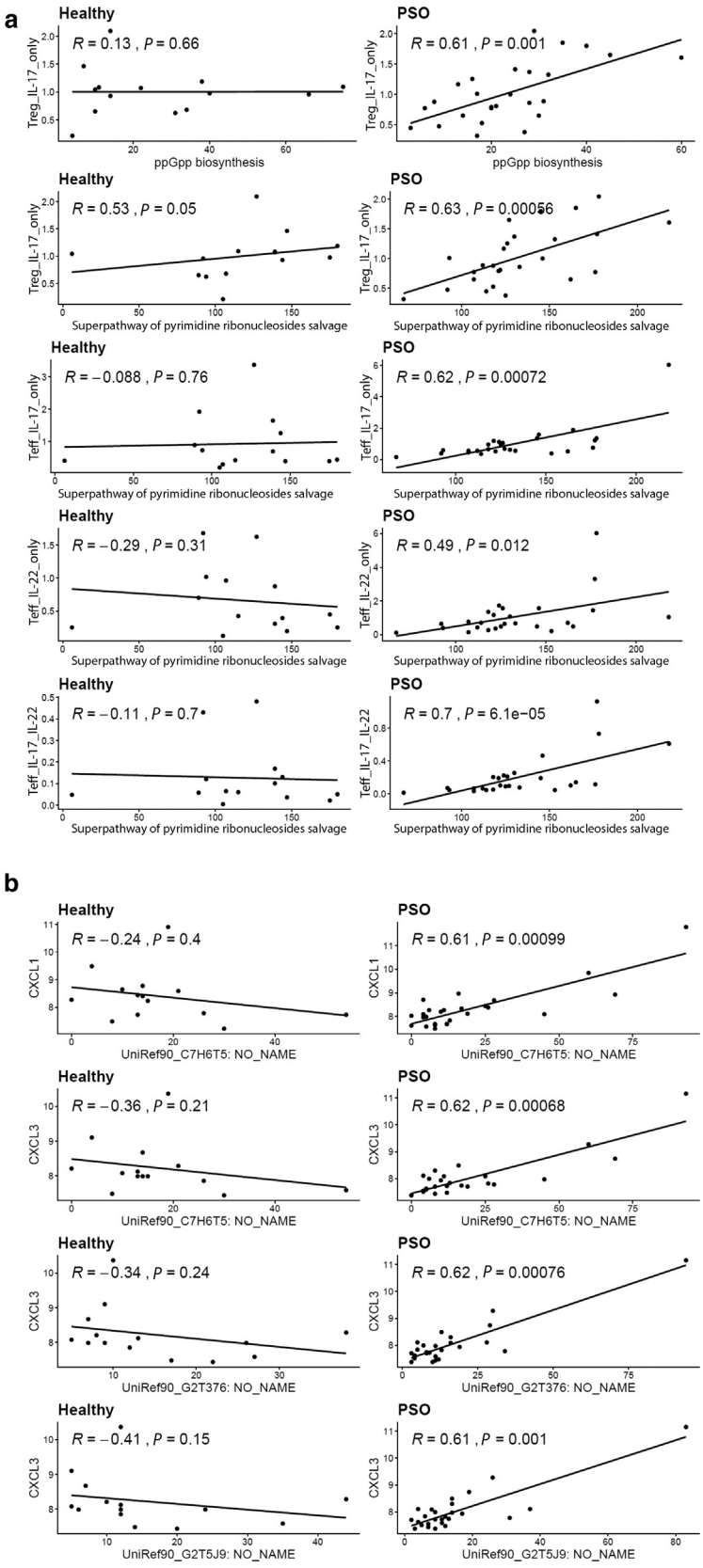

Supplementary Figure S4. PSO-specific correlations between microbial functions and proinflammatory host response. (**a**) Scatter plots show positive correlations between microbial MetaCyc pathways and IL-17 production in psoriatic PBMCs but not in healthy PBMCs. (**b**) Scatter plots show a positive correlation between microbial UniRef90 gene families with the colonic expression of CXCL1 and CXCL3 in patients with PSO but not in healthy control. The correlations were calculated by Spearman's rank-order correlation. PSO, psoriasis; Teff, effector T cell; Treg, regulatory T cell.

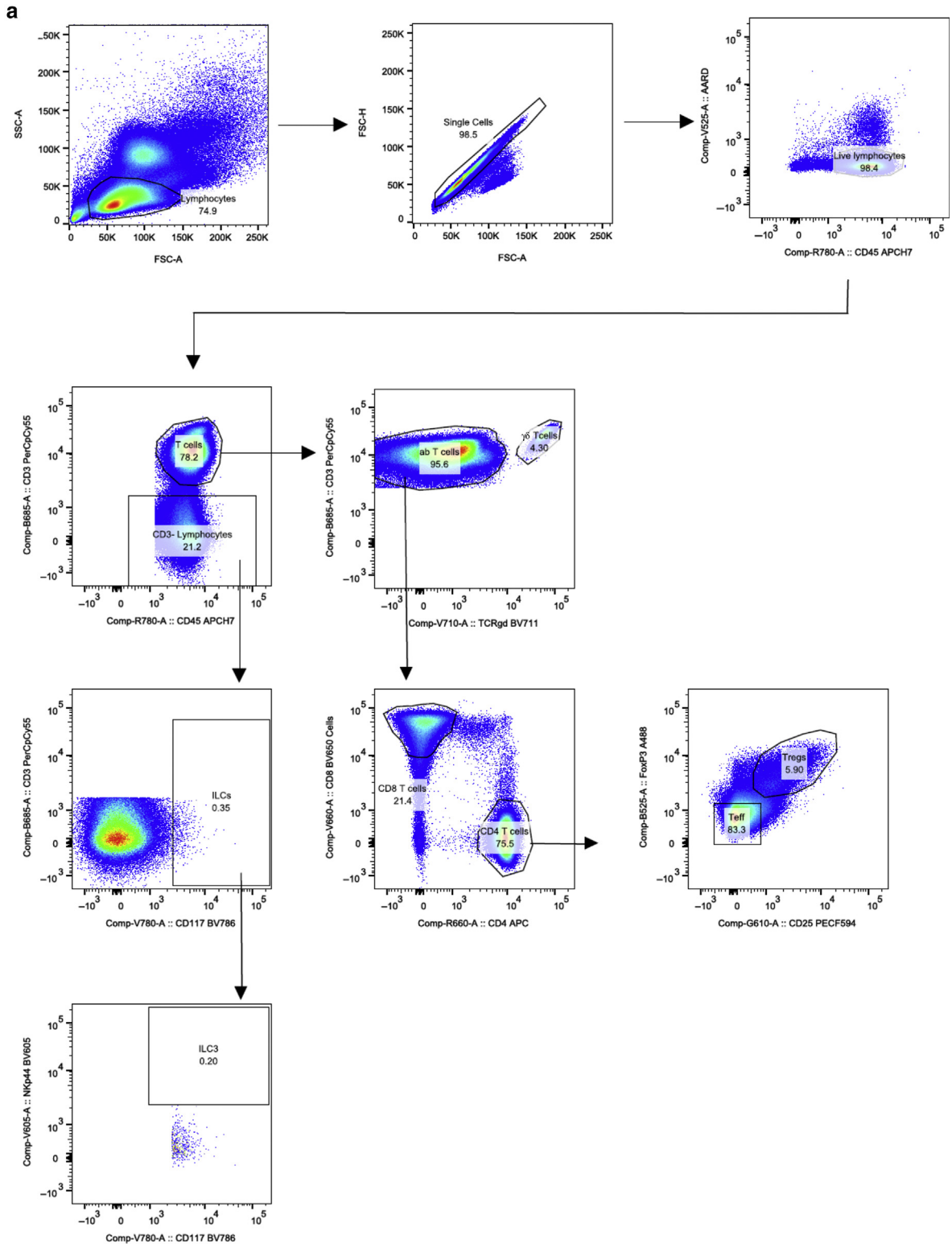

Supplementary Figure S5. Representative flow cytometry gating for identifying various cell populations. (**a**) Cell populations (CD4+ Teff, CD4+ Treg, CD8+ T cell, γδ T cell, and innate lymphoid cells) and (**b**) their memory and activation state. APC, allophycocyanin; FSC-A, forward scatter area; FSC-H, forward scatter height; K, thousand; PE, phycoerythrin; Q, quadrant; SSC-A, side scatter area; Teff, effector T cell; Treg, regulatory T cell.

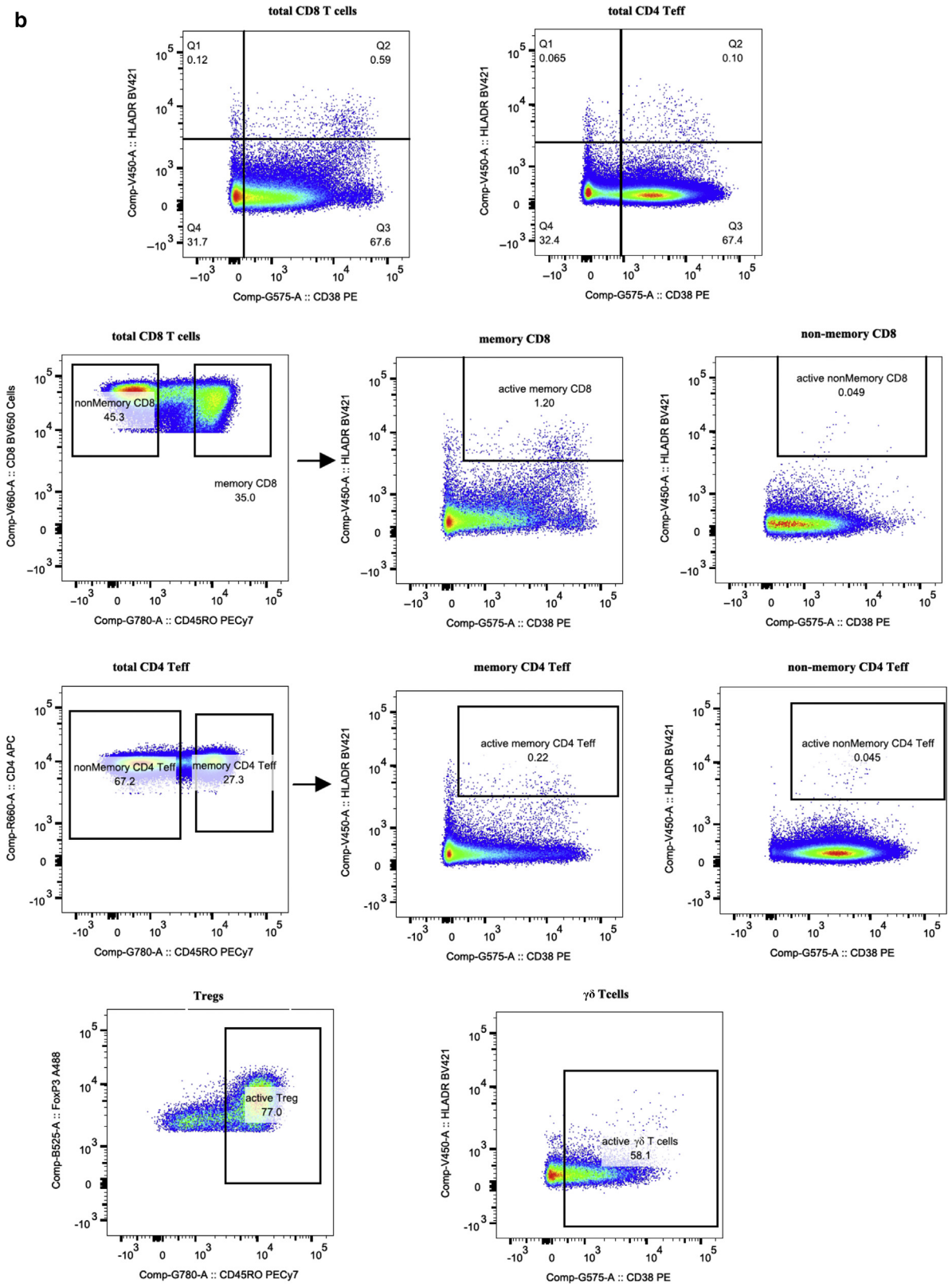

Supplementary Figure S5. *Continued.*

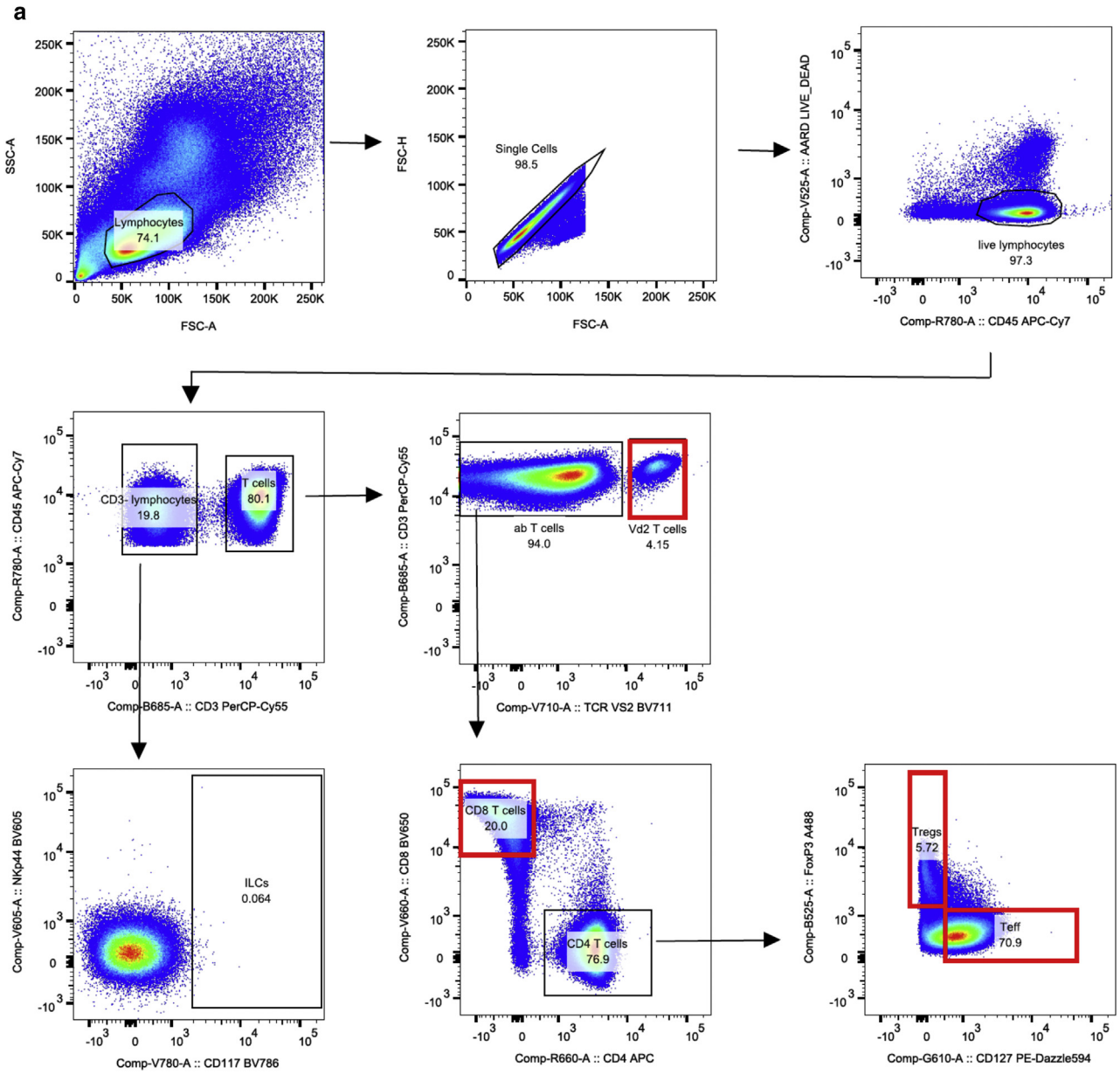

Supplementary Figure S6. Representative flow cytometry gating for measuring cytokine production in various cell populations after 4 hours of PMA and ionomycin stimulation. (**a**) Gating strategies for identification of Teff, Treg, CD8+ T cells, and γδ T cells. (**b**) Gating strategies for measuring the production of IL-17A, IL-22, TNF-α, and IFNγ. APC, allophycocyanin; FSC-A, forward scatter area; FSC-H, forward scatter height; K, thousand; PMA, phorbol myristate acetate; Teff, effector T cell; Treg, regulatory T cell; vs. versus.

Supplementary Figure S6. *Continued.*

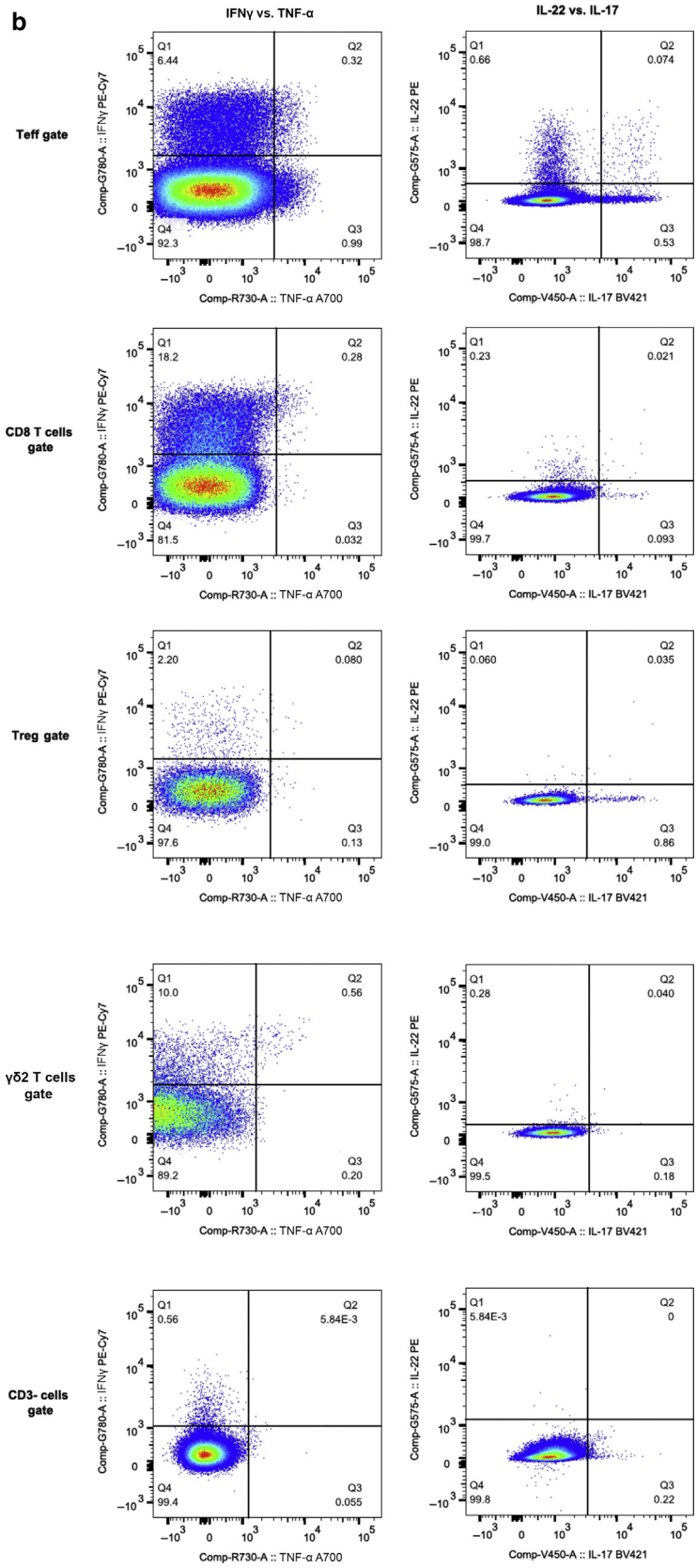

Supplementary Table S1. List of Microbial Species that Are Differentially Abundant between Psoriasis and Healthy Samples

Microbial Species	Base Mean	Log_2 Fold Change	*P*-Value	*P*adj
Prevotella_disiens	12.48	26.94	5.07382E−16	2.08027E−14
Clostridium_sp_KLE_1755	95.27	26.20	3.98903E−15	9.08612E−14
Bacteroides_coprocola	1,787.37	22.57	1.30691E−11	1.33958E−10
Erysipelotrichaceae_bacterium_5_2_54FAA	4.22	21.86	5.56657E−11	5.18704E−10
Dorea_unclassified	2.09	20.75	4.90663E−10	3.59236E−09
Prevotella_buccae	2.70	18.20	4.78393E−08	3.26902E−07
Brachyspira_unclassified	0.73	16.74	5.16488E−07	3.30875E−06
Haemophilus_pittmaniae	4.37	16.29	9.98499E−07	6.02036E−06
Gemella_sanguinis	3.32	15.09	5.99289E−06	3.41262E−05
Roseburia_unclassified	1,416.55	14.32	1.53925E−05	8.09092E−05
Bacteroides_oleiciplenus	12.19	13.46	5.31623E−05	0.000272457
Burkholderiales_bacterium_1_1_47	579.13	12.17	3.16928E−08	2.24035E−07
Weissella_unclassified	1.08	11.51	0.000557326	0.002393849
Lachnospiraceae_bacterium_9_1_43BFAA	56.00	10.31	0.001862232	0.007485442
Clostridium_hylemonae	3.72	10.17	0.002285859	0.008841529
Anaerotruncus_unclassified	7.27	9.86	0.003047001	0.011567319
Megasphaera_unclassified	3,017.86	9.60	0.001021066	0.004186369
Collinsella_stercoris	11.98	9.54	0.004187753	0.015061219
Enterococcus_faecium	291.35	9.24	0.003988014	0.014598981
Dialister_invisus	11,846.88	9.16	0.00038163	0.001738535
Eubacterium_dolichum	126.53	8.43	0.000771769	0.003228827
Parabacteroides_goldsteinii	179.97	6.59	0.010261261	0.035346823
Parasutterella_excrementihominis	232.32	4.89	0.006925784	0.024479064
Sutterella_wadsworthensis	2,783.26	4.82	0.011048633	0.037130653
Bacteroides_vulgatus	16,890.23	2.08	0.003156479	0.01176506
Clostridiaceae_bacterium_JC118	68.59	−5.10	0.010345412	0.035346823
Phascolarctobacterium_succinatutens	16,877.87	−7.49	0.012182033	0.040279303
Bifidobacterium_pseudocatenulatum	843.21	−8.15	0.000560511	0.002393849
Peptostreptococcaceae_noname_unclassified	407.41	−8.64	6.40326E−05	0.00031254
Streptococcus_mitis_oralis_pneumoniae	31.93	−9.77	1.50858E−05	8.09092E−05
Atopobium_parvulum	1.79	−10.15	0.002104515	0.008296648
Coprococcus_sp_ART55_1	17,348.22	−11.50	0.000206357	0.000961438
Lactobacillus_delbrueckii	5.36	−11.56	0.000500643	0.002231124
Mitsuokella_multacida	247.94	−12.11	9.84218E−05	0.00046922
Fusobacterium_ulcerans	188.80	−13.32	6.19636E−05	0.000309818
Mitsuokella_unclassified	1,185.04	−14.76	1.95683E−06	1.14614E−05
Leuconostoc_lactis	12.28	−14.80	8.64274E−06	4.78854E−05
Gemella_unclassified	1.35	−16.59	6.05617E−07	3.76217E−06
Desulfovibrio_desulfuricans	43.84	−17.53	1.0359E−07	6.85032E−07
Proteus_penneri	0.22	−20.93	3.3238E−10	2.52363E−09
Citrobacter_freundii	1.54	−21.36	1.38522E−10	1.09219E−09
Leuconostoc_gelidum	0.28	−21.40	1.32504E−10	1.08653E−09
Proteus_unclassified	0.29	−21.44	1.22431E−10	1.04577E−09
Streptococcus_anginosus	6.60	−21.57	9.26092E−11	8.2543E−10
Porphyromonas_somerae	4.71	−21.89	5.18674E−11	5.06325E−10
Lactobacillus_curvatus	13.67	−22.92	5.84E−12	6.30105E−11
Alloscardovia_omnicolens	2.16	−23.22	3.21802E−12	3.66497E−11
Lactobacillus_sakei	1.23	−23.34	2.45901E−12	2.96528E−11
Streptococcus_sp_BS35b	2.20	−23.89	7.47425E−13	9.57638E−12
Enterococcus_avium	2.11	−24.12	4.44676E−13	6.07724E−12
Bacteroides_gallinarum	16.02	−24.34	2.59664E−13	3.80222E−12
Carnobacterium_maltaromaticum	12.49	−24.74	1.15388E−13	1.81958E−12
candidate_division_TM7_single_cell_isolate_TM7c	0.18	−25.12	4.69133E−14	8.01436E−13
Weissella_cibaria	6.65	−25.57	1.65562E−14	3.08547E−13
Subdoligranulum_variabile	28.34	−25.57	1.27799E−14	2.61988E−13
Bacteroides_sp_1_1_6	133.01	−26.24	3.4666E−15	8.88316E−14
Citrobacter_unclassified	4.40	−26.39	1.9069E−15	5.58448E−14

(*continued*)

Supplementary Table S1. Continued

Microbial Species	Base Mean	Log_2 Fold Change	*P*-Value	*P*adj
Butyricicoccus_pullicaecorum	12.00	−26.47	1.86029E−15	5.58448E−14
Bacteroides_sp_2_1_22	425.75	−29.27	1.42946E−18	7.326E−17
Corynebacterium_glutamicum	1.95	−29.98	2.24401E−19	1.54839E−17
Ruminococcus_champanellensis	1,472.34	−30.00	2.26594E−19	1.54839E−17
Campylobacter_hominis	1.51	−30.00	2.09163E−19	1.54839E−17

Abbreviation: adj, adjusted.

Supplementary Table S2. List of Microbial Gene Families that Are Differentially Abundant between Psoriasis and Healthy Samples

UniRef90_Genefamilies	Base Mean	Log_2 Fold Change	*P*-Value	*P*adj
UniRef90_D4JKB5: NO_NAME	20.44971008	8.184774568	3.76E−07	3.33E−05
UniRef90_D4JKB4: NO_NAME	9.737750875	7.318193992	2.7E−06	0.000218
UniRef90_D4JKB3: NO_NAME	5.604615949	5.972567491	2.98E−06	0.000239
UniRef90_C6JHT6: NO_NAME	11.59795247	3.503976143	3.74E−06	0.000297
UniRef90_V8CCN6: NO_NAME	7.911723223	−8.466033916	2.02E−05	0.001506
UniRef90_R5HHX1: NO_NAME	3.291298903	5.617246745	2.23E−05	0.001652
UniRef90_B0MUZ9: NO_NAME	17.2243469	7.779663835	2.63E−05	0.001914
UniRef90_B0NKZ9: NO_NAME	4.866770601	4.68406674	0.000104	0.007173
UniRef90_E1YTP4: NO_NAME	9.980238914	4.364093512	0.000124	0.008475
UniRef90_C0EYV3: NO_NAME	5.843250501	−1.156773775	0.00013	0.008856
UniRef90_K9DSD1: NO_NAME	20.70420605	7.4409631	0.000134	0.009178
UniRef90_D4V9S6: Toxin-antitoxin system, antitoxin component family protein	3.433982731	3.624603291	0.000137	0.009363
UniRef90_T4Z7D4: NO_NAME	12.26511689	−1.374370748	0.00014	0.009561
UniRef90_A7A642: NO_NAME	9.61390528	−3.999917984	0.00018	0.012157
UniRef90_C4Z8L3: NO_NAME	8.953334146	4.14025387	0.000198	0.013365
UniRef90_D4L5Q7: Dockerin type I repeat	3.709257355	4.458714365	0.000214	0.014395
UniRef90_C4ZDT0: NO_NAME	11.02944175	2.61803876	0.000221	0.014875
UniRef90_Q89YV2: NO_NAME	3.960842604	2.459102717	0.000231	0.015496
UniRef90_R5ENA9: NO_NAME	7.31968454	2.809734777	0.000273	0.018301
UniRef90_R5VN00: NO_NAME	6.66944193	2.726824008	0.000283	0.018902
UniRef90_C0FYT5: NO_NAME	5.608127022	5.494622505	0.000289	0.019302
UniRef90_U2DKA0: Toxin-antitoxin system, antitoxin component, Xre family	2.41752419	−2.07552754	0.000315	0.021031
UniRef90_U2NXE6: NO_NAME	0.823846701	4.956194737	0.000317	0.0212
UniRef90_R5F076: NO_NAME	6.570912784	2.6,53219048	0.000329	0.021951
UniRef90_I7ASX7: Aminoglycoside 6-adenylyltransferase	5.981679914	−1.229156672	0.000339	0.022617
UniRef90_D6E2K8: NO_NAME	6.220313047	7.882367351	0.00035	0.023302
UniRef90_C4ZCN8: NO_NAME	4.739971235	4.531804983	0.000367	0.02438
UniRef90_A8SDV6: NO_NAME	3.111716292	−6.463421902	0.00037	0.024535
UniRef90_A7B7Y7: NO_NAME	3.835647149	−4.216283036	0.000381	0.02528
UniRef90_R5DHM8: 50S ribosomal protein L14	8.05231442	−1.091553729	0.000387	0.025643
UniRef90_F7JRF6: NO_NAME	2.10652993	−2.258144862	0.000397	0.026326
UniRef90_R5ENA5: NO_NAME	6.145444386	2.76594925	0.000404	0.026733
UniRef90_C4ZB30: NO_NAME	13.98634953	6.26094269	0.000416	0.027527
UniRef90_C4ZHW5: NO_NAME	7.601796234	2.21832247	0.000424	0.028048
UniRef90_A6NXS5: NO_NAME	3.085119571	−1.949411921	0.000431	0.028513
UniRef90_R5ES70: NO_NAME	6.142418982	2.70370766	0.000447	0.029252
UniRef90_R5ENC3: NO_NAME	6.187279035	2.701041839	0.00045	0.029276
UniRef90_R5VTV0: NO_NAME	11.84385896	−8.859754987	0.000484	0.031431
UniRef90_R5ES82: NO_NAME	6.218044543	2.631291787	0.000495	0.03205
UniRef90_A8SDV1: PTS system, lactose/cellobiose family IIC component	1.577472175	−5.394020156	0.000498	0.032135
UniRef90_R5F071: NO_NAME	5.795869956	2.671859836	0.0005	0.032226
UniRef90_R5EN96: NO_NAME	6.316661771	2.597760365	0.000522	0.033606
UniRef90_D4LVD7: Bacterial mobilisation protein (MobC)	2.997706936	−3.203584633	0.000527	0.033927
UniRef90_R5EP09: NO_NAME	6.497763827	2.664311777	0.000545	0.035039
UniRef90_A8SDV2: PTS system, Lactose/Cellobiose specific IIB subunit	1.67041892	−5.420005822	0.000571	0.036645
UniRef90_R5ENY1: NO_NAME	6.055002091	2.605312597	0.000597	0.038285
UniRef90_R5EXU5: NO_NAME	6.640770231	2.590729061	0.000608	0.039021
UniRef90_R5B346: Peptidyl-prolyl cis-trans isomerase	1.333716976	−2.172687536	0.000617	0.039563
UniRef90_R5F1R6: NO_NAME	6.195974482	2.670392787	0.00062	0.039746
UniRef90_R5ENZ3: NO_NAME	5.847885346	2.536486311	0.000661	0.042259
UniRef90_R5F1S4: NO_NAME	6.301820127	2.594059152	0.000673	0.043049

(*continued*)

Supplementary Table S2. Continued

UniRef90_Genefamilies	Base Mean	Log_2 Fold Change	*P*-Value	*P*adj
UniRef90_F9Z9M1: Putative transposase	3.863722566	2.56148742	0.000689	0.044002
UniRef90_R5F5V1: NO_NAME	6.214726081	2.736286892	0.000691	0.044147
UniRef90_C0B519: NO_NAME	2.42564728	−2.370035967	0.000713	0.045513
UniRef90_J9GFK7: Transposase	10.34428213	3.257865985	0.000716	0.045681
UniRef90_R5F1T5: NO_NAME	7.6286111	2.573141893	0.000747	0.047598
UniRef90_R5ES58: NO_NAME	6.279915456	2.537809692	0.000753	0.047953
UniRef90_R5END3: NO_NAME	6.459389346	2.620179025	0.000759	0.048362
UniRef90_C4ZAI7: Putative regulatory components of sensory transduction system	8.358269459	1.883595829	0.000763	0.04859
UniRef90_R5ENB7: NO_NAME	6.194816868	2.563624339	0.000778	0.049511

Abbreviation: adj, adjusted.

Supplementary Table S3. List of Microbial Metacyc Pathways that Are Differentially Abundant between Psoriasis and Healthy Samples

MetaCyc_Pathway	Base Mean	Log_2 Fold Change	*P*-Value	*P*adj
P163-PWY: L-lysine fermentation to acetate and butanoate	0.174625879	−17.84752508	8.47E−08	1.63E−05
PWY-5304: superpathway of sulfur oxidation (Acidianus ambivalens)	0.135640038	−18.83320162	1.60E−08	6.16E−06
PWY-7200: superpathway of pyrimidine deoxyribonucleoside salvage	0.627023649	12.74062955	6.12E−05	0.007856

Abbreviation: adj, adjusted.

Supplementary Table S4. Summary of Statistics of Diet Survey

Diet	*P*-Value (Disease Status)	*P*-Value (Enterotype)
Milk	0.76	0.88
Fruit	0.66	0.16
Cereal	0.12	0.93
Soda	0.51	0.52
Pure fruit juices	0.87	0.86
Sweetened tea or coffee	0.25	0.49
Sweetened fruit drinks	0.6	0.87
Salad	0.44	0.48
Fried potatoes	0.1	0.07
Other kinds of potatoes	0.0564	0.09
Beans	0.29	0.18
Brown rice	0.64	0.67
Other veggies	0.48	0.28
Salsa	0.11	0.0958
Pizza	0.38	0.69
Tomato sauces	0.68	0.12
Cheese	0.47	0.46
Red meat	0.65	0.65
Processed meat	0.13	0.28
Whole grain bread	0.74	0.1
Chocolate/candy	0.84	0.62
Doughnuts	0.46	0.33
Pastries	0.5	0.07
Frozen desserts	0.79	0.23
Popcorn	0.52	0.75

Supplementary Table S5. List of Microbial Species that Are Differentially Abundant between Different Subgroup in the Cohort

Microbial Species	Base Mean	Log_2 Fold Change	*P*-Value	*P*adj	Comparison Pair
Turicibacter unclassified	148.1650263	−25.09944303	1.48E−25	2.77E−23	c2c1
Coprococcus sp ART55 1	17,348.22439	−30	4.07E−22	3.80E−20	c2c1
Phascolarctobacterium succinatutens	16,877.86806	−30	5.75E−20	3.58E−18	c2c1
Turicibacter sanguinis	30.89947547	−23.71828011	1.25E−19	5.84E−18	c2c1
Coprococcus sp ART55 1	17,348.22439	−32.10303282	4.81E−18	9.82E−16	c2c3
P. succinatutens	16,877.86806	−27.87316104	1.19E−12	8.08E−11	c2c3
Turicibacter unclassified	148.1650263	−20.02159204	2.65E−12	1.35E−10	c2c3
Megamonas unclassified	13,738.87404	−10.70556321	1.26E−06	1.03E−05	c2c1
Megamonas unclassified	13,738.87404	−12.64875264	1.93E−06	2.81E−05	c2c3
T. sanguinis	30.89947547	−15.01564462	2.39E−06	3.25E−05	c2c3
Ruminococcaceae bacterium D16	318.9654536	−8.1375798	0.000312498	0.003363951	c3c1
T. sanguinis	30.89947547	−8.702635493	0.000532915	0.005417965	c3c1
Lachnospiraceae bacterium 1 1 57FAA	2,253.140867	−6.756348377	0.000705118	0.006791396	c3c1
Streptococcus thermophilus	2,905.078536	−4.197322843	0.002619562	0.020410751	c2c1
Prevotella copri	69,851.06368	−4.796452699	0.003805748	0.028466996	c2c1
S. thermophilus	2,905.078536	−5.017689601	0.002810256	0.035830762	c2c3
Bacteroides xylanisolvens	1,773.658642	3.277724558	0.005561142	0.039997442	c2c1

Abbreviation: adj, adjusted.

Supplementary Table S6. List of Microbial Gene Families that Are Differentially Abundant between Different Subgroups in the Cohort

UniRef90_Genefamilies	Base Mean	Log_2 Fold Change	*P*-Value	*P*adj	Comparison Pair
UniRef90_R5F5T8: NO_NAME	6.13241864	3.855214514	8.38E−09	9.43E−06	c2c3
UniRef90_R5F5U3: NO_NAME	7.146133182	3.742380578	6.57E−09	7.87E−06	c2c3
UniRef90_R5F5U7: NO_NAME	5.872476462	3.736858351	3.22E−09	5.40E−06	c2c3
UniRef90_R5F5V1: NO_NAME	6.214726081	3.729014981	1.70E−07	8.76E−05	c2c3
UniRef90_R5F5V6: NO_NAME	6.843317692	3.810172235	7.23E−08	4.24E−05	c2c3
UniRef90_R5F6I7: NO_NAME	5.66902435	3.508892329	1.28E−08	1.30E−05	c2c3
UniRef90_R5F7E6: NO_NAME	7.654869731	3.781212969	8.36E−08	4.80E−05	c2c3
UniRef90_R5F7E9: NO_NAME	6.014946714	3.700272305	1.07E−07	5.95E−05	c2c3
UniRef90_R5F7F4: NO_NAME	6.252090198	3.70429003	2.70E−09	4.97E−06	c2c3
UniRef90_R5F7F6: NO_NAME	7.03037544	3.73575232	6.86E−08	4.14E−05	c2c3
UniRef90_R5F826: NO_NAME	6.25853359	3.553654489	5.32E−06	0.002125	c2c3
UniRef90_R5F830: NO_NAME	4.020772359	3.303446928	0.000126	0.041501	c2c3
UniRef90_R6BXA1: Pyridoxal biosynthesis lyase PdxS	18.20827345	−4.738434723	0.000139	0.025007	c2c1
UniRef90_R6EYN1: Phosphoenolpyruvate carboxykinase [ATP]	12.14532041	−5.300791062	0.000284	0.045255	c2c1
UniRef90_R5UHP6: NO_NAME	7.404456209	−2.502048554	0.000151	0.048523	c2c3
UniRef90_R5V1S5: NO_NAME	6.469822898	3.674332424	3.90E−08	2.69E−05	c2c3
UniRef90_R5VEH7: NO_NAME	5.638179874	3.783296451	3.44E−08	2.46E−05	c2c3
UniRef90_R5VN00: NO_NAME	6.66944193	3.804730154	9.58E−10	2.11E−06	c2c3
UniRef90_R6FSV7: dTDP-4-dehydrorhamnose 3 5-epimerase	3.836852934	−4.712602303	0.00015	0.026547	c2c1
UniRef90_UPI00046F6872: NO_NAME	3.841073774	−3.288653597	7.37E−05	0.025081	c2c3
UniRef90_R6YLJ5: dTDP-glucose 4 6-dehydratase	25.36463194	−5.501203549	4.07E−05	0.008208	c2c1
UniRef90_R6YTB4: Virulence protein	6.475252167	3.598839048	1.42E−11	5.13E−08	c3c1
UniRef90_R7ERI0: Protein phosphatase 2C	3.917056058	2.488315558	0.000229	0.03792	c2c1
UniRef90_W1I1K8: Uncultured bacterium extrachromosomal DNA RGI00018	44.18955643	−8.421153783	7.98E−05	0.027004	c2c3
UniRef90_W1I4A6: Uncultured bacterium extrachromosomal DNA RGI00018	19.44468222	−5.622500646	0.000293	0.046458	c2c1

Abbreviation: adj, adjusted.

Supplementary Table S7. List of Microbial Metacyc Pathways that Are Differentially Abundant between Different Subgroups in the Cohort

MetaCyc_Pathway	Base Mean	Log_2 Fold Change	*P*-Value	*P*adj	Comparison Pair
NAD-BIOSYNTHESIS-II: NAD salvage pathway II	6.885975523	−2.032470385	0.004596	0.081003	c2c1
POLYAMINSYN3-PWY: super pathway of polyamine biosynthesis II	16.58305195	−2.61298583	0.002204	0.069068	c2c1
PWY-5121: superpathway of geranylgeranyl diphosphate biosynthesis II (via MEP)	39.92534701	−1.094952419	0.003983	0.081003	c2c1
PWY-5384: sucrose degradation IV (sucrose phosphorylase)	6.824519225	−3.287493629	0.0009	0.061079	c2c1
PWY-6147: 6-hydroxymethyl-dihydropterin diphosphate biosynthesis I	54.32244565	−0.893067591	0.002654	0.074673	c2c1
PWY-6167: flavin biosynthesis II (archaea)	5.972757342	−5.596005317	0.005971	0.098575	c2c1
PWY-6270: isoprene biosynthesis I	88.15679759	−1.066870021	0.006642	0.098575	c2c1
PWY-6859: all-trans-farnesol biosynthesis	4.012058217	−3.717715695	0.001083	0.061079	c2c1
PWY-7392: taxadiene biosynthesis (engineered)	9.386270018	−3.60306079	0.000283	0.042061	c2c1
PWY-7560: methylerythritol phosphate pathway II	79.44418324	−1.069297573	0.007032	0.099156	c2c1
ANAEROFRUCAT-PWY: homolactic fermentation	143.8794075	0.779635572	0.0046	0.097618	c2c3
COLANSYN-PWY: colanic acid building blocks biosynthesis	35.8384929	1.550221291	0.0044	0.097618	c2c3
HEXITOLDEGSUPER-PWY: superpathway of hexitol degradation (bacteria)	54.54908312	0.909153433	0.002063	0.066483	c2c3
OANTIGEN-PWY: O-antigen building blocks biosynthesis (*E. coli*)	99.70191306	−1.121948089	0.006771	0.097618	c2c3
PHOSLIPSYN-PWY: superpathway of phospholipid biosynthesis I (bacteria)	70.46008483	1.331355977	0.001855	0.066483	c2c3
PWY4FS-7: phosphatidylglycerol biosynthesis I (plastidic)	51.5490991	1.391404667	0.006811	0.097618	c2c3
PWY-5101: L-isoleucine biosynthesis II	66.49625492	1.214578922	0.005292	0.097618	c2c3
PWY-6168: flavin biosynthesis III (fungi)	172.2879499	0.689038903	0.005629	0.097618	c2c3
PWY-7323: superpathway of GDP-mannose-derived O-antigen building blocks biosynthesis	25.89416668	1.771497516	0.002522	0.067784	c2c3
UDPNAGSYN-PWY: UDP-N-acetyl-D-glucosamine biosynthesis I	67.18613175	−1.506925835	0.001515	0.066483	c2c3
ARG+POLYAMINE-SYN: super pathway of arginine and polyamine biosynthesis	69.58601257	−0.960789029	0.000298	0.042061	c2c1
ARG+POLYAMINE-SYN: super pathway of arginine and polyamine biosynthesis	69.58601257	−1.05230553	0.000918	0.066483	c2c3
ARGININE-SYN4-PWY: L-ornithine de novo biosynthesis	91.08538996	1.466876718	0.001004	0.066483	c2c3
ARGININE-SYN4-PWY: L-ornithine de novo biosynthesis	91.08538996	1.144773909	0.001917	0.069068	c2c1
PWY-6471: peptidoglycan biosynthesis IV (Enterococcus faecium)	10.68397596	−2.509515632	0.004524	0.081003	c2c1
PWY-6471: peptidoglycan biosynthesis IV (Enterococcus faecium)	10.68397596	−3.293509459	0.001507	0.066483	c2c3
PYRIDOXSYN-PWY: pyridoxal 5-phosphate biosynthesis I	83.95260245	1.49487838	0.002165	0.066483	c2c3
PYRIDOXSYN-PWY: pyridoxal 5-phosphate biosynthesis I	83.95260245	1.201030452	0.002913	0.074673	c2c1

Abbreviation: adj, adjusted.

Supplementary Table S8. List of Differentially Expressed Genes that Are Differentially Abundant between Different Subgroups in the Cohort

Ensembl_Gene_ID	Base Mean	Log_2 Fold Change	*P*adj	Gene Name	Comparison Pair
ENSG00000155966	70.519	3.74964	0.000392968	*AFF2*	c3c1
ENSG00000233680	35.444	3.02891	0.001437268	*HNRNPA1P27*	c2c1
ENSG00000187527	19.131	2.03977	0.049354713	*ATP13A5*	c2c3
ENSG00000214671	84.817	0.83427	0.022303138	*RPL6P12*	c2c1
ENSG00000214595	713.756	1.01421	0.018629526	*EML6*	c3c1
ENSG00000173040	124.774	−0.84891	0.038601379	*EVC2*	c2c3
ENSG00000238025	58.599	−1.37982	0.039362413	*ZDHHC4P1*	c2c1
ENSG00000162897	190.900	1.35991	0.02346219	*FCAMR*	c3c1
ENSG00000086205	10.244	−2.40497	0.000829552	*FOLH1*	c2c3
ENSG00000181867	0.673	−20.54710	0.000897703	*FTMT*	c2c1
ENSG00000158089	21.123	2.26847	0.013980259	*GALNT14*	c3c1
ENSG00000274618	372.111	1.52264	0.008495718	*HIST1H4F*	c3c1
ENSG00000166736	16.410	−3.99495	0.032119336	*HTR3A*	c2c3
ENSG00000166736	16.410	3.54715	0.013195954	*HTR3A*	c3c1
ENSG00000241244	319.624	−1.36024	0.020133239	*IGKV1D-16*	c2c3
ENSG00000129451	40.860	−4.35734	0.035837072	*KLK10*	c2c3
ENSG00000129451	40.860	3.74074	0.025102134	*KLK10*	c3c1
ENSG00000225128	0.677	23.60138	0.005620613	*LINC00972*	c2c3
ENSG00000225128	0.677	−17.31295	0.038958367	*LINC00972*	c3c1
ENSG00000182333	0.399	12.17337	0.003881171	*LIPF*	c2c3
ENSG00000264251	0.669	10.28858	0.024886441	*RN7SL819P*	c2c3
ENSG00000182333	0.399	−12.36307	5.74E−05	*LIPF*	c3c1
ENSG00000249333	0.470	−14.41122	1.34E−06	*LL22NC03-23C6.12*	c2c1
ENSG00000234031	27.687	1.34310	0.039573133	*RPS3AP44*	c2c3
ENSG00000249333	0.470	−16.86785	1.46E−05	*LL22NC03-23C6.12*	c2c3
ENSG00000271765	63.342	0.91097	0.038601379	*RN7SKP299*	c2c3
ENSG00000118308	1,060.651	1.25761	0.049743284	*LRMP*	c3c1
ENSG00000266276	0.285	−17.22075	0.004989858	*MIR4743*	c3c1
ENSG00000240666	3.840	−5.06250	0.015579404	*MME-AS1*	c2c3
ENSG00000228232	975.118	−1.27782	0.014609163	*GAPDHP1*	c2c3
ENSG00000215182	291.333	−4.57590	0.005872574	*MUC5AC*	c2c3
ENSG00000215182	291.333	4.07199	0.002093636	*MUC5AC*	c3c1
ENSG00000185697	288.454	1.51200	0.012506363	*MYBL1*	c3c1
ENSG00000160505	11.579	−5.48847	0.008074731	*NLRP4*	c2c3
ENSG00000265018	49.486	−2.47429	0.009651198	*AGAP12P*	c2c3
ENSG00000160505	11.579	4.54221	0.006739737	*NLRP4*	c3c1
ENSG00000163545	1,334.424	−0.72970	0.030687143	*NUAK2*	c2c3
ENSG00000278561	12.597	−3.56800	0.024920457	*PTPN20CP*	c2c3
ENSG00000189233	376.826	−1.37169	0.015794615	*NUGGC*	c2c3
ENSG00000160191	3,535.762	1.00276	0.026512132	*PDE9A*	c2c1
ENSG00000236717	0.463	−23.22885	6.47E−16	*RP11-100G15.10*	c2c1
ENSG00000236717	0.463	−23.12038	1.84E−08	*RP11-100G15.10*	c2c3
ENSG00000231090	0.555	−13.99578	7.79E−05	*RP11-101C11.1*	c2c1
ENSG00000231090	0.555	−17.07458	0.000194189	*RP11-101C11.1*	c2c3
ENSG00000257513	3.422	−4.72468	0.008074731	*NPIPB1P*	c2c3
ENSG00000272988	0.267	−15.44717	0.023939688	*RP11-150D20.5*	c3c1
ENSG00000259772	165.237	−0.83726	0.011698659	*RP11-16E12.2*	c2c3
ENSG00000282950	0.907	−26.60203	6.09E−05	*RP11-174O3.6*	c2c3
ENSG00000260303	23.670	−4.86844	0.01227057	*RP11-203B7.2*	c2c3
ENSG00000260303	23.670	4.12079	0.010443355	*RP11-203B7.2*	c3c1
ENSG00000258675	0.457	−12.87191	0.006683019	*RP11-299L17.3*	c3c1
ENSG00000275314	0.741	10.03950	0.024849813	*RP11-32A1.2*	c2c3
ENSG00000275314	0.741	−10.90604	0.000262234	*RP11-32A1.2*	c3c1
ENSG00000259476	1.221	13.39380	0.001571351	*RP11-50C13.2*	c2c3
ENSG00000259476	1.221	−13.63577	2.56E−05	*RP11-50C13.2*	c3c1
ENSG00000206532	8.420	−3.15479	0.04914993	*RP11-553A10.1*	c2c3
ENSG00000249877	3.764	−13.38306	0.010980955	*RP11-706F1.2*	c3c1

(*continued*)

Supplementary Table S8. Continued

Ensembl_Gene_ID	Base Mean	Log_2 Fold Change	*P*adj	Gene Name	Comparison Pair
ENSG00000280022	44.512	−5.02298	0.001165293	*RP11-707O23.1*	c2c1
ENSG00000258962	113.659	2.06291	0.004479337	*RP11-747H7.1*	c2c1
ENSG00000260711	1,768.668	1.06849	0.039573133	*RP11-747H7.3*	c2c3
ENSG00000203620	0.321	13.96751	0.032593228	*RP11-84A19.2*	c2c3
ENSG00000203620	0.321	−13.23645	0.008565686	*RP11-84A19.2*	c3c1
ENSG00000231654	8.334	−2.42875	0.024773164	*RPS6KA2-AS1*	c2c1
ENSG00000170054	54.004	6.27792	0.001444378	*SERPINA9*	c3c1
ENSG00000142583	152.205	1.50167	0.008107758	*SLC2A5*	c3c1
ENSG00000243770	14.943	−1.76051	0.02152624	*RN7SL65P*	c3c1
ENSG00000198203	1,020.018	−1.26205	0.000897703	*SULT1C2*	c2c1
ENSG00000198203	1,020.018	−1.24560	0.049945372	*SULT1C2*	c2c3
ENSG00000196228	130.871	−1.37044	0.006397675	*SULT1C3*	c2c1
ENSG00000157303	105.695	1.10998	0.013195954	*SUSD3*	c3c1
ENSG00000187621	53.221	2.55063	0.013195954	*TCL6*	c3c1
ENSG00000088992	54.739	1.29575	0.013195954	*TESC*	c3c1
ENSG00000160182	2,794.990	1.52164	0.038058354	*TFF1*	c3c1
ENSG00000160181	62.719	1.80337	0.021301346	*TFF2*	c3c1
ENSG00000169903	40.103	3.38885	0.012506363	*TM4SF4*	c3c1
ENSG00000275154	16.556	2.73116	0.024773164	*U3*	c2c1
ENSG00000175567	592.509	−0.78874	0.006712427	*UCP2*	c2c3
ENSG00000112303	146.742	−1.84313	0.027895978	*VNN2*	c2c3
ENSG00000112303	146.742	1.50589	0.040547819	*VNN2*	c3c1
ENSG00000101842	47.686	−2.79232	0.049611364	*VSIG1*	c2c3
ENSG00000101842	47.686	2.42312	0.034021561	*VSIG1*	c3c1
ENSG00000158023	52.914	1.39125	0.012506363	*WDR66*	c3c1

Abbreviations: adj, adjusted; ID, identification.

Supplementary Table S9. Comparison of Immune Profiles from Flow Cytometry and Cibersort among Different Psoriasis Subgroups

		AVG ± SD				Significance (Wilcox Test)					
Data Source	**Immune Population**	**Healthy**	**PSO1**	**PSO2**	**PSO3**	**Healthy Versus PSO1**	**Healthy Versus PSO2**	**Healthy Versus PSO3**	**PSO1 Versus PSO2**	**PSO1 Versus PSO3**	**PSO2 Versus PSO3**
Immunephenotype	Teff (CD3+ CD4+ CD25− FoxP3−)	80.49 ± 5.98%	83.33 ± 3.15%	83.49 ± 3.71%	80.8 ± 3.29%	n.s.	n.s.	n.s.	n.s.	n.s.	n.s.
	Active Teff (CD3+ CD4+ CD25+ FoxP3− CD38+ HLADR+)	0.13 ± 0.09%	0.27 ± 0.26%	0.09 ± 0.03%	0.36 ± 0.25%	n.s.	n.s.	0.035	n.s.	n.s.	0.024
	Memory Teff (CD3+ CD4+ CD25− FoxP3− CD45RO+)	33.72 ± 10.14%	34.55 ± 13.64%	35.81 ± 12.12%	36.3 ± 10.2%	n.s.	n.s.	n.s.	n.s.	n.s.	n.s.
	Active memory Teff (CD3+ CD4+ CD25− FoxP3− CD45RO+ CD38+ HLADR+)	0.31 ± 0.34%	0.55 ± 0.55%	0.18 ± 0.08%	0.67 ± 0.56%	n.s.	n.s.	n.s.	0.018	n.s.	0.02
	Tregs (CD3+ CD4+ CD25+ FoxP3+)	6.46 ± 2.66%	5.81 ± 1.03%	6.13 ± 1.22%	6.53 ± 1.26%	n.s.	n.s.	n.s.	n.s.	n.s.	n.s.
	Activated Tregs (CD3+ CD4+ CD25+ FoxP3+, CD45RO+)	70.65 ± 11.6%	67.99 ± 9.84%	66.94 ± 10.33%	69.95 ± 6.3%	n.s.	n.s.	n.s.	n.s.	n.s.	n.s.
Cytokine production	Teff (CD3+ CD4+ CD127+)	58.51 ± 15.43%	52.79 ± 18.71%	58.85 ± 10.83%	39.48 ± 18.33%	n.s.	n.s.	0.02	n.s.	n.s.	0.04
	Teff IL17+ only	0.93 ± 0.87%	1.1 ± 1.56%	0.78 ± 0.53%	1.11 ± 0.5%	n.s.	n.s.	n.s.	n.s.	n.s.	n.s.
	Teff IL22+ only	0.66 ± 0.51%	0.68 ± 0.39%	1.75 ± 2%	0.89 ± 0.58%	n.s.	n.s.	n.s.	n.s.	n.s.	n.s.
	Teff IL17+ IL22+	0.13 ± 0.15%	0.15 ± 0.16%	0.32 ± 0.41%	0.15 ± 0.06%	n.s.	n.s.	n.s.	n.s.	n.s.	n.s.
	Teff TNF-α+ only	0.69 ± 0.77%	0.84 ± 0.87%	1.28 ± 1.37%	0.6 ± 0.21%	n.s.	n.s.	n.s.	n.s.	n.s.	n.s.
	Teff IFNγ+ only	10.73 ± 3.92%	11 ± 4.07%	12.02 ± 7.43%	11.81 ± 4.17%	n.s.	n.s.	n.s.	n.s.	n.s.	n.s.
	Teff TNF-α+ IFNγ+	0.63 ± 0.71%	0.44 ± 0.3%	1 ± 1.64%	0.44 ± 0.23%	n.s.	n.s.	n.s.	n.s.	n.s.	n.s.
CIBERSORTx	Th1	0.02 ± 0.02%	0.01 ± 0.01%	0.03 ± 0.02%	0.02 ± 0.02%	n.s.	n.s.	n.s.	0.012	n.s.	n.s.
	Th17	0.08 ± 0.02%	0.08 ± 0.02%	0.09 ± 0.02%	0.09 ± 0.03%	n.s.	n.s.	n.s.	n.s.	n.s.	n.s.
	Treg	0.05 ± 0%	0.05 ± 0%	0.05 ± 0.01%	0.06 ± 0.01%	n.s.	n.s.	n.s.	n.s.	n.s.	0.02
	Tcm	0.02 ± 0%	0.02 ± 0%	0.02 ± 0%	0.02 ± 0%	n.s.	n.s.	n.s.	n.s.	n.s.	n.s.
	Tfh	0.01 ± 0%	0.01 ± 0%	0.01 ± 0%	0.01 ± 0%	n.s.	n.s.	n.s.	n.s.	n.s.	n.s.
	Activated CD4 T	0.14 ± 0.03%	0.14 ± 0.02%	0.14 ± 0.02%	0.11 ± 0.01%	n.s.	n.s.	0.014	n.s.	0.024	0.02

Immunephenotype	CD8(CD3+ CD8+)	30.19 ± 10.33%	32.09 ± 12.33%	24.66 ± 9.14%	31 ± 12.52%	n.s.	n.s.	n.s.	n.s.	n.s.	n.s.
	Active CD8 (CD3+ CD8+ CD38+ HLADR+)	0.52 ± 0.28%	1.3 ± 1.65%	0.44 ± 0.25%	1.09 ± 0.81%	n.s.	n.s.	n.s.	n.s.	n.s.	n.s.
	Memory CD8 (CD3+ CD8+ CD45RO+)	15.36 ± 6.22%	15.57 ± 8.13%	25.34 ± 6.52%	16.45 ± 6.41%	n.s.	0.002	n.s.	0.02	n.s.	0.029
	Activated memory CD8 (CD3+ CD8+ CD45RO+ CD38+ HLADR+)	2.04 ± 1.61%	3.5 ± 4.8%	1.18 ± 1.01%	3.09 ± 1.81%	n.s.	n.s.	n.s.	n.s.	n.s.	0.04
Cytokine production	CD8 (CD3+ CD8+)	27.21 ± 10.1%	30.32 ± 12.55%	23.69 ± 9.09%	27.08 ± 13.52%	n.s.	n.s.	n.s.	n.s.	n.s.	n.s.
	CD8+ IL17+ only	0.12 ± 0.08%	0.15 ± 0.08%	0.28 ± 0.36%	0.17 ± 0.08%	n.s.	n.s.	n.s.	n.s.	n.s.	n.s.
	CD8+ IL22+ only	0.14 ± 0.19%	0.07 ± 0.06%	0.47 ± 0.64%	0.08 ± 0.04%	n.s.	n.s.	n.s.	0.023	n.s.	n.s.
	CD8+ IL17+ IL22+	0.02 ± 0.01%	0.02 ± 0.01%	0.15 ± 0.2%	0.02 ± 0.03%	n.s.	n.s.	n.s.	n.s.	n.s.	n.s.
	CD8+ TNF-α+ only	0.04 ± 0.07%	0.09 ± 0.22%	0.14 ± 0.18%	0.06 ± 0.06%	n.s.	n.s.	n.s.	n.s.	n.s.	n.s.
	CD8+ IFNγ+ only	16.47 ± 7.85%	16.09 ± 9.52%	20.17 ± 12.71%	20.45 ± 8.55%	n.s.	n.s.	n.s.	n.s.	n.s.	n.s.
	CD8+ TNF-α+ IFNγ+	0.4 ± 0.29%	0.35 ± 0.35%	0.46 ± 0.65%	0.66 ± 0.58%	n.s.	n.s.	n.s.	n.s.	n.s.	n.s.
CIBERSORTx	CD8 T	0.00375 ± 0.0065%	0.00326 ± 0.00408%	0.00053 ± 0.00133%	0.01483 ± 0.01089%	n.s.	n.s.	0.026	0.043	0.042	0.011

Abbreviations: AVG, average; n.s., not significant; Tcm, T central memory; Teff, effector T cell; tfh, T follicular helper; Th, T helper; Treg, regulatory T cell.

Supplementary Table S10. Summary of Datasets Used in Multiomic Analysis

Dataset	Measurement Type	Inclusion Criteria	No. of Features Included	Normalization Method
Microbial spp. (n = 40)	Shotgun metagenomics from stool samples	Nonzero counts in at least 10 samples	142	Counts per million
Microbial UniRef90 gene families (n = 40)	Shotgun metagenomics from stool samples	At least three counts for 80% of all metagenomics samples (total is 52 samples)	2,488	Counts per million
Microbial MetaCyc pathways (n = 40)	Shotgun metagenomics from stool samples	All metacyc pathways identified by humann2	334	Counts per million
Flow cell population (n = 40)	Flow cytometry from PBMCs	Include all data collected	25	Percentage of parental gate
Flow cytokine production (n = 40)	Flow cytometry from PBMCs	Include all data collected	29	Percentage of parental gate
Host RNA-seq (n = 40)	RNA-seq from sigmoidal colon biopsies	Top 500 most variable genes + all DE genes identified by either disease comparison or PSO subgroup comparisons + inflammatory genes	601	vst transformation to ensure variance is constant across the data

Abbreviations: DE, differentially expressed; No., number; PSO, psoriasis; RNA-seq, RNA sequencing; vst, variance stabilizing transformation.

Supplementary Table S11. List of Significant Associations in Host Microbial Multiomics Network

From	To	Cor	*P*-Value	*P*adj	Greedy Membership
Significant associations in health-associated network					
s__Catenibacterium_mitsuokai	CD8_TNFa_only	0.80837	0.000118	0.047311	1
PWY4FS-7: phosphatidylglycerol biosynthesis I (plastidic)	Teff_IFNg_Only	0.643956	0.00019	0.095866	
PWY4FS-8: phosphatidylglycerol biosynthesis II (non-plastidic)	Teff_IFNg_Only	0.643956	0.00019	0.095866	
PWY4FS-7: phosphatidylglycerol biosynthesis I (plastidic)	Teff_TNFa_INFg	0.621978	1.49E−06	0.003106	
PWY4FS-8: phosphatidylglycerol biosynthesis II (non-plastidic)	Teff_TNFa_INFg	0.621978	1.49E−06	0.003106	
CD8_TNFa_only	IL1R2	−0.68647	2.35E−06	0.006511	
s__Catenibacterium_mitsuokai	NOS2	0.805281	0.000223	0.096093	
Teff_TNFa_INFg	NOS2	0.775824	0.000257	0.091006	
CD8_TNFa_only	ST6GAL2	−0.64466	3.23E−05	0.030873	
s__Catenibacterium_mitsuokai	ST6GAL2	−0.66447	4.78E−06	0.005155	
PHOSLIPSYN-PWY: superpathway of phospholipid biosynthesis I (bacteria)	CD8_IFNg_only	0.767033	0.000162	0.092121	2
Treg_INFg_only	CCDC144A	0.749451	0.000105	0.062263	
Treg_INFg_only	RP11-219A15.1	0.796066	2.5E−05	0.02777	
CD8_IFNg_only	RP11-336A10.5	0.818482	2.1E−05	0.02777	
CD8_IL22_only	RP11-336A10.5	0.752476	0.000181	0.080494	
Treg_INFg_only	RP11-336A10.5	0.673268	0.000104	0.062263	
Treg_TNFa_IFNg	RP11-336A10.5	0.790289	0.000219	0.088193	
Treg_INFg_only	USP32P1	0.783672	0.000112	0.06403	
PWY-6125: superpathway of guanosine nucleotides de novo biosynthesis II	activated.memory.Teff	0.686469	0.000357	0.021066	3
PWY-7184: pyrimidine deoxyribonucleotides de novo biosynthesis I	activated.memory.Teff	0.638767	0.000445	0.025005	
PWY-7197: pyrimidine deoxyribonucleotide phosphorylation	activated.memory.Teff	0.613862	0.001624	0.073648	
s__Escherichia_coli	activated.memory.Teff	0.60066	1.89E−05	0.003131	
FUC-RHAMCAT-PWY: super pathway of fucose and rhamnose degradation	Active.Teff	0.786207	0.001056	0.051489	
PWY-6125: super pathway of guanosine nucleotides de novo biosynthesis II	Active.Teff	0.63631	0.001602	0.073212	
PWY-6628: superpathway of L-phenylalanine biosynthesis	Active.Teff	0.728019	7.38E−06	0.0016	
s__Escherichia_coli	Active.Teff	0.660784	8.59E−06	0.001669	
UniRef90_K6B179: NO_NAME	Active.Teff	0.604715	1.58E−06	0.041485	
s__Eubacterium_ventriosum	IGLV8-61	−0.73511	0.000141	0.073261	4
s__Ruminococcus_obeum	IGLV8-61	−0.6	0.000147	0.0755	
UniRef90_A5ZMH0: NO_NAME	IGLV8-61	−0.81588	2.75E−06	0.065021	
UniRef90_D4LLH7: ATPases involved in chromosome partitioning	IGLV8-61	−0.76686	3.19E−06	0.070247	
UniRef90_R6S2S2: Ketol-acid reductoisomerase	IGLV8-61	−0.71356	5.13E−06	0.091049	
GLYCOLYSIS: glycolysis I (from glucose 6-phosphate)	memory.CD8	0.78022	0.000181	0.011891	5
PWY-5484: glycolysis II (from fructose 6-phosphate)	memory.CD8	0.789011	0.000203	0.013021	
UniRef90_D4M0P1: ADP-ribose pyrophosphatase	memory.CD8	0.899252	1.03E−05	0.087323	
NONOXIPENT-PWY: pentose phosphate pathway (non-oxidative branch)	RP11-716A19.3	0.61012	7.69E−06	0.031569	6
UniRef90_R7JV77: NO_NAME	RP11-716A19.3	0.610793	4.62E−06	0.086393	
NONOXIPENT-PWY: pentose phosphate pathway (non-oxidative branch)	RP4-672N11.1	0.61012	7.69E−06	0.031569	
UniRef90_R7JV77: NO_NAME	RP4-672N11.1	0.610793	4.62E−06	0.086393	
PPGPPMET-PWY: ppGpp biosynthesis	activated.memory.CD8	0.601323	0.001952	0.08521	7
PWY-821: superpathway of sulfur amino acid biosynthesis (Saccharomyces cerevisiae)	activated.memory.CD8	0.686806	7.64E−05	0.006382	

(*continued*)

Supplementary Table S11. Continued

From	To	Cor	*P*-Value	*P*adj	Greedy Membership
NONMEVIPP-PWY: methylerythritol phosphate pathway I	ADGRG7	0.868132	2.01E−05	0.062622	8
s__Prevotella_copri	ADGRG7	0.871288	3.52E−05	0.0262	
GLUCUROCAT-PWY: superpathway of β-D-glucuronide and D-glucuronate degradation	SULT1C2	−0.92527	2.97E−05	0.078414	9
UniRef90_D4K8E3: Predicted phosphatase homologous to the C-terminal domain of histone macroH2A1	SULT1C2	−0.9083	7.16E−07	0.027384	
CD8_Immune.function	ZG16	0.732674	0.000189	0.080761	10
CD8_Immune.Pop	ZG16	0.767033	3.68E−05	0.065578	
UniRef90_C7H1R7: NO_NAME	MST1L	−0.90309	1.41E−06	0.040723	11
UniRef90_C7H1R7: NO_NAME	MST1P2	−0.89428	3.41E−07	0.020076	
s__Eubacterium_hallii	AP000350.5	0.91339	9.22E−05	0.05574	12
s__Eubacterium_hallii	AP000350.6	0.792502	0.000112	0.062974	
UniRef90_D4K1Q8: Predicted integral membrane protein	HELLPAR	0.719472	1.51E−06	0.04237	13
UniRef90_E2ZN70: NO_NAME	HELLPAR	0.803967	4.87E−06	0.089006	
s__Bacteroides_dorei	LL22NC03-23C6.12	0.61662	7.52E−05	0.049355	14
s__Bacteroides_dorei	RP11-174O3.6	0.604902	9.1E−05	0.055665	
UniRef90_G2SYP7: NO_NAME	RP11-745A24.3	0.704199	2.9E−06	0.065432	15
UniRef90_G2T527: Filamentation induced by cAMP protein Fic	RP11-745A24.3	0.72507	3.86E−06	0.07883	
Teff_TNFa_only	IGHV6-1	−0.80968	2.48E−05	0.02777	16
Teff_TNFa_only	REG1A	0.610445	7.99E−05	0.062263	
PWY-7219: adenosine ribonucleotides de novo biosynthesis	ITGA2	−0.91969	2.74E−05	0.076724	17
s__Dorea_formicigenerans	Teff_Immune.Pop	−0.91209	0.000234	0.020021	18
Treg_IL17_IL22	IGLV2-18	−0.76005	0.000208	0.086495	19
CD8_TNFa_IFNg	TM4SF1	−0.65714	0.000312	0.098059	20
UniRef90_R6LGS5: NO_NAME	AC131056.3	−0.89989	2.79E−06	0.065021	21
ILC3	IGHD	0.748352	7.96E−06	0.018936	22
UniRef90_R5TP61: 50S ribosomal protein L30	IGHV3-33	−0.70751	1.16E−06	0.036628	23
UniRef90_R9HTU6: NO_NAME	FTMT	0.612826	1.82E−07	0.012321	24
PWY-5177: glutaryl-CoA degradation	CDA	0.816282	1.43E−05	0.049172	25
s__Ruminococcus_lactaris	EML6	0.76199	4.06E−05	0.029981	26
PWY-7328: superpathway of UDP-glucose-derived O-antigen building blocks biosynthesis	IL17F	0.780793	2.95E−05	0.078414	27
UniRef90_D4KCX5: Rhamnulose-1-phosphate aldolase	CD177P1	0.963551	2.32E−06	0.056574	28
PWY0-1061: superpathway of L-alanine biosynthesis	CD8_IL17_only	0.760754	4.74E−06	0.006165	29
s__Ruminococcus_sp_5_1_39BFAA	CD19	0.781079	0.000124	0.066737	30

(*continued*)

Supplementary Table S11. Continued

From	To	Cor	*P*-Value	*P*adj	Greedy Membership
Significant associations in psoriasis-associated network					
1CMET2-PWY: N10-formyl-tetrahydrofolate biosynthesis	GAPDHP1	−0.6841	9.75E−05	0.064441	1
ARGININE-SYN4-PWY: L-ornithine de novo biosynthesis	GAPDHP1	−0.7126	2.17E−05	0.023794	
PWY-3841: folate transformations II	GAPDHP1	−0.65402	0.00017	0.092741	
PWY-5101: L-isoleucine biosynthesis II	GAPDHP1	−0.68194	0.000136	0.080946	
PWY-6353: purine nucleotides degradation II (aerobic)	GAPDHP1	0.663131	0.000167	0.091415	
PWY-7282: 4-amino-2-methyl-5-phosphomethylpyrimidine biosynthesis (yeast)	GAPDHP1	−0.69345	2.78E−05	0.027634	
PWY0-845: super pathway of pyridoxal 5-phosphate biosynthesis and salvage	GAPDHP1	−0.71761	9.73E−06	0.013577	
PYRIDOXSYN-PWY: pyridoxal 5-phosphate biosynthesis I	GAPDHP1	−0.71319	1.28E−05	0.01645	
UniRef90_A7V4G2: NO_NAME	GAPDHP1	−0.75316	5.57E−06	0.058996	
UniRef90_Q5LC85: Elongation factor 4	GAPDHP1	−0.75949	1.37E−06	0.02837	
UniRef90_Q5LES4: Sulfate adenylyltransferase subunit 2	GAPDHP1	−0.78468	1.2E−06	0.027047	
ARGININE-SYN4-PWY: L-ornithine de novo biosynthesis	MIR222HG	0.677723	0.000185	0.098183	
PWY-6703: preQ0 biosynthesis	MIR222HG	0.635198	0.000171	0.092877	
PWY0-845: super pathway of pyridoxal 5-phosphate biosynthesis and salvage	MIR222HG	0.697094	0.000186	0.098528	
s__Bacteroides_uniformis	MIR222HG	0.718291	8.08E−05	0.030159	
PWY-6353: purine nucleotides degradation II (aerobic)	MTND1P23	−0.73465	9.63E−05	0.06407	
s__Bacteroides_uniformis	NPIPB15	−0.60205	0.000127	0.043035	
PWY-6703: preQ0 biosynthesis	NUAK2	−0.69266	0.000187	0.098672	
ARGININE-SYN4-PWY: L-ornithine de novo biosynthesis	RN7SKP299	0.705078	0.000141	0.082044	
PWY-5101: L-isoleucine biosynthesis II	RN7SKP299	0.773598	1.22E−05	0.01603	
ARGININE-SYN4-PWY: L-ornithine de novo biosynthesis	RP11-16E12.2	−0.71602	0.000189	0.098755	
UniRef90_R5EN96: NO_NAME	AP001627.1	0.718549	7.47E−06	0.070498	2
UniRef90_R5ENA5: NO_NAME	AP001627.1	0.705786	5.84E−06	0.060871	
UniRef90_R5ENA9: NO_NAME	AP001627.1	0.651182	7.75E−06	0.072187	
UniRef90_R5ENB7: NO_NAME	AP001627.1	0.676065	4.98E−06	0.05694	
UniRef90_R5ENC3: NO_NAME	AP001627.1	0.695925	6.58E−06	0.065657	
UniRef90_R5END3: NO_NAME	AP001627.1	0.660024	8.62E−06	0.075666	
UniRef90_R5ENY1: NO_NAME	AP001627.1	0.678813	5.08E−06	0.057196	
UniRef90_R5ENZ3: NO_NAME	AP001627.1	0.660032	9.77E−06	0.080475	
UniRef90_R5EP09: NO_NAME	AP001627.1	0.607497	9.06E−06	0.077542	
UniRef90_R5ES58: NO_NAME	AP001627.1	0.712702	7.09E−06	0.068494	
UniRef90_R5ES70: NO_NAME	AP001627.1	0.698935	5.74E−06	0.06032	
UniRef90_R5ES82: NO_NAME	AP001627.1	0.726586	7.68E−06	0.072187	
UniRef90_R5EXU5: NO_NAME	AP001627.1	0.665197	7.19E−06	0.069054	
UniRef90_R5F071: NO_NAME	AP001627.1	0.690192	6.4E−06	0.064816	
UniRef90_R5F076: NO_NAME	AP001627.1	0.759732	4.82E−06	0.056148	
UniRef90_R5F1R6: NO_NAME	AP001627.1	0.669014	9.65E−06	0.080053	
UniRef90_R5F1S4: NO_NAME	AP001627.1	0.698402	5.46E−06	0.058301	
UniRef90_R5F1T5: NO_NAME	AP001627.1	0.677638	3.89E−06	0.051875	
UniRef90_R5VN00: NO_NAME	AP001627.1	0.707391	5.26E−06	0.057636	
UniRef90_C7H6T5: NO_NAME	CXCL1	0.607639	1.68E−07	0.006928	3
UniRef90_C7H6T5: NO_NAME	CXCL3	0.62271	3.3E−08	0.002159	
UniRef90_G2T376: NO_NAME	CXCL3	0.61847	9.73E−10	0.000185	
UniRef90_G2T5J9: NO_NAME	CXCL3	0.607058	2.91E−08	0.001971	

(*continued*)

Supplementary Table S11. Continued

From	To	Cor	*P*-Value	*P*adj	Greedy Membership
PWY-7196: superpathway of pyrimidine ribonucleosides salvage	Teff_IL17_IL22	0.703267	0.00045	0.078835	4
PWY-7196: superpathway of pyrimidine ribonucleosides salvage	Teff_IL17_only	0.62053	0.000127	0.064567	
PPGPPMET-PWY: ppGpp biosynthesis	Treg_IL17_only	0.607528	0.000525	0.085532	
PWY-7196: superpathway of pyrimidine ribonucleosides salvage	Treg_IL17_only	0.630174	0.000704	0.095585	
COLANSYN-PWY: colanic acid building blocks biosynthesis	IGHV3-30	−0.6278	0.000129	0.077505	5
PWY-7323: super pathway of GDP-mannose-derived O-antigen building blocks biosynthesis	IGHV3-30	−0.62012	5.2E−05	0.043212	
COLANSYN-PWY: colanic acid building blocks biosynthesis	RP11-16E12.2	−0.61959	0.00017	0.092741	
ANAGLYCOLYSIS-PWY: glycolysis III (from glucose)	IGHV2-70	−0.69299	2.94E−05	0.028746	6
CALVIN-PWY: Calvin-Benson-Bassham cycle	IGHV2-70	−0.75205	9.6E−06	0.01349	
NONOXIPENT-PWY: pentose phosphate pathway (non-oxidative branch)	IGHV2-70	−0.75603	1.87E−05	0.021434	
PWY-1042: glycolysis IV (plant cytosol)	IGHV2-70	−0.73312	2.18E−06	0.00494	
PWY-7242: D-fructuronate degradation	IGHV2-70	−0.69802	8.1E−05	0.056949	
COA-PWY: coenzyme A biosynthesis I	MTND2P28	−0.61331	1.79E−05	0.020776	7
FAO-PWY: fatty acid β-oxidation I	MTND2P28	−0.64143	2.21E−05	0.023794	
PWY-5100: pyruvate fermentation to acetate and lactate II	MTND2P28	−0.66359	5.47E−05	0.044043	
PWY-5136: fatty acid β-oxidation II (peroxisome)	MTND2P28	−0.61916	3.21E−05	0.030777	
PWY-1269: CMP-3-deoxy-D-manno-octulosonate biosynthesis I	Vd2	0.679672	0.000179	0.071033	8
PWY-1269: CMP-3-deoxy-D-manno-octulosonate biosynthesis I	Vd2T	0.661191	0.000251	0.022565	
PWY-1269: CMP-3-deoxy-D-manno-octulosonate biosynthesis I	IGHV2-26	−0.63313	0.000189	0.098755	
HEME-BIOSYNTHESIS-II: heme biosynthesis I (aerobic)	IGKV1-17	−0.74011	4.13E−05	0.036607	9
PWY-5918: super pathway of heme biosynthesis from glutamate	IGKV1-17	−0.71627	0.000159	0.087773	
s__Streptococcus_parasanguinis	KRTAP13-2	−0.6127	1.05E−05	0.006086	10
s__Streptococcus_parasanguinis	RN7SL65P	−0.62108	5.04E−06	0.003209	
s__Dorea_formicigenerans	CD8_TNFa_IFNg	0.651556	0.000876	0.036379	11
UniRef90_G1WU72: NO_NAME	CD8_TNFa_IFNg	0.641326	6.26E−05	0.083128	
PWY-5384: sucrose degradation IV (sucrose phosphorylase)	AGAP12P	0.660269	2.54E−05	0.026031	12
PWY-5384: sucrose degradation IV (sucrose phosphorylase)	NPIPB1P	0.648085	0.000185	0.098183	
UniRef90_C9YMF0: Sigma-24 (Feci)	IL1RN	0.810404	8.15E−06	0.074295	13
UniRef90_D4L1Z0: DNA-directed RNA polymerase specialized sigma subunit, sigma24 homolog	IL1RN	0.807528	7.07E−06	0.068494	
PWY-3001: super pathway of L-isoleucine biosynthesis I	Treg_TNFa_IFNg	−0.63367	0.000231	0.071033	14
THRESYN-PWY: super pathway of L-threonine biosynthesis	Treg_TNFa_IFNg	−0.72483	7.24E−05	0.050646	
P461-PWY: hexitol fermentation to lactate, formate, ethanol and acetate	SIGLEC12	0.722109	7.4E−05	0.053292	15
UniRef90_R6SAP9: Orotate phosphoribosyltransferase	SIGLEC12	0.743519	2.73E−06	0.040374	
FUC-RHAMCAT-PWY: super pathway of fucose and rhamnose degradation	RP11-693J15.5	0.622961	0.000178	0.095618	16
UniRef90_R5DXN6: NO_NAME	TMEM72	−0.6137	9.9E−06	0.081082	17

(*continued*)

Supplementary Table S11. Continued

From	To	Cor	*P*-Value	*P*adj	Greedy Membership
PWY-5695: urate biosynthesis/inosine 5-phosphate degradation	IGHV3-53	−0.7541	0.000161	0.088313	18
UniRef90_R5J0A8: Transposase IS605 OrfB family central region	SLC6A14	0.727059	9.13E−06	0.077542	19
UniRef90_R9HTU6: NO_NAME	RPL6P12	0.644934	1.12E−05	0.087267	20
UniRef90_D4K3E4: Desulfoferrodoxin ferrous iron-binding domain	IGLV5-45	0.677288	6.46E−06	0.065139	21
s__Odoribacter_splanchnicus	PCK1	−0.67833	4.84E−05	0.020322	22
UniRef90_C7H7L8: NO_NAME	LL22NC03-23C6.12	0.603595	6.12E−09	0.000802	23
Vd2T_TNFa_IFNg	KLK10	0.719637	7.31E−09	2.1E−05	24
UniRef90_C4ZEM9: NO_NAME	REG1A	0.653404	3.24E−07	0.010793	25
UniRef90_R5J281: NO_NAME	Treg_TNFa	0.66736	2.24E−07	0.004274	26
UniRef90_A8SCB2: NO_NAME	GSTA1	−0.64042	4E−06	0.052695	27
Treg_INFg_only	FOS	0.640109	1.57E−05	0.015843	28
PWY-5345: super pathway of L-methionine biosynthesis (by sulfhydrylation)	Teff_IFNg_Only	−0.67739	0.000424	0.078253	29
P185-PWY: formaldehyde assimilation III (dihydroxyacetone cycle)	IGLV4-60	−0.68048	9.42E−05	0.063081	30
UniRef90_V8CHB5: NO_NAME	DSG3	0.644924	2.65E−06	0.039778	31
PWY0-1296: purine ribonucleosides degradation	ALDH1L1	0.623461	0.000178	0.095618	32
HEMESYN2-PWY: heme biosynthesis II (anaerobic)	Teff_Immune.Pop	−0.6012	0.001917	0.065199	33
s__Alistipes_shahii	ADAMTS4	0.607468	0.000263	0.071968	34
s__Bacteroidales_bacterium_ph8	IL22	0.621457	1.92E−07	0.000212	35
Significant associations in PSO1-associated network					
activated.memory.CD8	RP11-299L17.3	0.650444	1.13E−06	0.00596	1
activated.nonMemory.CD8	RP11-299L17.3	0.650444	1.79E−07	0.001895	
activeCD8	RP11-299L17.3	0.650444	2.14E−06	0.007538	
UniRef90_D4JPG6: NO_NAME	RP11-299L17.3	0.65273	1.51E−06	0.090737	
UniRef90_U4D938: NO_NAME	RP11-299L17.3	0.651584	1.37E−07	0.030625	
UniRef90_D4LM01: Site-specific recombinase XerD	activated.memory.CD8	0.804932	0.000156	0.095101	
UniRef90_D4LWR3: RNA polymerase sigma factor, sigma-70 family	activated.memory.CD8	0.712285	1.54E−05	0.033677	
UniRef90_D4MWC2: Replication initiator protein A (RepA) N-terminus	activated.memory.CD8	0.642109	3.2E−05	0.047927	
UniRef90_U4D938: NO_NAME	activated.memory.CD8	0.612961	3.6E−05	0.047962	
UniRef90_D4LWR3: RNA polymerase sigma factor, sigma-70 family	activated.memory.Teff	0.648507	2.11E−05	0.038011	
UniRef90_C4Z761: Citrate synthase	activeCD8	0.617548	0.000109	0.08439	
UniRef90_G2T5D6: Glutathione synthase	activeCD8	0.624565	3.18E−05	0.047927	

(*continued*)

Supplementary Table S11. Continued

From	To	Cor	*P*-Value	*P*adj	Greedy Membership
s__Flavonifractor_plautii	activated.nonMemory.Teff	0.666676	6.31E−10	1.56E−07	2
s__Ruminococcus_sp_5_1_39BFAA	activated.nonMemory.Teff	0.616463	0.000705	0.069518	
UniRef90_C6JCI4: NO_NAME	activated.nonMemory.Teff	0.645614	0.000177	0.098154	
UniRef90_D4LLE0: Aldehyde dehydrogenase, molybdenum-binding subunit apoprotein	activated.nonMemory.Teff	0.660215	9.81E−05	0.082059	
UniRef90_R5HR90: NO_NAME	activated.nonMemory.Teff	0.635567	6.87E−05	0.069169	
UniRef90_R5HVG1: NO_NAME	activated.nonMemory.Teff	0.690686	1.74E−05	0.034534	
UniRef90_R5I7T7: ATP-dependent 6-phosphofructokinase	activated.nonMemory.Teff	0.695959	0.000192	0.098154	
UniRef90_R5XT20: Rhamnulose-1-phosphate aldolase	activated.nonMemory.Teff	0.706504	0.000132	0.092377	
UniRef90_R6GH13: NO_NAME	activated.nonMemory.Teff	0.731108	3.57E−05	0.047962	
UniRef90_R6PH30: NO_NAME	activated.nonMemory.Teff	0.682456	1.65E−05	0.034534	
UniRef90_R6Q745: NO_NAME	activated.nonMemory.Teff	0.742962	2.36E−05	0.040223	
UniRef90_R7CD60: NO_NAME	activated.nonMemory.Teff	0.695959	8.4E−05	0.076379	
UniRef90_R7CD72: NO_NAME	activated.nonMemory.Teff	0.695959	0.000145	0.092467	
UniRef90_R7CDD0: NO_NAME	activated.nonMemory.Teff	0.700709	0.000163	0.096324	
UniRef90_R7CGR6: NO_NAME	activated.nonMemory.Teff	0.685965	0.00013	0.092377	
UniRef90_R7CGS0: NO_NAME	activated.nonMemory.Teff	0.73592	0.000135	0.092377	
UniRef90_R7CGX0: Nicotinate phosphoribosyltransferase	activated.nonMemory.Teff	0.64437	0.000179	0.098154	
UniRef90_R7CGX6: NO_NAME	activated.nonMemory.Teff	0.607018	0.00012	0.09182	
UniRef90_R7CH88: NO_NAME	activated.nonMemory.Teff	0.697716	0.000174	0.098154	
UniRef90_R7CIC0: NO_NAME	activated.nonMemory.Teff	0.666676	0.000155	0.095101	
UniRef90_R7CIF8: NO_NAME	activated.nonMemory.Teff	0.64386	0.000128	0.092377	
UniRef90_R7CK52: NO_NAME	activated.nonMemory.Teff	0.741653	0.000141	0.092467	
UniRef90_R7CLQ2: Cyclic pyranopterin monophosphate synthase accessory protein	activated.nonMemory.Teff	0.674929	9.2E−05	0.080527	
UniRef90_R7CLX2: NO_NAME	activated.nonMemory.Teff	0.655537	0.000181	0.098154	
UniRef90_R7CPD9: NO_NAME	activated.nonMemory.Teff	0.652022	3.76E−05	0.048	
UniRef90_R7CPY8: NO_NAME	activated.nonMemory.Teff	0.721193	0.000124	0.092377	
UniRef90_R7CR35: ATP synthase	activated.nonMemory.Teff	0.698246	0.000102	0.082059	
UniRef90_R7CRE2: Acetylglutamate kinase	activated.nonMemory.Teff	0.700709	0.00019	0.098154	
UniRef90_R7CSG7: NO_NAME	activated.nonMemory.Teff	0.675439	8.46E−05	0.076379	
UniRef90_R7CSS1: NO_NAME	activated.nonMemory.Teff	0.734623	0.000134	0.092377	
UniRef90_R7DCE8: NO_NAME	activated.nonMemory.Teff	0.601055	5.27E−05	0.058851	
UniRef90_R7NEY7: Acetyltransferases	activated.nonMemory.Teff	0.625457	1.66E−06	0.008485	
UniRef90_T5LV87: IS605 OrfB family transposase	activated.nonMemory.Teff	0.624561	0.000135	0.092377	
UniRef90_T5M0M6: NO_NAME	activated.nonMemory.Teff	0.711034	6.03E−05	0.062774	

(*continued*)

Supplementary Table S11. Continued

From	To	Cor	*P*-Value	*P*adj	Greedy Membership
UniRef90_E1YTP4: NO_NAME	activated.nonMemory.Teff	0.790135	5.17E−07	0.003527	3
UniRef90_R7CII3: NO_NAME	activated.nonMemory.Teff	0.670823	0.000184	0.098154	
UniRef90_R7CQN6: TrkA-N domain-containing protein	activated.nonMemory.Teff	0.699664	0.000171	0.098154	
UniRef90_D4LQI2: Site-specific recombinases, DNA invertase Pin homologs	Teff_IL17_IL22	0.652583	2.91E−06	0.015436	
UniRef90_C6J953: NO_NAME	Teff_IL17_only	0.671967	1.62E−06	0.011888	
UniRef90_C6JBL1: NO_NAME	Teff_IL17_only	0.610238	4.71E−05	0.065888	
UniRef90_C6JEF2: NO_NAME	Teff_IL17_only	0.62527	2.19E−05	0.047594	
UniRef90_D4LQI1: Site-specific recombinases, DNA invertase Pin homologs	Teff_IL17_only	0.698422	4.94E−05	0.066521	
UniRef90_D4LQI2: Site-specific recombinases, DNA invertase Pin homologs	Teff_IL17_only	0.627224	3.5E−06	0.016735	
UniRef90_E1YTP4: NO_NAME	Teff_IL17_only	0.62082	6.42E−06	0.022067	
UniRef90_R5XAV3: Heavy-metal-associated domain	Teff_IL17_only	0.62566	9.01E−07	0.008609	
UniRef90_R7CFY1: NO_NAME	Teff_IL17_only	0.669696	2.91E−05	0.054164	
UniRef90_R7CHB7: Na+/H+ antiporter NhaC	Teff_IL17_only	0.811625	1.33E−05	0.035418	
UniRef90_R7CII3: NO_NAME	Teff_IL17_only	0.610643	0.000114	0.091508	
UniRef90_R7CMK6: NO_NAME	Teff_IL17_only	0.637328	1.29E−07	0.002051	
UniRef90_R7CN26: NO_NAME	Teff_IL17_only	0.666082	3.98E−06	0.017267	
UniRef90_R7CQN6: TrkA-N domain-containing protein	Teff_IL17_only	0.61839	0.00011	0.090629	
UniRef90_A5ZNM4: NO_NAME	Teff_IL17_IL22	0.734266	5.1E−06	0.019503	4
UniRef90_A5ZYV3: NO_NAME	Teff_IL17_IL22	0.706294	3.54E−05	0.06035	
UniRef90_A5ZYV6: NO_NAME	Teff_IL17_IL22	0.686516	2.57E−06	0.015322	
UniRef90_C6JC21: NO_NAME	Teff_IL17_IL22	0.607808	6.47E−06	0.022067	
UniRef90_D4JAB3: Glyoxalase/Bleomycin resistance protein/Dioxygenase superfamily	Teff_IL17_IL22	0.794387	0.000109	0.090629	
UniRef90_D4LKT7: 50S ribosomal protein L7/L12	Teff_IL17_IL22	0.684624	0.000117	0.091508	
UniRef90_D4LRE4: Transcriptional regulator, BadM/Rrf2 family	Teff_IL17_IL22	0.666693	9.86E−05	0.086726	
UniRef90_D4LVZ1: Predicted transcriptional regulators	Teff_IL17_IL22	0.766035	8.23E−07	0.008609	
UniRef90_D4MTV2: Transcriptional regulator, MerR family	Teff_IL17_IL22	0.713542	5.75E−05	0.073251	
UniRef90_D4MUD3: Transcriptional regulator, MarR family	Teff_IL17_IL22	0.729829	1.16E−06	0.009737	
UniRef90_F7JEX2: NO_NAME	Teff_IL17_IL22	0.711285	3.92E−06	0.017267	
UniRef90_R5Z6G3: NO_NAME	Teff_IL17_IL22	0.678483	2.85E−06	0.015436	
UniRef90_R7CCT5: NO_NAME	Teff_IL17_IL22	0.678393	0.000148	0.099236	
UniRef90_D4MUD3: Transcriptional regulator, MarR family	Teff_IL17_only	0.75747	8.66E−08	0.002044	
s__Bacteroides_thetaiotaomicron	CD300E	0.640982	2.63E−05	0.02332	5
UniRef90_G2T376: NO_NAME	CXCL2	0.735024	1.52E−06	0.090737	
s__Bacteroides_thetaiotaomicron	CXCL3	0.704029	3.68E−06	0.007238	
UniRef90_G2T376: NO_NAME	CXCL3	0.699686	6.32E−07	0.045297	
UniRef90_G2T5J9: NO_NAME	CXCL3	0.727956	7.33E−07	0.0507	
UniRef90_G2T376: NO_NAME	LRFN5	0.657281	4.08E−07	0.040956	
s__Bacteroides_thetaiotaomicron	SOCS3	0.704029	8.85E−05	0.050575	

(*continued*)

Supplementary Table S11. Continued

From	To	Cor	*P*-Value	*P*adj	Greedy Membership
UniRef90_D4LVH8: KaiC	activated.memory.CD8	0.78459	0.000144	0.092467	6
UniRef90_R9JXY1: 50S ribosomal protein L33	activated.nonMemory.Teff	0.648507	0.000165	0.096324	
UniRef90_A7B829: NO_NAME	Active.Teff	0.620145	0.000188	0.098154	
UniRef90_D4LVH8: KaiC	Active.Teff	0.697716	0.000175	0.098154	
UniRef90_G2T5D0: NO_NAME	Active.Teff	0.651408	0.000155	0.095101	
UniRef90_K1S8B5: Transcriptional regulator	Active.Teff	0.739437	0.000158	0.09531	
UniRef90_R9JXY1: 50S ribosomal protein L33	Active.Teff	0.669014	0.00014	0.092467	
UniRef90_U2PAU4: NO_NAME	Active.Teff	0.870181	5.14E−07	0.003527	
s__Barnesiella_intestinihominis	LL22NC03-23C6.12	0.651584	9.5E−05	0.052803	7
UniRef90_C7H7L9: ABC transporter, ATP-binding protein	LL22NC03-23C6.12	0.65273	2.34E−07	0.036053	
s__Barnesiella_intestinihominis	SERPINA9	0.747806	3.18E−05	0.026686	
s__Eubacterium_hallii	GSTA1	0.72028	0.000187	0.078443	8
UniRef90_E2ZGA1: NO_NAME	GSTA1	−0.82312	1.06E−06	0.071004	
s__Eubacterium_ventriosum	Vd2T_TNFa_only	0.797189	5.33E−05	0.006695	9
UniRef90_B0NZF6: NO_NAME	Vd2T_TNFa_only	0.64675	0.000105	0.090542	
UniRef90_D4M5F3: dTDP-glucose pyrophosphorylase	memory.Teff	−0.88422	0.000101	0.082059	10
UniRef90_D4M5F3: dTDP-glucose pyrophosphorylase	nonMemory.Teff	0.880707	5.17E−05	0.058792	
DZ_duration	CD8_IL17_IL22	0.654946	0.000478	0.040147	11
PWY-5104: L-isoleucine biosynthesis IV	DZ_duration	0.736492	0.000281	0.068952	
UniRef90_B0G2Q7: NO_NAME	Treg_IL17_IL22	0.776803	7.01E−05	0.077728	12
UniRef90_D4J5V6: Site-specific recombinase XerD	Treg_IL17_IL22	0.693832	9.86E−05	0.086726	
UniRef90_A5ZSX2: NO_NAME	CD8_TNFa_IFNg	0.907182	7.34E−05	0.077728	13
UniRef90_D4JAA1: Phage integrase family	CD8_TNFa_IFNg	0.795496	6.81E−05	0.077728	
s__Parabacteroides_distasonis	IL17A	0.649429	0.000219	0.085842	14
s__Parabacteroides_distasonis	LINC00939	0.751742	2.07E−05	0.020128	
s__Bacteroides_dorei	FOSB	0.605649	4.51E−05	0.033931	15
s__Bacteroides_dorei	Treg_IL22_only	0.643114	3.18E−05	0.004358	
Treg_INFg_only	RP11-301M17.1	0.650444	2.22E−06	0.009133	16
UniRef90_G2SYP7: NO_NAME	Teff_TNFa_only	0.704243	5.65E−06	0.020765	17
UniRef90_C4Z763: GTP pyrophosphokinase	Teff_TNFa_INFg	0.804196	0.000117	0.091508	18
PWY0-1297: superpathway of purine deoxyribonucleosides degradation	PASI	0.713137	1.85E−05	0.018036	19
UniRef90_C0FPA9: BAAT/acyl-CoA thioester hydrolase C-terminal domain protein	nonMemory.CD8	−0.87834	0.000123	0.092377	20
s__Alistipes_putredinis	CD55	0.881119	0.000117	0.059771	21
s__Dorea_formicigenerans	TRHDE	0.895105	4.16E−05	0.032046	22
s__Coprococcus_comes	CCDC85A	−0.63398	0.000222	0.086043	23
s__Lachnospiraceae_bacterium_3_1_46FAA	UCA1	0.609458	0.000162	0.072164	24
THRESYN-PWY: super pathway of L-threonine biosynthesis	Treg_TNFa_IFNg	−0.85365	7.05E−06	0.016049	25
UniRef90_C7H2P0: NO_NAME	CD8_TNFa_only	0.704029	8.19E−05	0.079819	26
s__Roseburia_inulinivorans	CD177	−0.83916	1.39E−06	0.003509	27
PYRIDNUCSAL-PWY: NAD salvage pathway I	URAD	0.882718	1.02E−07	0.005333	28

(*continued*)

Supplementary Table S11. Continued

From	To	Cor	*P*-Value	*P*adj	Greedy Membership
Significant associations in PSO2-associated network					
BIOTIN-BIOSYNTHESIS-PWY: biotin biosynthesis I	CYP2B7P	0.833333	2.98E−05	0.009035	1
FASYN-ELONG-PWY: fatty acid elongation – saturated	CYP2B7P	0.833333	1.4E−05	0.005053	
FASYN-INITIAL-PWY: super pathway of fatty acid biosynthesis initiation (*E. coli*)	CYP2B7P	0.826362	2.64E−05	0.008035	
GLUDEG-I-PWY: GABA shunt	CYP2B7P	0.714286	0.000278	0.074586	
PWY-5022: 4-aminobutanoate degradation V	CYP2B7P	0.714286	0.000334	0.087365	
PWY-5971: palmitate biosynthesis II (bacteria and plants)	CYP2B7P	0.833333	2.8E−05	0.008503	
PWY-6113: superpathway of mycolate biosynthesis	CYP2B7P	0.833333	4.57E−05	0.013734	
PWY-6282: palmitoleate biosynthesis I (from (5Z)-dodec-5-enoate)	CYP2B7P	0.833333	7.21E−05	0.021414	
PWY-6284: super pathway of unsaturated fatty acids biosynthesis (*E. coli*)	CYP2B7P	0.833333	4.07E−05	0.012269	
PWY-6519: 8-amino-7-oxononanoate biosynthesis I	CYP2B7P	0.833333	3.09E−05	0.009339	
PWY-7388: octanoyl-[acyl-carrier protein] biosynthesis (mitochondria, yeast)	CYP2B7P	0.833333	1.83E−05	0.006357	
PWY-7664: oleate biosynthesis IV (anaerobic)	CYP2B7P	0.833333	1.18E−05	0.004438	
PWY0-862: (5Z)-dodec-5-enoate biosynthesis	CYP2B7P	0.833333	2.54E−05	0.007747	
PWYG-321: mycolate biosynthesis	CYP2B7P	0.833333	1.31E−05	0.004806	
BIOTIN-BIOSYNTHESIS-PWY: biotin biosynthesis I	STC1	−0.7619	0.00013	0.03689	
FASYN-ELONG-PWY: fatty acid elongation – saturated	STC1	−0.7619	0.000173	0.047907	
FASYN-INITIAL-PWY: super pathway of fatty acid biosynthesis initiation (*E. coli*)	STC1	−0.7545	0.000271	0.073002	
PWY-5971: palmitate biosynthesis II (bacteria and plants)	STC1	−0.7619	0.000209	0.05735	
PWY-6113: super pathway of mycolate biosynthesis	STC1	−0.7619	0.000287	0.076805	
PWY-6282: palmitoleate biosynthesis I (from (5Z)-dodec-5-enoate)	STC1	−0.7619	0.00028	0.075069	
PWY-6284: super pathway of unsaturated fatty acids biosynthesis (*E. coli*)	STC1	−0.7619	0.000347	0.090509	
PWY-6519: 8-amino-7-oxononanoate biosynthesis I	STC1	−0.7619	0.0002	0.055236	
PWY-7388: octanoyl-[acyl-carrier protein] biosynthesis (mitochondria, yeast)	STC1	−0.7619	0.00016	0.044499	
PWY-7664: oleate biosynthesis IV (anaerobic)	STC1	−0.7619	0.000235	0.063921	
PWY0-862: (5Z)-dodec-5-enoate biosynthesis	STC1	−0.7619	0.000229	0.062421	
PWYG-321: mycolate biosynthesis	STC1	−0.7619	0.00012	0.0343	
s__Bacteroides_ovatus	Teff_TNFa_only	0.666667	0.000994	0.091836	2
s__Bacteroides_ovatus	Vd2T_IL17_only	0.761905	0.00021	0.043201	
UniRef90_C0FN95: NO_NAME	Vd2T_IL17_only	0.880952	5.48E−07	0.026184	
UniRef90_D6E3G6: Site-specific recombinase XerD	Vd2T_IL17_only	0.90368	1.25E−07	0.011927	
ANAEROFRUCAT-PWY: homolactic fermentation	FOS	−0.97619	0.000119	0.034027	3
GLYCOLYSIS: glycolysis I (from glucose 6-phosphate)	FOS	−0.95238	8.01E−05	0.023227	
PWY-5484: glycolysis II (from fructose 6-phosphate)	FOS	−0.95238	5.05E−05	0.015132	
ANAEROFRUCAT-PWY: homolactic fermentation	PDE4C	−0.90476	9.72E−05	0.028114	

(*continued*)

Supplementary Table S11. Continued

From	To	Cor	*P*-Value	*P*adj	Greedy Membership
ARGSYN-PWY: L-arginine biosynthesis I (via L-ornithine)	PASI	0.754505	0.001298	0.055236	4
PENTOSE-P-PWY: pentose phosphate pathway	PASI	0.833333	0.002607	0.055236	
PWY-5154: L-arginine biosynthesis III (via N-acetyl-L-citrulline)	PASI	0.785714	0.001279	0.055236	
PWY-7400: L-arginine biosynthesis IV (archaebacteria)	PASI	0.754505	0.001234	0.055236	
ARGSYN-PWY: L-arginine biosynthesis I (via L-ornithine)	XIST	−0.64672	7.14E−06	0.00271	
ARGSYNBSUB-PWY: L-arginine biosynthesis II (acetyl cycle)	XIST	−0.92857	4.15E−06	0.001618	
GLUTORN-PWY: L-ornithine biosynthesis	XIST	−0.6627	2.01E−07	9.8E−05	
PWY-5154: L-arginine biosynthesis III (via N-acetyl-L-citrulline)	XIST	−0.63474	1.07E−05	0.004031	
PWY-7400: L-arginine biosynthesis IV (archaebacteria)	XIST	−0.62655	1.07E−05	0.004046	
PWY-6121: 5-aminoimidazole ribonucleotide biosynthesis I	BMX	−0.95238	0.000205	0.056554	5
PWY-6122: 5-aminoimidazole ribonucleotide biosynthesis II	BMX	−0.97619	0.000225	0.061454	
PWY-6277: super pathway of 5-aminoimidazole ribonucleotide biosynthesis	BMX	−0.97619	0.000225	0.061454	
PWY-6121: 5-aminoimidazole ribonucleotide biosynthesis I	CCDC129	−0.88095	0.000105	0.030152	
PWY-6122: 5-aminoimidazole ribonucleotide biosynthesis II	CCDC129	−0.90476	0.000107	0.030556	
PWY-6277: superpathway of 5-aminoimidazole ribonucleotide biosynthesis	CCDC129	−0.90476	0.000107	0.030556	
PWY-6121: 5-aminoimidazole ribonucleotide biosynthesis I	SH2D6	−0.97619	2.49E−05	0.007595	
PWY-6122: 5-aminoimidazole ribonucleotide biosynthesis II	SH2D6	−0.95238	7.94E−05	0.023078	
PWY-6277: superpathway of 5-aminoimidazole ribonucleotide biosynthesis	SH2D6	−0.95238	7.94E−05	0.023078	
PWY-6121: 5-aminoimidazole ribonucleotide biosynthesis I	SH2D7	−0.95238	0.000325	0.085378	
PWY-6122: 5-aminoimidazole ribonucleotide biosynthesis II	SH2D7	−0.97619	0.000326	0.08554	
PWY-6277: super pathway of 5-aminoimidazole ribonucleotide biosynthesis	SH2D7	−0.97619	0.000326	0.08554	
P461-PWY: hexitol fermentation to lactate, formate, ethanol and acetate	MT1X	−0.85714	7.8E−05	0.022737	6
P461-PWY: hexitol fermentation to lactate, formate, ethanol, and acetate	MYBL1	−0.90476	0.000309	0.081754	
P461-PWY: hexitol fermentation to lactate, formate, ethanol, and acetate	NTRK2	−0.95238	0.000321	0.084551	
s__Clostridium_bartlettii	IL17F	0.76835	0.000202	0.059482	7
s__Veillonella_unclassified	IL17F	0.76835	2.91E−05	0.011329	
s__Clostridium_bartlettii	RN7SL301P	0.76835	0.00012	0.038644	
s__Veillonella_unclassified	RN7SL301P	0.76835	7.23E−05	0.025955	
s__Eggerthella_lenta	Vd2	0.89822	0.000353	0.054394	8
s__Flavonifractor_plautii	Vd2	0.785714	0.000613	0.072663	
s__Eggerthella_lenta	RP11-707O23.5	0.76835	1.96E−06	0.001075	
s__Flavonifractor_plautii	RP11-707O23.5	0.763763	0.000134	0.04259	
s__Eubacterium_siraeum	Vd2T_IL22_only	0.814386	0.000264	0.048712	9
s__Eubacterium_siraeum	IL17C	0.76835	7.73E−06	0.003364	
s__Subdoligranulum_unclassified	IRX2	0.754505	0.000291	0.083959	10
s__Subdoligranulum_unclassified	PAX8-AS1	−0.83333	0.000316	0.087851	
s__Roseburia_hominis	C5orf17	0.904762	0.000139	0.043995	11
s__Roseburia_hominis	RP11-726G1.1	0.904762	0.000122	0.038958	

(*continued*)

Supplementary Table S11. Continued

From	To	Cor	*P*-Value	*P*adj	Greedy Membership
GALACTUROCAT-PWY: D-galacturonate degradation I	GHR	0.928571	0.000275	0.073927	12
PWY-6507: 4-deoxy-L-threo-hex-4-enopyranuronate degradation	GHR	0.97619	5.83E−05	0.017377	
CITRULBIO-PWY: L-citrulline biosynthesis	PCK1	0.904762	0.00033	0.086443	13
PWY-4984: urea cycle	PCK1	0.904762	0.000355	0.092057	
PWY-6305: putrescine biosynthesis IV	CXCL8	0.97619	0.000123	0.034844	14
PWY-6305: putrescine biosynthesis IV	IGHV4-31	0.928571	0.000159	0.044272	
FAO-PWY: fatty acid β-oxidation I	IGKV1D-16	0.946125	0.000305	0.080971	15
PWY-5136: fatty acid β-oxidation II (peroxisome)	IGKV1D-16	0.952381	7.44E−05	0.022051	
P42-PWY: incomplete reductive TCA cycle	IGLV7-46	−0.97619	0.000353	0.091828	16
PWY-5104: L-isoleucine biosynthesis IV	IGLV7-46	−0.95238	0.000101	0.029049	
s__Lachnospiraceae_bacterium_1_4_56FAA	CD8_IL22_only	0.809524	0.000137	0.036152	17
s__Lachnospiraceae_bacterium_1_4_56FAA	Teff_TNFa_INFg	0.718576	6.25E−05	0.020997	
PWY-5189: tetrapyrrole biosynthesis II (from glycine)	CA1	−0.78571	0.000311	0.082075	18
PWY-5189: tetrapyrrole biosynthesis II (from glycine)	CD274	0.928571	0.000299	0.079439	
FOLSYN-PWY: super pathway of tetrahydrofolate biosynthesis and salvage	TMEM37	0.934148	3.07E−06	0.001317	19
PWY-6612: superpathway of tetrahydrofolate biosynthesis	TMEM37	0.904762	4.47E−06	0.001739	
Treg_IL17_only	FCRL1	−0.97619	6.99E−05	0.041248	20
Treg_IL17_only	FCRLA	−1	0.000158	0.087172	
PWY-6969: TCA cycle V (2-oxoglutarate:ferredoxin oxidoreductase)	REG1A	−0.76376	0.000365	0.094544	21
s__Bacteroides_xylanisolvens	REG1A	0.736989	0.000162	0.048778	
GLCMANNANAUT-PWY: super pathway of N-acetylglucosamine, N-acetylmannosamine, and N-acetylneuraminate degradation	C11orf86	−0.83333	5.42E−06	0.002104	22
GLUCONEO-PWY: gluconeogenesis I	IGLV3-10	−0.7619	0.000271	0.073002	23
s__Ruminococcus_bromii	IGHM	0.904762	1.28E−05	0.005526	24
PWY-621: sucrose degradation III (sucrose invertase)	CLCA4	−0.97619	1.29E−05	0.00476	25
PWY-2941: L-lysine biosynthesis II	NLGN4Y	0.912328	0.000273	0.073524	26
PHOSLIPSYN-PWY: super pathway of phospholipid biosynthesis I (bacteria)	IGLV5-37	−0.90476	0.000222	0.060934	27
UniRef90_B0GA46: NO_NAME	CD8_TNFa_IFNg	0.8485	2.77E−06	0.088269	28
TRNA-CHARGING-PWY: tRNA charging	CHIT1	−0.92857	1.07E−05	0.004046	29
RHAMCAT-PWY: L-rhamnose degradation I	DZ_duration	0.886243	0.00443	0.078996	30
s__Clostridium_bolteae	Active.Teff	−0.87427	0.000195	0.092483	31
PWY0-1297: superpathway of purine deoxyribonucleosides degradation	MYEOV	0.904762	3.78E−05	0.011407	32
NONOXIPENT-PWY: pentose phosphate pathway (non-oxidative branch)	CLIC6	0.904762	0.000182	0.050256	33
PWY-3001: super pathway of L-isoleucine biosynthesis I	CIDEC	−0.88095	0.000207	0.056999	34
s__Bilophila_wadsworthia	NLRP2	−0.95238	4.72E−05	0.018207	35
PWY-5005: biotin biosynthesis II	KRT8P36	0.922172	0.000142	0.040129	36
PWY0-1061: superpathway of L-alanine biosynthesis	RP11-575F12.2	0.970077	0.000254	0.068804	37
PWY0-1296: purine ribonucleosides degradation	SULT1C2	−0.97619	0.000106	0.030556	38
MET-SAM-PWY: super pathway of S-adenosyl-L-methionine biosynthesis	FRMD1	−0.80952	0.000175	0.048401	39
LACTOSECAT-PWY: lactose and galactose degradation I	IGHV1-3	0.952381	0.000237	0.064542	40
s__Bilophila_unclassified	RPS6KA2-AS1	−1	1.82E−05	0.007734	41

(*continued*)

Supplementary Table S11. Continued

From	To	Cor	*P*-Value	*P*adj	Greedy Membership
PWY-7383: anaerobic energy metabolism (invertebrates, cytosol)	IGLV4-60	−0.92857	0.000302	0.080129	42
HEME-BIOSYNTHESIS-II: heme biosynthesis I (aerobic)	RP11-958N24.2	0.788009	0.000292	0.077896	43
PWY-7234: inosine-5-phosphate biosynthesis III	HERC2P4	−0.92857	0.000167	0.0464	44
PWY0-162: super pathway of pyrimidine ribonucleotides de novo biosynthesis	ARL14	−0.97008	6.97E−05	0.020733	45
PWY-7229: superpathway of adenosine nucleotides de novo biosynthesis I	CTAGE15	0.857143	0.000298	0.079314	46
Vd2T_IFNg_only	IGLC7	0.880952	0.000167	0.08878	47
PWY-6897: thiamin salvage II	MME-AS1	0.76835	0.000346	0.09024	48
PWY-5030: L-histidine degradation III	AC131056.3	0.952381	0.000379	0.097971	49
s__Eubacterium_eligens	RP11-259G18.3	−0.95181	6.08E−05	0.022759	50
Treg_IL17_IL22	IGKV1D-43	0.730552	6.75E−05	0.041248	51
s__Lachnospiraceae_bacterium_7_1_58FAA	ZBTB16	0.928571	0.000347	0.095663	52
s__Coprococcus_catus	THNSL2	1	5.97E−05	0.02245	53
s__Erysipelotrichaceae_bacterium_6_1_45	PTGS2	−0.83333	0.000359	0.098475	54
s__Bifidobacterium_longum	Vd2T_TNFa_only	−0.91573	0.000601	0.072663	55
List of significant associations in PSO3 associated network					
P122-PWY: heterolactic fermentation	EDDM3DP	0.664211	1.49E−05	0.022213	1
P122-PWY: heterolactic fermentation	RP11-100G15.10	0.664211	1.49E−05	0.022213	
PWY-5083: NAD/NADH phosphorylation and dephosphorylation	EDDM3DP	0.695608	4.42E−07	0.001001	
PWY-5083: NAD/NADH phosphorylation and dephosphorylation	RP11-100G15.10	0.695608	4.42E−07	0.001001	
PWY-821: super pathway of sulfur amino acid biosynthesis (Saccharomyces cerevisiae)	RP11-100G15.10	0.695608	7.39E−05	0.070103	
PWY-821: super pathway of sulfur amino acid biosynthesis (Saccharomyces cerevisiae)	EDDM3DP	0.695608	7.39E−05	0.070103	
PWY0-1061: superpathway of L-alanine biosynthesis	RP11-100G15.10	0.654654	9.11E−05	0.081919	
PWY0-1061: superpathway of L-alanine biosynthesis	EDDM3DP	0.654654	9.11E−05	0.081919	
s__Bacteroides_xylanisolvens	EDDM3DP	0.654654	0.000129	0.063831	
s__Bacteroides_xylanisolvens	RP11-100G15.10	0.654654	0.000129	0.063831	
s__Haemophilus_parainfluenzae	EDDM3DP	0.654654	3.59E−07	0.000407	
s__Haemophilus_parainfluenzae	RP11-100G15.10	0.654654	3.59E−07	0.000407	
PWY-5188: tetrapyrrole biosynthesis I (from glutamate)	MYBL1	−1	1.56E−05	0.022439	2
PWY-5188: tetrapyrrole biosynthesis I (from glutamate)	PAX5	−1	4.29E−05	0.046051	
PWY-5188: tetrapyrrole biosynthesis I (from glutamate)	AFF2	−1	1.32E−05	0.020625	
PWY-5188: tetrapyrrole biosynthesis I (from glutamate)	TCL1A	−0.88571	1.28E−05	0.020213	
PWY-5188: tetrapyrrole biosynthesis I (from glutamate)	CD79B	−0.88571	3.53E−05	0.040084	
PWY-5345: superpathway of L-methionine biosynthesis (by sulfhydrylation)	PWP2	−0.94286	1.25E−05	0.019878	3
PWY-5345: super pathway of L-methionine biosynthesis (by sulfhydrylation)	IGKV1-9	−0.94286	8.57E−05	0.078976	
SULFATE-CYS-PWY: super pathway of sulfate assimilation and cysteine biosynthesis	IGKV1-9	−0.89865	8.22E−05	0.076628	
COBALSYN-PWY: adenosylcobalamin salvage from cobinamide I	ATP13A5	−1	8.76E−05	0.079978	4
DTDPRHAMSYN-PWY: dTDP-L-rhamnose biosynthesis I	ATP13A5	−1	3.25E−05	0.037635	
DTDPRHAMSYN-PWY: dTDP-L-rhamnose biosynthesis I	RGS13	−0.94286	6.46E−05	0.063204	

(*continued*)

Supplementary Table S11. Continued

From	To	Cor	*P*-Value	*P*adj	Greedy Membership
s__Roseburia_intestinalis	IL36RN	0.845154	7.21E−05	0.042737	5
s__Roseburia_intestinalis	SLC44A5	0.771429	0.000123	0.061427	
s__Roseburia_intestinalis	RP11-313J2.1	−0.82857	6.98E−05	0.041714	
s__Lachnospiraceae_bacterium_7_1_58FAA	RP11-462B18.1	0.654654	0.000174	0.083495	6
s__Lachnospiraceae_bacterium_7_1_58FAA	TM4SF4	0.885714	3.85E−05	0.024936	
s__Lachnospiraceae_bacterium_7_1_58FAA	IGHV3-66	−1	6.57E−06	0.005182	
GOLPDLCAT-PWY: superpathway of glycerol degradation to 1,3-propanediol	NARF	−1	0.000113	0.097624	7
GOLPDLCAT-PWY: superpathway of glycerol degradation to 1,3-propanediol	PNLIPRP2	−1	4.67E−05	0.04818	
MET-SAM-PWY: superpathway of S-adenosyl-L-methionine biosynthesis	TMEM150B (DRAM-3 regulate autophagy)	1	3.53E−05	0.040084	8
PWY-5347: superpathway of L-methionine biosynthesis (transsulfuration)	TMEM150B	1	8.06E−05	0.075717	
FAO-PWY: fatty acid β-oxidation I	TEKT4P2	−1	2.74E−05	0.035602	9
PWY-5136: fatty acid β-oxidation II (peroxisome)	TEKT4P2	−1	3.71E−05	0.040923	
UniRef90_A7B4W0: NO_NAME	AQP5	0.970588	4.31E−07	0.015343	10
UniRef90_D6DY27: ABC-type antimicrobial peptide transport system, ATPase component	AQP5	0.955882	1.67E−06	0.057497	
UniRef90_C6JCY5: NO_NAME	IGLV4-60	−0.98561	2.08E−06	0.070312	11
NAD-BIOSYNTHESIS-II: NAD salvage pathway II	NLGN4Y	0.941124	7.1E−05	0.068116	12
CALVIN-PWY: Calvin-Benson-Bassham cycle	HBEGF	1	7.11E−05	0.068116	13
GLUCONEO-PWY: gluconeogenesis I	RP11-575F12.3	1	7.47E−06	0.013124	14
PWY-5097: L-lysine biosynthesis VI	RP11-30P6.6	−1	4.54E−05	0.047844	15
PYRIDNUCSYN-PWY: NAD biosynthesis I (from aspartate)	RP11-747H7.3	1	5.69E−05	0.055963	16
UniRef90_G1WWG9: NO_NAME	CD55	1	2.77E−06	0.090568	17
PWY-5005: biotin biosynthesis II	TDRD1	0.941124	8.24E−05	0.076628	18
OANTIGEN-PWY: O-antigen building blocks biosynthesis (*E. coli*)	ISG15	1	4.61E−05	0.048107	19
UniRef90_D4L1Y1: Site-specific recombinases, DNA invertase Pin homologs	SERPINA9	−1	1.8E−08	0.000665	20
PWY-2941: L-lysine biosynthesis II	PI15	0.828571	4.83E−05	0.049266	21
PWY4LZ-257: superpathway of fermentation (Chlamydomonas reinhardtii)	IGLC7	−0.94286	8.84E−05	0.080307	22
UniRef90_D4KBZ1: Ribonuclease H	HRCT1	−1	2.95E−06	0.094916	23
UniRef90_C7H3L3: NO_NAME	FOSB	−0.95618	1.65E−06	0.057497	24
CRNFORCAT-PWY: creatinine degradation I	VWA5B1	1	5.56E−06	0.010772	25
s__Anaerostipes_hadrus	RP11-424G14.1	0.845154	2.53E−07	0.000295	26

Abbreviations: adj, adjusted; Cor, correlation value.

Supplementary Table S12. Available Clinical and Experimental Data

PID	Status	Gender	Age	PASI	PSO onset	Disease Duration	Metagenomics Data (Stool)	Host Transcriptomic Data (Sigmoid)	Flow Cytometry Data (PBMCs)	PSO Subgroups Identified
6532	Healthy	M	61	NA	NA	NA	Yes	Yes	Yes	Healthy
7300	PSO	F	58	5.9	18	37	Yes	Yes	Yes	PSO2
7301	PSO	M	37	27.8	24	10	Yes	Yes	Yes	PSO2
7303	PSO	F	35	NA	18	14	Yes	Yes	Yes	PSO2
7304	PSO	F	41	1.2	19	19	Yes	Yes	Yes	PSO2
7305	PSO	M	58	19.4	33	22	Yes	Yes	Yes	PSO1
7306	PSO	M	70	2.1	20	47	Yes	Yes	Yes	PSO1
7307	PSO	M	58	15.6	50	5	Yes	Yes	Yes	PSO3
7308	PSO	F	60	5.2	48	10	Yes	Yes	Yes	PSO1
7309	PSO	F	29	0.2	10	16	Yes	Yes	Yes	PSO3
7310	PSO	M	54	7.7	44	10	Yes	Yes	Yes	PSO1
7311	PSO	M	58	5.6	20	47	Yes	Yes	Yes	PSO2
7312	PSO	M	39	4.3	10	26	Yes	Yes	Yes	PSO1
7313	PSO	F	76	7.5	60	14	Yes	Yes	Yes	PSO2
7314	PSO	M	29	4	7	19	Yes	Yes	Yes	PSO3
7315	PSO	M	55	3.9	42	10	Yes	Yes	Yes	PSO1
7317	PSO	F	28	2.6	10	15	Yes	Yes	Yes	PSO1
7320	PSO	F	60	13.2	29	32	Yes	Yes	Yes	PSO3
7322	PSO	F	42	3.4	10	32	Yes	Yes	Yes	PSO1
7323	PSO	F	53	31.1	22	31	Yes	Yes	Yes	PSO3
7324	PSO	M	57	7.8	55	2	Yes	Yes	Yes	PSO1
7325	PSO	F	22	27.8	15	7	Yes	Yes	Yes	PSO1
7327	PSO	F	29	11.3	6	23	Yes	Yes	Yes	PSO2
7328	PSO	F	28	13.2	8	20	Yes	Yes	Yes	PSO2
7330	PSO	F	28	16.1	16	12	Yes	Yes	Yes	PSO1
7331	PSO	F	29	18.7	12	17	Yes	Yes	Yes	PSO3
7332	PSO	M	28	19.8	24	4	Yes	Yes	Yes	PSO1
7352	Healthy	F	60	NA	NA	NA	Yes	No	No	Healthy
7353	Healthy	M	25	NA	NA	NA	Yes	Yes	Yes	Healthy
7355	Healthy	F	23	NA	NA	NA	Yes	Yes	Yes	Healthy
7358	Healthy	F	69	NA	NA	NA	Yes	Yes	Yes	Healthy
7360	Healthy	F	38	NA	NA	NA	Yes	Yes	Yes	Healthy
7364	Healthy	M	53	NA	NA	NA	Yes	Yes	Yes	Healthy
7365	Healthy	F	57	NA	NA	NA	Yes	Yes	Yes	Healthy
7368	Healthy	F	49	NA	NA	NA	Yes	Yes	Yes	Healthy
7369	Healthy	M	38	NA	NA	NA	Yes	Yes	Yes	Healthy
7371	Healthy	M	47	NA	NA	NA	Yes	Yes	Yes	Healthy
7372	Healthy	M	59	NA	NA	NA	Yes	Yes	Yes	Healthy
7374	Healthy	M	35	NA	NA	NA	Yes	Yes	Yes	Healthy
7375	Healthy	M	36	NA	NA	NA	Yes	Yes	Yes	Healthy
7376	Healthy	F	37	NA	NA	NA	Yes	Yes	Yes	Healthy
N1	PSO	M	52	23.9	27	25	Yes	No	No	PSO3
N11	PSO	F	31	31.9	5	16	Yes	No	No	PSO3
N2	PSO	M	49	8.8	26	23	Yes	No	No	PSO1
N3	PSO	M	37	22.7	27	10	Yes	No	No	PSO1
N4	PSO	M	32	66.6	25	7	Yes	No	No	PSO1
N6	PSO	M	35	6.8	35	1	Yes	No	No	PSO2
N9	PSO	F	29	18.7	27	2	Yes	No	No	PSO3

Abbreviations: F, female; M, male; NA, not available; PSO, psoriasis.